



<https://theses.gla.ac.uk/>

Theses Digitisation:

<https://www.gla.ac.uk/myglasgow/research/enlighten/theses/digitisation/>

This is a digitised version of the original print thesis.

Copyright and moral rights for this work are retained by the author

A copy can be downloaded for personal non-commercial research or study, without prior permission or charge

This work cannot be reproduced or quoted extensively from without first obtaining permission in writing from the author

The content must not be changed in any way or sold commercially in any format or medium without the formal permission of the author

When referring to this work, full bibliographic details including the author, title, awarding institution and date of the thesis must be given

Enlighten: Theses

<https://theses.gla.ac.uk/>  
[research-enlighten@glasgow.ac.uk](mailto:research-enlighten@glasgow.ac.uk)

# Non-Relativistic QCD on the Lattice

Andrew John Lidsey

Thesis submitted to the University of Glasgow  
for the degree of Doctor of Philosophy

March 1995

ProQuest Number: 10391121

All rights reserved

INFORMATION TO ALL USERS

The quality of this reproduction is dependent upon the quality of the copy submitted.

In the unlikely event that the author did not send a complete manuscript and there are missing pages, these will be noted. Also, if material had to be removed, a note will indicate the deletion.



ProQuest 10391121

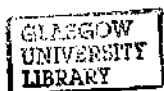
Published by ProQuest LLC (2017). Copyright of the Dissertation is held by the Author.

All rights reserved.

This work is protected against unauthorized copying under Title 17, United States Code  
Microform Edition © ProQuest LLC.

ProQuest LLC.  
789 East Eisenhower Parkway  
P.O. Box 1346  
Ann Arbor, MI 48106 – 1346

Thesis  
10102  
Copy 2



*Dedicated to my Mum and Dad*

## Acknowledgements

I would like to thank my supervisor Christine Davies and other members of the NRQCD collaboration, especially John Sloan and Junko Shigemitsu. Thanks of course to all the people in the theory group, Luke, Brian, Paul, Steven, Douglas, Gordon, Susan, Saad, Elizabeth, David R, David K, Jack, Gerry, Carolyn, Garry and David A.

This work was funded by the Particle Physics and Astronomy Research Council (PPARC).

## Declaration

In this thesis chapter 1 and 2 are introductions into Lattice QCD and Non-Relativistic QCD. Chapter 3, 4 and 5 is original work done by myself and my supervisor Dr Christine Davies.

## Abstract

Traditional perturbative techniques for solving QCD are unable to successfully describe the properties of hadrons, where non-perturbative effects are likely to be present. One way to solve QCD non-perturbatively is to use Lattice QCD which offers a solution of QCD from first principles. This thesis describes the solution of bound states of heavy quarks using a Non-Relativistic formulation of QCD (NRQCD) together with Lattice techniques.

Chapter 1 is an introduction to QCD as well as Lattice QCD, introducing the discretized action for relativistic fermions and the gauge field action. Chapter 2 describes potential models which to some extent can successfully predict the spectrum of Quarkonium states composed of Charm or Bottom quarks. NRQCD is then defined as an effective field theory in the continuum and relativistic corrections are derived as a power series of the typical quark velocity inside the Quarkonium. In Chapter 3 NRQCD is derived on the Lattice and the evolution of the quark Greens function given. The importance of tadpole-improved perturbation theory is stressed and its effect on spin-splittings is noted. Operators for various spin and orbital angular momentum states are derived and smearing of these operators are done to increase the signal to noise ratio. Chapter 4 describes the calculation in detail of the spectrum of Charmonium. To extract ground state masses to high precision and also excited states, fits of multiple correlation functions to multi-exponential terms are done. The spectrum for Upsilon is calculated on a coarser lattice than has previously been done to try to quantify any remaining lattice spacing errors. The spectrum for  $B_c$  mesons is also calculated. These exotic heavy mesons have not been observed experimentally yet and the low lying states calculated can act as a prediction. In chapter 5 the two most important systematic errors remaining in the simulation are estimated using a simple Schrödinger equation. These errors are quenching and  $\mathcal{O}(a)^2$  corrections in the gluonic action. Adjusting for  $\mathcal{O}(a)^2$  corrections it is possible to observe scaling of mass-independent splittings on going from a finer to coarser lattice. This indicates there is no significant error left from lattice spacing errors. Chapter 6 is the conclusion.

# Contents

<b>1</b>	<b>Introduction to Lattice QCD</b>	<b>3</b>
1.1	Introduction . . . . .	3
1.2	Defining QCD . . . . .	4
1.3	Lattice QCD . . . . .	5
1.4	Numerical Simulations . . . . .	7
1.5	Hadron Correlators . . . . .	8
<b>2</b>	<b>Non-Relativistic QCD</b>	<b>11</b>
2.1	Introduction . . . . .	11
2.2	Potential Models . . . . .	11
2.3	Relativistic Corrections to Potential Models . . . . .	13
2.4	Non-Relativistic QCD as an effective field theory . . . . .	16
2.5	Energy Scales in Quarkonium . . . . .	16
2.6	Power Counting for NRQCD in Quarkonium . . . . .	17
2.7	Heavy Wilson Fermions . . . . .	19
2.8	Why use NRQCD for Quarkonium ? . . . . .	21
<b>3</b>	<b>Non-Relativistic QCD on the Lattice</b>	<b>24</b>
3.1	Introduction . . . . .	24
3.2	Lattice NRQCD Operators . . . . .	24
3.3	Lattice spacing errors to Lattice NRQCD operators . . . . .	27
3.4	Evolution of the quark Greens function . . . . .	28
3.5	Improved Perturbation . . . . .	30
3.6	Meson Correlation functions . . . . .	32
3.7	Meson operators . . . . .	32
3.8	Coding up Meson Correlators . . . . .	37
3.9	Smearred Operators . . . . .	41
3.10	Dispersion Relation . . . . .	46

3.11	Wavefunctions	50
<b>4</b>	<b>Simulation Results</b>	<b>52</b>
4.1	Multi-Exponential and Multi-Correlated Fitting Routines	52
4.2	Charmonium Spectroscopy	55
4.2.1	Fitting Simulation Data	56
4.2.2	Fitting results for the S, P and D states	62
4.2.3	Fits to Spin Splittings	72
4.2.4	Wavefunctions	74
4.2.5	Comparison with Experiment	77
4.3	Upsilon and $B_c$ Spectroscopy	82
4.3.1	Upsilon Spectroscopy	85
4.3.2	$B_c$ Spectroscopy	90
<b>5</b>	<b>Estimates of Quenching and <math>O(a)^2</math> Gluonic corrections</b>	<b>95</b>
5.1	Introduction	95
5.2	Schrödinger equation on the lattice	95
5.3	Quenching	98
5.4	$O(a)^2$ Gluonic Corrections	101
5.5	Decay Constants	107
<b>6</b>	<b>Conclusion</b>	<b>109</b>

# Chapter 1

## Introduction to Lattice QCD

### 1.1 Introduction

In particle theory today there is a highly successful model of particle interactions called the Standard Model (SM). In the SM the fundamental particles of nature are fermions interacting with each other via exchange of virtual gauge bosons. To understand the interaction requires gauge invariance and the SM demands invariance under  $SU(3) \otimes SU(2) \otimes U(1)$  rotations.  $SU(3)$  describes QCD the interaction of quarks and gluons.  $SU(2) \otimes U(1)$  is the electroweak interaction describing the interaction between leptons and the  $W$  and  $Z$  particles with the symmetry breaking at low energies to  $U(1)$  of electromagnetism and the weak interaction.

Traditionally to calculate quantities of physical interest, scattering amplitudes and matrix elements, requires the use of perturbation theory where a power series in the typical coupling constant between the appropriate fermion and gauge boson is used. Higher terms in the series represent more complex possibilities for exchange of virtual gauge bosons between fermions. Collectively these differing processes are called Feynman diagrams. For QED the characteristic coupling constant  $\alpha_e \approx \frac{1}{137}$  and the series is very convergent making QED relatively simple to solve. However for QCD the coupling constant  $\alpha_s \approx \mathcal{O}(1)$  and will cause perturbation theory to break down. QCD has the property of asymptotic freedom where the typical coupling constant increases as the momentum scale at which one wants to solve QCD decreases. The opposite is true for QED. One immediate consequence of asymptotic freedom is that the quarks are confined into bound states called hadrons. The coupling constant increases as the separation of the quarks increases or the typical momentum exchange between such quarks decreases ( $\Delta p \Delta x \approx 1$ ). In order to un-

derstand for example the mass spectrum of QCD, where such bound states rely on the mechanism of confinement and hence non-perturbative QCD, another way to solve QCD other than from perturbative methods needs to be found.

In the next sections the formulation of QCD is given and it is shown how through the path integral approach it is possible to extract non-perturbative QCD physics using the method of Lattice QCD [1].

## 1.2 Defining QCD

QCD, like all gauge field theories, is defined through a Lagrangian density  $\mathcal{L}_{QCD}$  or equivalently the action  $S_{QCD} = \int d^4x \mathcal{L}_{QCD}$ . In analogy to U(1) of QED the Lagrangian density in Euclidean space [2, 3, 4, 5] is

$$\mathcal{L}_{QCD} = \mathcal{L}_F + \mathcal{L}_G \quad (1.1)$$

where

$$\mathcal{L}_G = \frac{1}{2} \text{Tr} [F_{\mu\nu} F^{\mu\nu}] \quad (1.2)$$

with

$$F_{\mu\nu}(x) = \partial_\mu A_\nu(x) - \partial_\nu A_\mu(x) - ig [A_\mu(x), A_\nu(x)] \quad (1.3)$$

and

$$\begin{aligned} \mathcal{L}_F &= \bar{\psi}(x) (\gamma_\mu (\partial_\mu + ig_0 A_\mu) + M_0) \psi(x) \\ \{\gamma_\mu, \gamma_\nu\} &= 2\delta_{\mu\nu} \quad \gamma_\mu^\dagger = \gamma_\mu \end{aligned} \quad (1.4)$$

Under local  $SU(3)$  rotations the quark and gluon fields transform as

$$\begin{aligned} \psi'(x) &\rightarrow G(x)\psi(x) \\ A_\mu(x) &\rightarrow G(x)A_\mu(x)G^{-1}(x) - \frac{i}{g} G(x)\partial_\mu G^{-1}(x) \end{aligned} \quad (1.5)$$

$\mathcal{L}_F$  and  $\mathcal{L}_G$  are invariant and colour charge at any space-time point is conserved. After writing down a formulation for QCD it is necessary to extract measurable quantities which are then compared to experiment to test the theory. One way to do this is to use the path integral representation of quantum field theory where the expectation values of time ordered product of interpolating fields are calculated.

The path interal is defined as a partition function given by

$$\mathcal{Z} = \int \mathcal{D}\bar{\psi} \mathcal{D}\psi \mathcal{D}A e^{-S_{QCD}} \quad (1.6)$$

where  $\mathcal{D}\bar{\psi}$ ,  $\mathcal{D}\psi$  and  $\mathcal{D}A$  is a short hand notation for intergrating over all possible quantum fluctuations of the quark, anti-quark and gluonic fields. Defining a collection of time ordered product of fields as  $\mathcal{O}(\bar{\psi}, \psi, A)$  its expectation value is given by

$$\langle \mathcal{O}(\bar{\psi}, \psi, A) \rangle = \frac{1}{\mathcal{Z}} \int \mathcal{D}\bar{\psi} \mathcal{D}\psi \mathcal{D}A \mathcal{O}(\bar{\psi}, \psi, A) e^{-S_{QCD}} \quad (1.7)$$

In perturbation theory the total QCD action is split up into the free action for the fermion and the gauge fields and the interacting part of the action. Hence

$$S_{QCD} = S_{\text{free}} + S_{\text{int}} \quad (1.8)$$

and the exponential for the interaction part of the action is expanded in the coupling constant  $g_0$ . By doing this a series of Feynman diagrams can be built up and the amplitudes for the various processes calculated analytically. There are a number of drawbacks to this, notably one has to have  $g_0$  small enough for perturbation to be valid. Also the calculation involves integrals which are in general divergent and will need to be regulated. If it is required to solve QCD in the non-perturbative region where  $g_0$  is  $\mathcal{O}(1)$  then a new method to evaluate equ (1.7) will need to be found. This is where Lattice QCD comes into play.

### 1.3 Lattice QCD

In Lattice QCD space-time is split up into a set of discrete points on a finite volume. This introduces a natural cut off in momentum space of order of the inverse of the lattice spacing  $a^{-1}$ . The path integral in equ (1.6) is well defined and not necessarily divergent. Instead of expanding in  $g_0$  the whole exponential term containing the interaction part of the action is kept and the path integral evaluated numerically. This allows a study of non-perturbative effects.

The formulation of QCD in the continuum requires gauge invariance which must also be the case on the lattice. To define a gauge invariant action the following path ordered quantity is introduced

$$U(y, x) = P e^{(ig_0 \int_x^y dz_\mu A_\mu)} \quad (1.9)$$

and under a general gauge transformation  $G(x)$  the quantity transforms as

$$U(y, x) = G(x)U(y, x)G^{-1}(y) \quad (1.10)$$

It is then straight forward to produce a gauge invariant object like for example

$$\bar{\psi}(x)U(y,x)\psi(y) \quad (1.11)$$

Discretizing the fermion Lagrangian  $\mathcal{L}_f$  is achieved by replacing

$$\partial_\mu \psi(x) \rightarrow \frac{1}{2a} (\psi(x+a\mu) - \psi(x-a\mu)) \quad (1.12)$$

on a lattice with spacing  $a$ . For gauge invariance the path ordered integral equ (1.9) between two lattice points is defined as

$$U(x,\mu) = e^{i g A_\nu(x)a} \quad (1.13)$$

From this it follows that the action for fermions in the interacting case is given by

$$S_F = a^4 \sum_{x,\mu} \bar{\psi} \left( \gamma_\mu \frac{1}{a} [U(x,\mu)\psi(x+a\mu) - U^\dagger(x-a,\mu)\psi(x-a\mu)] + M_0\psi(x) \right) \quad (1.14)$$

Looking at the dispersion relation for such fermions in the free field case one has

$$E^2 = M^2 + (a^{-1})^2 \sum_i \sin^2 q_i a \quad (1.15)$$

where  $-\frac{\pi}{a} < q_i \leq \frac{\pi}{a}$ . For  $q_i \rightarrow 0$ ,  $E^2 \rightarrow M^2$  which is the continuum energy for a fermion with zero momentum in the low energy region. However for  $q_i \rightarrow \frac{\pi}{a}$   $E^2 \rightarrow M^2$  as well. There is then an extra particle in the low energy region even though its momentum is high. This is purely a lattice artifact and in  $d$  dimensions one has  $2^d$  fermions using the naive action equ (1.14). To circumvent this problem extra operators can be added to the Lagrangian which disappear in the continuum. The most commonly used action is that given by Wilson [6] where the operator  $\frac{ar}{2} \bar{\psi}(x) \Delta^2 \psi(x)$  is added to equ (1.14) to give an action

$$S_{WF} = S_F - \frac{ar}{2} \sum_x a^4 \bar{\psi}(x) \Delta^2 \psi(x) \quad (1.16)$$

$\Delta^2$  is the lattice version of the continuum Laplacian and  $r$  is set to unity. From this action in the free field case the dispersion relation becomes

$$E^2 = \left[ M + a^{-1} (1 - \sum_i \cos q_i a) \right]^2 + (a^{-1})^2 \sum_i \sin^2 q_i a \quad (1.17)$$

Taking  $q_i \rightarrow 0$  as before one has  $E^2 = M^2$  but now when  $q_i \rightarrow \frac{\pi}{a}$   $E^2 \rightarrow (M + 2a^{-1})$ . Approaching the continuum  $a \rightarrow 0$  the effective mass becomes infinite and the extra  $2^d - 1$  fermions do not propagate and hence decouple from the theory.

As for the gauge field action on the lattice this too should be gauge invariant as in the continuum case. To make up a gauge invariant operator consisting of U fields

will involve taking a trace. The simplest example is to take a trace of a plaquette defined by

$$\text{Tr}U_{\mu\nu}^P(x) = \text{Tr}(U_\mu(x)U_\nu(x+a\mu)U_\mu^\dagger(x+a\nu)U_\nu^\dagger(x)) \quad (1.18)$$

which is invariant under the gauge transformation  $U_\mu(x) \rightarrow G(x)U_\mu(x)G^{-1}(x+a\mu)$ . Defining

$$U_{\mu\nu}^P(x) = e^{(ig_0 a^2 F_{\mu\nu}^L(x))} \quad (1.19)$$

and taking the naive continuum limit one finds that  $F_{\mu\nu}^L(x) \rightarrow F_{\mu\nu}(x) + \mathcal{O}(a)$  where  $F_{\mu\nu}(x)$  is given in equ (1.3). From this it is straightforward to show that the gauge field action on the lattice is

$$S_G = \beta \sum_{x,\mu,\nu>\mu} \left[ 1 - \frac{\text{Tr}}{6} (U_{\mu\nu}^P(x) + (U^P)_{\mu\nu}^\dagger(x)) \right] \quad (1.20)$$

with  $\beta = \frac{6}{g_0^2}$ .

## 1.4 Numerical Simulations

After defining the actions for the fermion and gauge fields of QCD it is necessary to show how the lattice can be used to calculate expectation values. The partition function is now given by

$$\mathcal{Z} = \int \mathcal{D}\bar{\psi} \mathcal{D}\psi \mathcal{D}U e^{-S_{QCD}} \quad (1.21)$$

where as before  $S_{QCD} = S_F + S_G$ . But now, because we are on a finite lattice, the integral is well defined. Since

$$\mathcal{D}\psi = \prod_n d\psi(n) \quad \mathcal{D}\bar{\psi} = \prod_n d\bar{\psi}(n) \quad \mathcal{D}U = \prod_{n,\mu} dU_\mu(n) \quad (1.22)$$

the integration measures in equ(??) are finite which in turn ensures that the partition function is finite and well defined. If we express  $S_{QCD}$  as

$$S_{QCD} = \sum_{y,x} \bar{\psi} M(U, y, x) \psi + S_G \quad (1.23)$$

then the integration over the Grassmann fermion fields can be done analytically to obtain

$$\mathcal{Z} = \int \mathcal{D}U \det M(U) e^{-S_G} \quad (1.24)$$

Expectation values of an operator  $\mathcal{O}(U, \bar{\psi}(y), \psi(x))$  can then be evaluated. One of the most used operators in Lattice QCD is given by  $\mathcal{O}(\bar{\psi}(y), \psi(x)) = \bar{\psi}(y)\psi(x)$  and

the expectation value  $\langle \bar{\psi}(y)\psi(x) \rangle$  is called the Greens function  $G(y, x)$ . It follows that

$$G(y, x) = \frac{1}{Z} \int \mathcal{D}U M^{-1}(U, y, x) \epsilon^{-S_G} \det M(U) \quad (1.25)$$

Initially to evaluate the expectation value numerically one would generate a random configuration of  $SU(3)$  matrices and evaluate  $\det M(U)\epsilon^{-S_G}$  for this configuration explicitly and then average over as many configurations as required. This however is computationally very expensive due to the large range in values of  $\epsilon^{-S_G}$ . A more efficient way is to use importance sampling where the gauge fields are generated with weight  $\det M(U)\epsilon^{-S_G}$ .

Then quark Greens function  $G(y, x)$  is estimated by evaluating

$$G(y, x) = \frac{1}{N_{conf}} \sum_{i=1}^{N_{conf}} G(U_i, y, x) \quad (1.26)$$

where  $M^{-1}(U, y, x)$  has been rewritten as  $G(U_i, y, x)$  for configuration  $i$ . Another approximation in the numerical procedure comes from neglecting to evaluate  $\det M(U)$ . This is a non-local quantity and is too costly to calculate for present computer power. In this so called quenched approximation which most lattice simulations use,  $\det M(U)$  is set to unity. In perturbation theory doing this is equivalent to neglecting internal quark loops.

In order to find  $G(U_i, y, x)$  it is necessary to solve an equation of the form

$$\sum_{x'} M(U_i, y, x') \tilde{G}_X(U_i, x', x) = \chi(y, x) \quad (1.27)$$

For  $\chi(y, x) = \delta_{y,x}$ ,  $\tilde{G}_X(U_i, x', x)$  is the usual Greens function  $G(U_i, x', x)$ . Since  $\tilde{G}_X(U_i, x', x) = \sum_z G(U_i, x', z)\chi(z, x)$  this is known as smearing the Greens function with the function  $\chi(z, x)$ .

## 1.5 Hadron Correlators

To simulate hadrons with specific quantum numbers it is necessary to write down the correct operator with the required quantum numbers. For simplicity consider a meson containing a quark and anti-quark with flavour  $f$  and  $f'$ . The operator will be of the form

$$O = \bar{f}' \Gamma f \quad (1.28)$$

where  $\Gamma$  is a specific collection of  $\gamma$  matrices and diagonal in colour space. For a pseudo-scalar meson  $\Gamma = \gamma_5$  where as for a vector meson  $\Gamma = \gamma_i$ . The propagation

of this meson from space-time point  $x$  to  $y$  is represented by the correlation function  $C(y, x)$

$$C(y, x) = \langle 0 | \mathcal{O}(y) \mathcal{O}^\dagger(x) | 0 \rangle = \langle 0 | \bar{f}(y) \Gamma f(y) \bar{f}(x) \Gamma^\dagger f(x) | 0 \rangle \quad (1.29)$$

Putting in explicitly colour and spin indices and using Wicks theorem to factorize the different flavour quarks it is possible to rewrite  $C(y, x)$  as

$$C(y, x) = \text{Tr} \left[ G^{f'}(x, y) \Gamma G^f(y, x) \Gamma^\dagger \right] \quad (1.30)$$

where the trace is over colour and spin indices. Therefore the procedure in numerical simulations of QCD is to find the inverse of the matrix  $M(U)$ , average over configurations to obtain the quark Green function and combine this appropriately to produce the required hadron correlator. But what physics can be learnt from knowing  $C(y, x)$ ? Consider

$$C(t) = \sum_{\mathbf{x}} \langle 0 | \mathcal{O}(\mathbf{x}, t) \mathcal{O}^\dagger(0, 0) | 0 \rangle \quad (1.31)$$

where we have made explicit in the RHS of equ (1.31) the spatial and time coordinates of  $\mathcal{O}$ . In the Feynman path integral approach the operator  $\mathcal{O}$  is in the Heisenberg representation and evolves in Euclidean time. Hence

$$\mathcal{O}(\mathbf{x}, t) = e^{-i\mathbf{q}\cdot\mathbf{x} + \mathcal{H}t} \mathcal{O}(0, 0) e^{+i\mathbf{q}\cdot\mathbf{x} - \mathcal{H}t} \quad (1.32)$$

for some Hamiltonian operator  $\mathcal{H}$ . Inserting a complete set of states into equ (1.31)

$$\sum_{\mathbf{q}, 0} |n\mathbf{q}\rangle \langle n\mathbf{q}| = 1 \quad (1.33)$$

where the base states have been normalized so that

$$\langle n\mathbf{q} | m\mathbf{p} \rangle = \delta_{nm} \delta_{\mathbf{p}\mathbf{q}} \quad (1.34)$$

$$\begin{aligned} C(t) &= \sum_{\mathbf{x}, \mathbf{q}, 0} \langle 0 | \mathcal{O}(\mathbf{x}, t) | n\mathbf{q} \rangle \langle n\mathbf{q} | \mathcal{O}^\dagger(0, 0) | 0 \rangle \\ &= \sum_{\mathbf{x}, \mathbf{q}, 0} |\langle 0 | \mathcal{O}(0, 0) | n\mathbf{q} \rangle|^2 e^{-E_n t + i\mathbf{q}\cdot\mathbf{x}} \\ &= \sum_{\mathbf{n}, \mathbf{q}} \delta_{\mathbf{q}, 0} |\langle 0 | \mathcal{O}(0, 0) | n\mathbf{q} \rangle|^2 e^{-E_n t} \\ &= \sum_{\mathbf{n}} |\langle 0 | \mathcal{O}(0, 0) | n \rangle|^2 e^{-M_n t} = |\langle 0 | \mathcal{O}(0, 0) | 1 \rangle|^2 e^{-M_1 t} + \dots \end{aligned} \quad (1.35)$$

In the large Euclidean time limit the hadron correlator decays exponentially fast. In the large time interval this is determined by the lowest mass  $M_1$  of the hadron with specific quantum numbers determined by the operator  $\mathcal{O}$ . In the simulation  $M_1$  can be found by evaluating

$$-\ln \left[ \frac{C(t-1)}{C(t)} \right] \quad (1.36)$$

as  $t \rightarrow \infty$ . The amplitude  $\langle 0|\mathcal{O}|1 \rangle$  is the matrix element for the decay of the hadron, a non-perturbative quantity which can only be calculated by Lattice simulations. This is also true for the calculation of the hadron mass.

## Chapter 2

# Non-Relativistic QCD

### 2.1 Introduction

Ever since the discovery of the Charm quark [7, 8] and even before the discovery of the Bottom quark [9, 10], potential models have been used with considerable success to predict the spectrum of heavy-heavy bound states. In this chapter a simple introduction to potential models is given and their basic features which can be used to explain the bulk of the the heavy meson spectrum. Next Non-Relativistic QCD (NRQCD) is introduced as an effective field theory of QCD in the heavy quark limit. Power counting in the typical quark velocity  $v^2$  is used to order the relativistic corrections away from the Non-Relativistic case. The relevant operators representing these corrections are written down and their significance for the meson spectrum described.

### 2.2 Potential Models

In the Standard Model there are six quarks (accepting now that the top quark does exist). They fall into two categories with the typical scale of QCD ( $\Lambda_{QCD}$ ) separating them. If one assumes that the typical momentum of quarks inside hadrons is  $\mathcal{O}(\Lambda_{QCD})$  then for quarks with mass  $\mathcal{O}(\Lambda_{QCD})$ , ie the u,d and s, they are considered to be relativistic with  $v^2 \approx c^2$ . For the other three c,b and t whose mass are very much greater than  $\Lambda_{QCD}$  they are considered to have velocities  $v^2 \ll c^2$ . It seems then appropriate to consider c and b and eventually t in terms of potential models. The starting point would be to pick an appropriate spin-independent potential and solve a Schrödinger type equation to predict spin-independent splittings for exam-

ple. To get an understanding of the type of potential to be chosen it is useful to calculate some elastic scattering between an equal mass quark and anti-quark and perform a non-relativistic expansion. This will not only tell us the form of the static heavy quark potential but also the type of relativistic corrections.

The matrix element for such a scattering  $M_{fi}^\Gamma$  between a quark and an anti-quark with initial momentum  $p_1, p_2$  into a final quark and anti-quark state with final momentum  $q_1, q_2$  can be expressed in the form

$$M_{fi}^\Gamma = \bar{u}(q_1)\Gamma u(p_1)V_\Gamma(p_1 - q_1)\bar{v}(p_2)\Gamma v(q_2) \quad (2.1)$$

where  $\Gamma$  determines the spin structure of the interaction. The  $\Gamma$ 's are made up of Dirac gamma matrices and classify the different types of potentials. In the non-relativistic limit the different potentials contribute according to [11]

$$\Gamma_{\text{scalar}} = 1 \rightarrow V_s \quad (2.2)$$

$$\Gamma_{\text{pseudoscalar}} = \gamma_5 \rightarrow 0 \quad (2.3)$$

$$\Gamma_{\text{vector}} = \gamma_\mu \rightarrow V_V \quad (2.4)$$

$$\Gamma_{\text{axial-vector}} = \gamma_\mu \gamma_5 - \sigma_1 \cdot \sigma_2 V_A \quad (2.5)$$

$$\Gamma_{\text{tensor}} = \sigma_{\mu\nu} \rightarrow \sigma_1 \cdot \sigma_2 V_T \quad (2.6)$$

There is no pseudoscalar static potential contribution at leading order. For the axial-vector and tensor terms this depends on the spin  $\sigma_1, \sigma_2$  of the quark and anti-quark at leading order. Consequently this would mean that spin-dependent splittings would be of the same order as spin-independent ones which clearly is not the case from experimental data. These two potentials are then ignored. One is left with the conclusion that at leading order the static potentials consist only of scalar and vector parts.

It is possible to calculate the matrix element perturbatively via one gluon exchange which leads to a potential of the form  $V \sim \frac{1}{q^2}$ . It is straight forward to show that the resulting potential in position space is  $V_V(r) = -\frac{4}{3} \frac{\alpha_s}{r}$ , the familiar coulombic type potential of QED. This will be the dominant potential at short distances where the momentum exchange is high and perturbation works. For the long range potential, because of confinement, perturbation is not applicable and a phenomenological potential will have to be used. This is taken to be of the form

$aR^n$  for  $n > 0$ . Therefore we know that the static heavy quark potential has a vector and/or scalar part and that at short distance the potential is coulombic and at large distances the potential increases with distance. It is normally taken that  $n = 1$  from spectroscopy considerations as well as lattice results. The next question to ask is whether these potentials are of vector or scalar or both in nature. For this we need to know what the relativistic corrections are.

### 2.3 Relativistic Corrections to Potential Models

One way to calculate relativistic corrections is to use the method of Eichten and Feinberg [12] where the spin-dependent potential correct up to order  $\frac{1}{m^2}$  is given by

$$V_{SD}(r) = \frac{\mathbf{L}_1 \cdot \mathbf{S}_1 - \mathbf{L}_2 \cdot \mathbf{S}_2}{m^2 r} \left( \frac{V_0'(r)}{2} + V_1'(r) \right) + \frac{\mathbf{L}_1 \cdot \mathbf{S}_2 + \mathbf{L}_2 \cdot \mathbf{S}_1}{m^2 r} V_2'(r) + \left( \frac{(\mathbf{r} \cdot \mathbf{S}_1)(\mathbf{r} \cdot \mathbf{S}_2)}{m^2 r^2} - \frac{\mathbf{S}_1 \cdot \mathbf{S}_2}{3m^2} \right) V_3(r) + \frac{\mathbf{S}_1 \cdot \mathbf{S}_2}{3m^2} V_4(r) \quad (2.7)$$

where  $\mathbf{L}_i = \mathbf{r} \times \mathbf{P}_i$  and  $V_0$  is the heavy quark static potential. The importance of writing it this way is because the  $V_i$ 's can be written in terms of cross-correlations between the chromo-magnetic and electric fields and this allows a non-perturbative treatment using, for example, lattice techniques [36]. A perturbative treatment is possible if we make the following identifications in terms of the vector ( $V_V$ ) scalar ( $V_S$ ) and pseudoscalar ( $V_P$ ) potentials

$$V_0(r) = V_V(r) + V_S(r) \quad (2.8)$$

$$V_1(r) = -V_S(r) \quad (2.9)$$

$$V_2(r) = V_V(r) \quad (2.10)$$

$$V_3(r) = \frac{V_V'(r) - V_P'(r)}{r} - (V_V''(r) - V_P''(r)) \quad (2.11)$$

$$V_4(r) = 2 \nabla^2 V_V(r) + \nabla^2 V_P(r) \quad (2.12)$$

Forgetting the pseudoscalar potential  $V_P(r)$  for now one ends up with the well known Breit-Fermi Hamiltonian

$$H = 2m + \frac{\mathbf{p}^2}{m} + \frac{\mathbf{p}^4}{4m^3} + V_0(r) + V_{SI}(r) + V_{LS}(r) + V_{SS}(r) + V_T(r) \quad (2.13)$$

where the following potentials are given by

$$V_{LS} = \frac{1}{2m^2 r} \left( 3 \frac{d}{dr} V_V(r) - \frac{d}{dr} V_S(r) \right) \mathbf{L} \cdot \mathbf{S} \quad (2.14)$$

$$V_{SS} = \frac{2}{3m^2} \mathbf{S}_1 \cdot \mathbf{S}_2 \nabla^2 V_V(r) \quad (2.15)$$

$$V_T = \frac{1}{12m^2} \left( \frac{1}{r} \frac{d}{dr} V_V(r) - \frac{d^2}{dr^2} V_V(r) \right) S_{12} \quad (2.16)$$

with the abbreviation

$$S_{12} \equiv 12 \left( \frac{(\mathbf{S}_1 \cdot \mathbf{x})(\mathbf{S}_2 \cdot \mathbf{x})}{r^2} - \frac{1}{3} \mathbf{S}_1 \cdot \mathbf{S}_2 \right) \quad (2.17)$$

Treating these interactions perturbatively it is possible to find expectation values of the appropriate operators using suitable wavefunctions. For this the expectation values of  $\mathbf{S} \cdot \mathbf{L}$ ,  $\mathbf{S}_1 \cdot \mathbf{S}_2$  and  $S_{12}$  will need to be evaluated. Decomposing the eigenvalues into the total spin  $\mathbf{S}$ , the relative orbital angular momentum  $\mathbf{L}$ , and the total momentum  $\mathbf{J} = \mathbf{L} + \mathbf{S}$  it follows that

$$\langle \mathbf{S} \cdot \mathbf{L} \rangle = \frac{1}{2} (J(J+1) - L(L+1) - S(S+1)) \quad (2.18)$$

$$\langle \mathbf{S}_1 \cdot \mathbf{S}_2 \rangle = \frac{1}{2} (S(S+1) - S_1(S_1+1) - S_2(S_2+1)) \quad (2.19)$$

For  $S_{12}$  with  $S_1 = \frac{1}{2}$  and  $S_2 = \frac{1}{2}$  it can be written in the form

$$S_{12} = 2 \left( 3 \frac{(\mathbf{S} \cdot \mathbf{x})^2}{r^2} - \mathbf{S}^2 \right) \quad (2.20)$$

and using the method of [14] to calculate the expectation values of tensors one has

$$\langle S_{12} \rangle = \frac{-12}{(2L-1)(2L+3)} \left( \langle \mathbf{S} \cdot \mathbf{L} \rangle^2 + \frac{1}{2} \langle \mathbf{S} \cdot \mathbf{L} \rangle - \frac{1}{3} S(S+1)L(L+1) \right) \quad (2.21)$$

Using these results we see that for either  $L=0$  or  $S=0$  the spin-orbit splitting vanishes as well as does the tensor term. Representing a two body equal mass bound state by the quantum numbers  $^{2S+1}L_J$  where  $L=0,1,2$  is replaced by S,P,D the above expectation values for various states can easily be calculated. For the ( $^3S_1, ^1S_0$ ) states,  $\langle \mathbf{S}_1 \cdot \mathbf{S}_2 \rangle = (\frac{1}{4}, -\frac{3}{4})$ . For ( $^3P_2, ^3P_1, ^3P_0$ ) states,  $\langle \mathbf{S} \cdot \mathbf{L} \rangle = (1, -1, -2)$ ,  $S_{12} = (-\frac{2}{3}, 2, -4)$  and  $\langle \mathbf{S}_1 \cdot \mathbf{S}_2 \rangle = \frac{1}{4}$ . The eigenvalues for the  $^1P_1$  state are zero except for  $\langle \mathbf{S}_1 \cdot \mathbf{S}_2 \rangle = -\frac{3}{4}$ .

From the knowledge obtained so far we know that the static potential has a vector and scalar contribution with a short distance coulombic potential and a linearly rising confining potential. We will now use the P hyperfine splittings to

deduce further the make up of the heavy quark potential and decide on which part of the potential is scalar and vector. To do this a parameter  $\rho$  is defined as

$$\rho = \frac{M(^3P_2) - M(^3P_1)}{M(^3P_1) - M(^3P_0)} \quad (2.22)$$

From the previous expressions the spin-orbit and tensor terms will contribute to this splitting, the spin-spin term if it does contribute at all to the P states will be the same for all P states with  $S=1$  and will not contribute to  $\rho$ . Lets assume first that the static potential is purely of vector type so that  $V_V = V_0$  and  $V_S = 0$ . Taking  $V_0 = -\frac{4}{3}\frac{\alpha_s}{r} + \sigma r$  then

$$\rho = \frac{1}{5} \frac{8\alpha_s \langle r^{-3} \rangle + 7\sigma \langle r^{-1} \rangle}{2\alpha_s \langle r^{-3} \rangle + \sigma \langle r^{-1} \rangle} \quad (2.23)$$

given the bounds  $\frac{4}{5} \leq \rho \leq \frac{7}{5}$  for  $\sigma = 0$  or  $\alpha_s = 0$ . This is not consistent with the experimental value  $\rho_{exp} \approx 0.6$ . Similarly a pure scalar is ruled out which would give a value  $\rho = 2$ . In conclusion the static potential has to be made up of both a scalar and a vector part. It is usual to identify the scalar part of the static potential with  $\sigma r$  the confining part of the potential and the vector part with  $-\frac{4}{3}\alpha_s r$ . The  $\rho$  parameter equ (2.23) now becomes

$$\rho = \frac{1}{5} \frac{8\alpha_s \langle r^{-3} \rangle + \frac{5}{2}\sigma \langle r^{-1} \rangle}{2\alpha_s \langle r^{-3} \rangle - \frac{1}{4}\sigma \langle r^{-1} \rangle} \quad (2.24)$$

which for a purely coulombic term  $\sigma = 0$  gives 0.8. Hence there must be a non-zero scalar confining part  $\sigma r$  which reduces the ratio equ (2.24) to agree with the experimental value [15, 16]. If we now substitute  $V_V = -\frac{4}{3}\frac{\alpha_s}{r}$  into the expression for the S hyperfine splitting equ (2.15) and evaluate perturbatively

$$\Delta V_{SS} = \frac{8\pi\alpha_s}{9m^2} \langle \mathbf{S}_1 \cdot \mathbf{S}_2 \rangle \Psi^2(0) \quad (2.25)$$

we see that the splitting is only going to effect states which have wavefunctions at the origin, for example the S states and will not effect P or D states. The  $^1P_1$  state then is not effected by either the spin-spin, spin-orbit or the tensor term. This is verified experimentally to a good approximation since the splitting between the  $^1P_1$  and the centre of gravity for the  $^3P_2, ^3P_1$  and  $^3P_0$  states is very small [17]. This indicates that the spin-spin interaction is absent in the P states and in turn suggests that indeed the vector potential is mostly coulombic in behaviour.

## 2.4 Non-Relativistic QCD as an effective field theory

Potential models described above can be very successful in accounting for the bulk effect of heavy-heavy meson spectroscopy. There are disadvantages to this approach in that it is only a model and not a calculation of the meson spectrum from first principles. For example the heavy quark potential has two free parameters which need to be adjusted. Normally the lowest ground states are used to fine-tune these parameters and then higher states can be predicted. Another drawback is that it is still not certain whether the scalar part of the heavy static potential is the confining part and whether the short range coulombic piece is vector in nature. However potential models should not be totally dismissed but should be used as a guide to solving heavy quark physics from first principles.

Looking at the spectrum for Charmonium and Upsilon one can see straight away the positronium type spectrum representative of non-relativistic behaviour. One important observation is the magnitude of spin-independent splittings relative to spin-dependent ones. For example in Charmonium and Upsilon the typical splitting between excited states or splittings between states of different angular momentum is about 500 MeV. Comparing this to spin-dependent splittings, for example, the S hyperfine or the P hyperfine in Charmonium these are typically of the order of 100 MeV. The same is true also of Upsilon where spin-splittings are of order 50 MeV. From potential models it is possible to calculate the typical quark velocity inside a heavy-heavy meson. The velocity for the Charm quark is  $v^2 \approx 0.3$  where as for the Bottom quark  $v^2 \approx 0.1$ . Looking at the spectrum for Charmonium and Upsilon it looks like spin-dependent quantities are down by the quark velocity and suggests that relativistic corrections can be added as a power series in  $v^2$ . This is the approach that Non-Relativistic QCD (NRQCD) takes. It is an effective field theory where corrections are added according to the importance or weight the corrections have on the physics involved.

## 2.5 Energy Scales in Quarkonium

In order to understand NRQCD more and why it is well situated to Quarkonium it is best to try and understand the different energy scales involved and the importance each one of them has. These scales are the heavy quark mass  $M$ , the quark's momentum  $Mv$  and the quark's kinetic energy  $Mv^2$ . The quark mass  $M$  sets the

overall scale of the meson and the scale for annihilation. The quark's momentum  $Mv$  determines the size of the meson ( $\frac{1}{Mv}$ ) and its kinetic energy  $Mv^2$  determines the size of spin-independent splittings. In such mesons, since the typical quark velocity  $v^2 \ll 1$ , there is a large disparity in the three energy scales. This will make it difficult to solve on the lattice if all three energy scales are present in the simulation. A first step would be to explicitly remove the mass scale from the theory. This will only alter the zero of energy and not for example the value of spin-splittings. It is still possible for quarks with average momentum  $Mv$  to fluctuate into relativistic states of value  $M$  but since this would occur for only a short period these relativistic corrections can be introduced as local interactions with coefficients determined perturbatively.

One starting point for the derivation of NRQCD is to perform a Foldy-Wouthuysen-Tani transformation [18] on the original QCD lagrangian. This transformation is a unitary transformation on the four fermi dirac fields which decouples the upper and lower components systematically in powers of  $\frac{1}{M}$  leaving a Non-Relativistic expansion. Following the example given in [19] one ends up after such a transformation with

$$\bar{\Psi}(D.\gamma - M)\Psi \rightarrow \psi^\dagger \left( iD_t - M + \frac{D^2}{2M} \right) \psi + \psi^\dagger \left( \frac{g}{2M} \sigma.B + \frac{g}{8M^2} \Delta.E \dots \right) \psi \quad (2.26)$$

Although this expansion is valid for an individual heavy quark one needs to ask whether this is an appropriate expansion for heavy quarks in Quarkonium. Looking at the expansion one sees that the  $\sigma.B$  term, which will presumably be responsible for spin-dependent splittings, comes in at order  $\frac{1}{M}$ . This is the same order in  $\frac{1}{M}$  as the kinetic energy operator which is mostly responsible for spin-independent splittings. This suggests that the two types of splittings will be of the same order which is clearly not the case. As previously mentioned spin-dependent splittings seem to be down by approximately  $v^2$  and it looks like this might be an appropriate expansion parameter rather than  $\frac{1}{M}$ . To derive NRQCD we perform the FWT transformation to produce the relevant relativistic corrections and evaluate the expectation values of the resulting terms in terms of  $v^2$  and order them appropriately.

## 2.6 Power Counting for NRQCD in Quarkonium

The work described below closely follows the work of [20] where the magnitude for various fields making up NRQCD in a Quarkonium state are estimated. To start with the estimated magnitude for the quark field  $\psi(x)$  (or equivalently the

anti-quark field  $\chi(x)$  is made. The number operator

$$\int d^3x \psi^\dagger(x) \psi(x) \quad (2.27)$$

which just counts the number of heavy quarks is one for Quarkonium. Since the quark is localised in a region  $\Delta x \sim \frac{1}{Mv}$

$$\int d^3x \psi^\dagger(x) \psi(x) \sim (\Delta x)^3 \psi^\dagger(x) \psi(x) \quad (2.28)$$

assuming the fields do not vary significantly over the region  $\Delta x$ . From this  $\psi(x) \sim (Mv)^{\frac{3}{2}}$ . The expectation value for the kinetic energy operator will be  $Mv^2$  hence

$$\int d^3x \psi^\dagger(x) \frac{\mathbf{D}^2}{2M} \psi(x) \sim Mv^2 \quad (2.29)$$

so  $\mathbf{D} \sim Mv$ . From the lowest order Schrödinger equation

$$\left( iD_t + \frac{\mathbf{D}^2}{2M} \right) \psi(x) = 0 \quad (2.30)$$

this leads to  $D_t \sim Mv^2$ . For a non-relativistic bound state the virial theorem tells us that the kinetic energy is balanced by the potential energy so that the potential energy  $g\phi(x) \sim Mv^2$ . To find the estimate for the vector potential term  $g\mathbf{A}(x)$  it is best to solve the field equations for the vector fields which gives  $g\mathbf{A}(x) \sim Mv^3$ . From these two estimates it is straight forward to obtain the estimate for the electric and magnetic fields

$$\begin{aligned} g\mathbf{E}(x) &= -\nabla g\phi(x) \sim M^2v^3 \\ g\mathbf{B}(x) &= g\nabla \times \mathbf{A}(x) \sim M^2v^4 \end{aligned} \quad (2.31)$$

using the fact that  $\nabla \sim (Mv)$ .

Using these estimates it is possible to build up various operators order by order in  $v^2$  away from the leading Schrödinger equation. In doing so the operators can not be arbitrary and must obey the symmetries of QCD ie charge conjugation, parity and gauge invariance. This limits the possibilities and to  $\mathcal{O}(v^2)$  the possible correction terms are

$$c_1 \frac{1}{8M^3} \psi^\dagger(x) \mathbf{D}^4 \psi(x) \quad (2.32)$$

$$c_3 \frac{g}{8M^2} \psi^\dagger(x) (\mathbf{D} \cdot \mathbf{E} - \mathbf{E} \cdot \mathbf{D}) \psi(x) \quad (2.33)$$

$$c_3 \frac{ig}{8M^2} \psi(x)^\dagger \boldsymbol{\sigma} \cdot (\mathbf{D} \times \mathbf{E} - \mathbf{E} \times \mathbf{D}) \psi(x) \quad (2.34)$$

$$c_4 \frac{g}{2M} \psi^\dagger(x) \boldsymbol{\sigma} \cdot \mathbf{B} \psi(x) \quad (2.35)$$

The first term is simply the first relativistic correction from the relativistic energy momentum dispersion relation  $E^2 = P^2 + M^2$ . The next is also a spin-independent relativistic correction and is the QCD equivalent of the Darwin term in QED. The last two are spin-dependent. The  $\boldsymbol{\sigma} \cdot \mathbf{B}$  term removes the degeneracy between states with different spin orientations and the  $\mathbf{D} \times \mathbf{E}$  will act as a spin-orbit coupling producing a P hyperfine splitting in the p states for example. We expect from the ordering of the operators in the typical quark velocity  $v$  that spin-dependent splittings should be down by about  $v^2$  compared to spin-independent splittings. This seems to be the case in the experimental determined spectrum for both the Charmonium and Upsilon. In a calculation in which only the above operators are used there will be systematic errors arising from the omission of relativistic corrections coming in at  $\mathcal{O}(v^6)$ . It is expected then that spin-independent splittings will have an accuracy of  $\mathcal{O}(v^4)$ , since the leading order corrections at  $\mathcal{O}(v^2)$  will effect these splittings. Similarly a relative accuracy of  $\mathcal{O}(v^2)$  in spin-dependent splittings is possible since they will be effected by operators which first occur at  $\mathcal{O}(v^4)$ , the next to leading order.

For full predictability of NRQCD the arbitrary coupling constants  $c_1, c_2, c_3, c_4$  need to be evaluated. These coupling constants will depend on the particular cut off  $\Lambda$  used and will cancel the cut-off dependence of the operators to ensure physical quantities are independent of  $\Lambda$  to some specific order in perturbation theory. To evaluate the coupling constants at tree level a FWT transformation can be performed to the appropriate order in  $\frac{1}{M}$  for which one finds that all  $c_i$ 's are unity. Another way to evaluate them is to calculate scattering amplitudes in full QCD at low energies and match these results in scattering amplitudes calculated in NRQCD [20]. Radiative corrections will occur away from tree-level values and will depend on  $\alpha_s(M)$  and the ratio  $\frac{\Lambda}{M}$  [33]. Taking  $\Lambda$  to infinity is not possible since the perturbative series breaks down which is just a reflection on the non-renormalizability of NRQCD. If however  $\Lambda \approx \frac{1}{M}$  the perturbation will work for large enough  $M$ . This will then leave two fundamental parameters left which are exactly those in the original QCD Lagrangian, the bare quark mass and the bare coupling constant.

## 2.7 Heavy Wilson Fermions

Any action defined on a lattice is an effective field theory, where the cut-off in momentum space is of the order of the inverse of the lattice spacing  $a^{-1}$ . As in any

effective theory one expects problems to arise when the highest momentum modes are greater than the cut-off. For example for heavy quarks with a bare mass of  $M_0$  it is expected that the Wilson formulation will break down when  $M_0 a > 1$ . To get some idea of why this is so a non-relativistic expansion of the energy-momentum relation for a Wilson quark can be performed to obtain the expression

$$E = M_1 + \frac{p^2}{2M_2} \quad (2.36)$$

with

$$M_1 = \log(1 + M_0 a) \quad (2.37)$$

$$M_2 \approx \frac{1}{M_0 a} \quad (2.38)$$

For small  $M_0 a$ ,  $M_1 = M_2$  and Lorentz invariance is restored at this order in the expansion. However this will not be the case when  $M_0 a > 1$ . Correction terms will have to be added to the original Wilson action to get the two definitions of the mass to be equal. A different interpretation of the problem is to recognise that just as in NRQCD the mass term  $M_1$  is redundant and only affects the zero of energy. It is the mass term  $M_2$  which determines the splitting between different orbital angular momentum states and hence sets the scale. If a dispersion relation similar to NRQCD is calculated so that the mass  $M_2$  is fixed to some physical quantity then it is expected that Wilson fermions can start to correctly describe heavy quarks. Of course the mass term appearing in the  $p^4$  term will be incorrect and a correction term will need to be added.

In Wilson fermions there are  $\mathcal{O}(a)$  corrections present which can be explicitly removed using the Symanzik improvement program [21]. The Wilson fermion action can be corrected from these  $\mathcal{O}(a)$  corrections by adding the term [22]

$$\Delta S = i g a \frac{c}{2} \kappa \sum_{x,\mu,\nu} \bar{\psi}(x) \sigma_{\mu\nu} F_{\mu\nu} \psi(x) \quad (2.39)$$

so that an Improved Heavy Wilson (IHW) action is defined by

$$S_{IHW} = S_{WF} + \Delta S \quad (2.40)$$

At tree-level  $c = 1$  and the remaining corrections will be  $\mathcal{O}(a^2)$ . Mean field estimates of radiative corrections changes  $c$  to 1.4. At tree-level the improvement term adjusts the mass  $M_3$  defined by the interaction  $\frac{\sigma \cdot \mathbf{B}}{2M_3}$  to be equal to  $M_2$  [23]. However the mass term appropriate to the spin-orbit interaction is incorrect and using equ (2.40) it is not possible to calculate the p spin-splittings correctly. Extra correction

terms will need to be added to achieve the same accuracy of NRQCD in its present form. Of course since it is the discretization errors which break Lorentz invariance in the Wilson formulation it is possible to take the lattice spacing explicitly to zero by brute force to obtain a fully Lorentz theory. Correction terms will then no longer be necessary. A comparison in the spectrum of Charmonium between the Wilson case and NRQCD will be made in section (4.2.5).

## 2.8 Why use NRQCD for Quarkonium ?

Before we can answer the question why use NRQCD to study Quarkonium it is best to ask the question why study heavy quarks at all. One simple answer is that there is a lot of experimental data now available to compare to. Decays of heavy quarks into other heavy quarks in heavy-light mesons depends on the parameters of the Cabibbo-Kobayashi-Maskawa matrix which are arbitrary parameters in the Standard Model (SM) [24]. Nailing down these parameters could offer an indication of physics beyond the SM, for example, deciding on whether the CKM matrix is unitary or not. Also if the objective is to try and solve QCD and understand the strong interactions it is best to study the most simple systems which for example heavy-heavy mesons are with their positronium-like behaviour.

The next question to ask is what is wrong with potential models since they can describe Quarkonium systems accurately. As we have seen, potential models lose their predictability to a certain degree by using experimental input to fix arbitrary constants in the heavy quark potential. One should not disregard potential models completely but they should be used as a guide of what to expect when using NRQCD. Of importance too is that they will be useful in deciding the effect of certain systematic errors present in lattice simulations. In particular to estimate finite volume effects using potential wavefunctions and help correct for the effect of quenching.

The answer to why use NRQCD to study Quarkonium is in two parts. The first part is that the dynamics are well suited to lattice simulations. For example the average size of a Charmonium or Upsilon is about 0.1 to 1 fm so finite volume effects which occur in much lighter mesons will be negligible here. From experimental data the decay of both Charmonium and Upsilon for states above threshold to a pair of heavy-light mesons is small indicating that sea quarks do not have a significant effect in such systems. This means that quenching is not expected to have a significant distortion on the spectrum. In simulations one considers pure

states whereas experimentally the observed states have wavefunctions containing a mixture of decay channels into lighter hadrons as well as the presence of hybrid states. Since most of the spectrum we will consider lies below threshold the first problem will not be significant. Decays into purely light quarks are suppressed by the Zweig rule. As for hybrids these are also suppressed in Quarkonium. The amplitude for emission of a gluon from a quark is  $\approx \alpha_s \approx v$  hence the probability for a hybrid state  $P_{Q\bar{Q}g}$  is  $\mathcal{O}(v^2)$  which is roughly 0.3 for Charmonium and 0.1 for Upsilon. Since the reaction time of a gluon is  $\frac{1}{v}$  times greater than that of a quark this explains why potential models which have a  $Q\bar{Q}$  pair interacting with each other by an instantaneous static potential work so well.

The other reason why NRQCD is more favoured over other theories to solve Quarkonium is the fact that NRQCD is a much more efficient field theory to solve on the lattice. Computationally the evolution of the Greens function is an initial value problem. Using the lowest order form of NRQCD the equation of motion for the Green's function  $G(x', x)$  satisfies

$$\left(iD_t + \frac{D^2}{2M}\right) G(x', x) = \delta_{x', x} \quad (2.41)$$

where  $x = (\mathbf{x}, t)$ . This means the Green's function can be obtained through one sweep of the lattice making the evaluation of the Green's functions very efficient. This is in contrast to the Dirac case where a large matrix needs to be inverted at each time step requiring many iterations. The iteration can also be done to as many time steps as required and does not suffer from the problem of periodic boundary conditions half way across the lattice. This is because in the Dirac case the quark and anti-quark fields are coupled together and as well as having particles travelling forward in time there will also be anti-quarks travelling backwards in time. In NRQCD the quark and anti-quark fields are separated and only the quark or only the anti-quark can propagate.

Other reasons which make Quarkonium an easy system to simulate is that Quarkonium is relatively small so different starting sites on the lattice can be used to propagate the Greens function increasing the statistics. Experimentally the spin-average 1P-1S splitting is independent of the quark mass and is therefore an ideal quantity to set the scale of the simulation. Unlike light quark simulations the correct bare mass can be chosen for the heavy quark case and no extrapolation from unrealistic high quark mass values to their physical ones needs to be done. Lastly because Quarkonium is a two body problem with the same type of quark and anti-quark only the quark or the anti-quark propagator needs to be calculated which is

then combined appropriately to form the required messon. All in all the reasons given above should make Quarkonium an ideal system to study not only to test QCD but also to give us some indications of the type of systematic errors which are involved in lattice simulations and a framework in which these can be corrected for.

## Chapter 3

# Non-Relativistic QCD on the Lattice

### 3.1 Introduction

This chapter explains how NRQCD can be adapted to the lattice. The connection between the relevant operators in the continuum and on the lattice is made and the particular quark Greens function which has been used in the simulation defined. An introduction to tadpole-improved perturbation theory is given and its importance for hyperfine splittings stressed. How meson operators with specific quantum numbers are formed from the individual quark and anti-quark fields is described. Smearing techniques are then introduced in order to improve the signal to noise ratio. Finally it is shown how to extract wavefunctions and the momentum dispersion relation which will be needed to fix the bare quark mass.

### 3.2 Lattice NRQCD Operators

To start with it is best to write down fully the NRQCD lagrangian in the continuum which we intend to discretize. In Euclidean space this is given by

$$\mathcal{L}_{\text{NRQCD}} = \psi^\dagger(x) \left( -D_t + \frac{\mathbf{D}^2}{2M} \right) \psi(x) + \delta\mathcal{L}_{\text{SI}} + \delta\mathcal{L}_{\text{SD}} \quad (3.1)$$

where

$$\delta\mathcal{L}_{\text{SI}} = \frac{1}{8M^3} \psi^\dagger(x) \mathbf{D}^4 \psi(x) - i \frac{g}{8M^2} \psi^\dagger(x) (\mathbf{D} \cdot \mathbf{E} - \mathbf{E} \cdot \mathbf{D}) \psi(x) \quad (3.2)$$

and

$$\delta\mathcal{L}_{\text{SD}} = \frac{g}{8M^2} \psi^\dagger(x) \boldsymbol{\sigma} \cdot (\mathbf{D} \times \mathbf{E} - \mathbf{E} \times \mathbf{D}) \psi(x) + \frac{g}{2M} \psi^\dagger(x) \boldsymbol{\sigma} \cdot \mathbf{B} \psi(x) \quad (3.3)$$

where the effect of the correction terms have on the Quarkonium spectrum is discussed in section (2.6)<sup>1</sup>. To discretize this action it is best to consider first the leading order term. This is a Schrödinger type term and to start with covariant derivatives in the continuum will need to be converted to covariant shift operators on the lattice. From section (1.2) gluonic fields are represented on the lattice by  $U_\mu(x)$  fields defined as

$$U_\mu(x) = e^{i g a A_\mu^L(x)} \quad (3.4)$$

where  $A_\mu^L(x) \rightarrow A_\mu^G(x)$  as the lattice spacing  $a$  goes to zero. Under a gauge transformation  $G(x)$  these  $U_\mu(x)$  fields transform as

$$U_\mu(x) \rightarrow G(x) U_\mu(x) G^{-1}(x+a) \quad (3.5)$$

This is in analogy with the continuum covariant derivative  $D_\mu$  which transforms as  $D_\mu \rightarrow G(x) D_\mu G^{-1}(x)$ . On the lattice we then simply replace

$$D_\mu \psi(x) \rightarrow \Delta_\mu^+ \psi(x) = U_\mu(x) \psi(x+a\hat{\mu}) - \psi(x) \quad (3.6)$$

which is a forward shift operation and for a backwards shift operation

$$\Delta_\mu^- \psi(x) = \psi(x) - U_{x-a\hat{\mu}}^\dagger \psi(x-a\hat{\mu}) \quad (3.7)$$

The symmetric difference can be defined also to be

$$\Delta_\mu^{(+)} = \frac{1}{2} (\Delta_\mu^+ + \Delta_\mu^-) \quad (3.8)$$

and the Laplacian is given by

$$\Delta^{(2)} = \sum_i \Delta_i^{(+)} \Delta_i^{(-)} \quad (3.9)$$

Using the equation of motions for the leading order term in equ (3.1) one ends up with the evolution equation for the quark propagator to be

$$G(\mathbf{x}, t+a; \mathbf{x}_0, t_0) = U_0^\dagger(\mathbf{x}, t) (1 - aH_0) G(\mathbf{x}, t; \mathbf{x}_0, t_0) \quad (3.10)$$

with

$$H_0 = - \sum_j \frac{\Delta_j^{(+)} \Delta_j^{(-)}}{2M a} \quad (3.11)$$

---

<sup>1</sup>from now on  $x$  denotes a vector in Euclidean space-time whereas  $\mathbf{x}$  will denote a three dimensional vector

and  $\mu = 0$  represents the time component in Euclidean space. Transforming this expression for the free field case into momentum space the evolution equation can be written as

$$G(\mathbf{p}, t + a; t_0) = \left( 1 - \sum_i \frac{4 \sin^2 \frac{p_i a}{2}}{2Ma} \right) G(\mathbf{p}, t; t_0) \quad (3.12)$$

For very high momentum there is an instability since at  $\mathbf{p}_i \approx \frac{\pi}{a}$

$$G(\mathbf{p}, t + a; t_0) = \left( 1 - \frac{12}{2Ma} \right) G(\mathbf{p}, t; t_0) \quad (3.13)$$

which will start to blow up for  $Ma < 3$ . To prevent this the evolution equation is replaced by

$$G(\mathbf{x}, t + a; \mathbf{x}_0, t_0) = U_0^1(\mathbf{x}, t) \left( 1 - a \frac{1}{n} H_0 \right)^n G(\mathbf{x}, t; \mathbf{x}_0, t_0) \quad (3.14)$$

which is now stable for  $Ma > \frac{3}{n}$ . The high momentum modes are expected to have little effect on the spectrum of Quarkonium which is determined by much lower momentum modes. The instability from the high momentum modes is just a numerical effect. The extra interactions which will occur to eliminate the instability will be suppressed by  $v^2$  as well as the lattice spacing  $a$ .

Considering the next to leading order in equ (3.2) and equ (3.3) this involves the calculation of the chromo-magnetic and electric fields on the lattice. In the continuum these fields are defined by

$$\mathbf{E}_i(x) = F_{0i}(x) \quad (3.15)$$

$$\mathbf{B}_i(x) = \frac{1}{2} \epsilon_{ijk} F_{jk}(x) \quad (3.16)$$

so we need a lattice equivalent of  $F_{\mu\nu}(x)$ . This is taken to be the cloverleaf term  $F_{\mu\nu}^c(x)$  defined by [25]

$$F_{\mu\nu}^c(x) = -\frac{1}{4a^2} \sum \mathcal{O}(P)$$

where

$$\mathcal{O}(P) = \frac{U^P(x) - (U^P)^\dagger(x)}{2i} - \frac{1}{3} \text{Im} (\text{Tr} (U^P(x))) \quad (3.17)$$

which is hermitian and traceless as in the case of the continuum version. The summation is over all the four plaquettes centred at point  $x$  and in the  $\mu, \nu$  direction.

### 3.3 Lattice spacing errors to Lattice NRQCD operators

Now that the appropriate NRQCD operators on the lattice have been defined it is necessary to identify lattice spacing errors and correct for them. In NRQCD it is not possible to take the lattice spacing explicitly to zero because the continuum is not well defined due to the non-renormalizability of the theory. Therefore a systematic improvement program must exist to reduce the effects of the lattice spacing errors.

Since NRQCD is an improvement program in  $v^2$  the effect of the lattice spacing errors in terms of  $v^2$  will need to be calculated. First consider the correction to the time derivative. Define  $t_\mu$  by

$$t_\mu \psi(x) = \psi(x + a\hat{\mu}) \quad (3.18)$$

where  $\mu = 0, 1, 2, 3$ . In the free field case

$$\Delta_0 \psi(x) = (t_0 - 1) \psi(x) \quad (3.19)$$

and in momentum space this is

$$\begin{aligned} \Delta_0 \sum_p \psi(p) e^{ip \cdot x} &= \sum_p \psi(p) e^{ip \cdot x} (\epsilon^{ip_0 a} - 1) \\ &\approx \sum_p \psi(p) e^{ip \cdot x} \left( ip_0 a - \frac{1}{2} p_0^2 a^2 + \dots \right) \end{aligned} \quad (3.20)$$

The lattice spacing correction in the time direction is of  $\mathcal{O}(p_0 a)$ . If we take the typical value of  $p_0$  to be  $\langle p_0 \rangle \approx K \approx mv^2$  and assume the lattice spacing is of order of the cut off  $a \approx \frac{1}{M}$  the correction term is  $\mathcal{O}(v^2)$ . The same can be done with spatial lattice spacing errors. These errors will appear in the laplacian which occurs in the kinetic energy operator at leading order. Defining the lattice laplacian as

$$\Delta^2 = \sum_i t_i + t_{i,j} - 2 \quad (3.21)$$

and going to momentum space for the free field case gives

$$\begin{aligned} \Delta^2 \sum_p \psi(p) e^{ip \cdot x} &= \sum_p \psi(p) e^{ip \cdot x} (\epsilon^{ip_0 a} + \epsilon^{-ip_0 a} - 2) \\ &\approx \sum_p \psi(p) e^{ip \cdot x} \left( -p_0^2 a^2 + \frac{1}{12} p_i^4 a^4 + \dots \right) \end{aligned} \quad (3.22)$$

There is then an  $\mathcal{O}(p_i^2 a^2)$  error away from the continuum. Again if one has  $a \approx \frac{1}{M}$  and assume the typical momentum  $p_i$  to be  $\langle p_i \rangle \approx mv$  then the correction is  $\mathcal{O}(v^2)$  as in the case of the time derivative. If an action correct to  $\mathcal{O}(v^4)$  in spin-independent terms is required then these errors need to be removed. For the laplacian a corrected version is simply

$$\tilde{\Delta}^2 = \Delta^2 - \frac{a^2}{12} \sum_i (\Delta_i^+ \Delta_i^-)^2 \quad (3.23)$$

When removing the time component lattice spacing error it is not possible to add higher derivatives in time in because this will prevent the evolution equation being an initial value one. Instead the lowest order hamiltonian is redefined as [20]

$$H_0 \rightarrow \bar{H}_0 = H_0 - \frac{a}{4n} H_0^2 \quad (3.24)$$

Other lattice spacing errors will occur for example in the chromo-magnetic and electric fields. This is an  $\mathcal{O}(a^2)$  effect and since these fields come in at  $\mathcal{O}(v^2)$  away from the leading order action they will only need to be corrected for with an action correct to  $\mathcal{O}(v^6)$ . There is also an  $\mathcal{O}(a^2)$  error present in the action for the gluonic gauge fields which is explained and corrected for in detail in [20].

These corrections are only correct at tree level where the fields are considered to be classical quantities. Quantum effects will undoubtedly have an effect and will need to be taken into account. A systematic way to account for the bulk of the radiative corrections is called tadpole-improvement and will be given in section (3.5).

### 3.4 Evolution of the quark Greens function

So far the action for NRQCD in the continuum correct to  $\mathcal{O}(v^4)$  have been derived. The conversion to the lattice of the appropriate operators corrected for lattice spacing errors has also been given. It is now necessary to define an evolution equation from which the quark Greens function can be calculated. For our particular evolution equation for the quark Greens function we define

$$G(\mathbf{x}, 1; \mathbf{x}_0, 0) = \left(1 - \frac{aH_0}{2n}\right)^n U_0^\dagger(\mathbf{x}, 0) \left(1 - \frac{aH_0}{2n}\right)^n \delta_{\mathbf{x}, \mathbf{x}_0} \quad (3.25)$$

and then continue to evolve this using the equation

$$G(\mathbf{x}, t+1; \mathbf{x}_0, t_0) = \left(1 - \frac{aH_0}{2n}\right)^n U_0^\dagger(\mathbf{x}, t) \left(1 - \frac{aH_0}{2n}\right)^n (1 - a\delta H) G(\mathbf{x}, t; \mathbf{x}_0, t_0) \quad (3.26)$$

The kinetic energy operator  $H_G$  is given by equ (3.11) and  $\delta H$  contains the relativistic and lattice spacing corrections defined by

$$\begin{aligned} \delta H = & -\frac{(\Delta^2)^2}{8M^3} + \frac{ig}{8M^2} (\Delta \cdot \mathbf{E} - \mathbf{E} \cdot \Delta) - \\ & \frac{g}{8M^2} \sigma \cdot (\Delta \times \mathbf{E} - \mathbf{E} \times \Delta) - \frac{g}{2M} \sigma \cdot \mathbf{B} + \frac{a^2 \Delta^4}{24M} - \frac{a(\Delta^2)^2}{16nM^2} \end{aligned} \quad (3.27)$$

The first four terms are the familiar relativistic corrections and the last two the lattice spacing corrections for the spatial and time direction. Here  $\Delta^4 = \sum_i (\Delta_i \Delta_{-i})^2$ .

The lowest order kinetic energy operator  $H_0$  will act on the the quark Greens function  $G(\mathbf{x}, t; \mathbf{x}_0, t_0)$  according to

$$\begin{aligned} \Delta^2 G(\mathbf{x}, t; \mathbf{x}_0, t_0) = & \sum_i^3 U_i(\mathbf{x}, t) G(\mathbf{x} + \mathbf{i}, t; \mathbf{x}_0, t_0) + \\ & U_i^\dagger(\mathbf{x} - \mathbf{i}, t) G(\mathbf{x} - \mathbf{i}, t; \mathbf{x}_0, t_0) - 2G(\mathbf{x}, t; \mathbf{x}_0, t_0) \end{aligned} \quad (3.28)$$

For the  $(\Delta^2)^2$  term this is just two of the above successive operations. For the  $\Delta^4$  term the effect on the quark Greens function is found by first considering the free field case

$$\begin{aligned} \sum_i^3 (\Delta_i \Delta_{-i})^2 G(\mathbf{x}, t; \mathbf{x}_0, t_0) = & \sum_i^3 G(\mathbf{x} + 2\mathbf{i}, t; \mathbf{x}_0, t_0) + G(\mathbf{x} - 2\mathbf{i}, t; \mathbf{x}_0, t_0) \\ & - 4G(\mathbf{x} + \mathbf{i}, t; \mathbf{x}_0, t_0) - 4G(\mathbf{x} - \mathbf{i}, t; \mathbf{x}_0, t_0) + 6G(\mathbf{x}, t; \mathbf{x}_0, t_0) \end{aligned} \quad (3.29)$$

and then for the interacting case since we want the quantity  $\psi^\dagger(\mathbf{x}) \Delta^4 \psi(\mathbf{x})$  to be gauge invariant this determines that

$$\begin{aligned} \sum_i^3 (\Delta_i \Delta_{-i})^2 G(\mathbf{x}, t; \mathbf{x}_0, t_0) = & \sum_i^3 U_i(\mathbf{x} + \mathbf{i}, t) U_i(\mathbf{x} + 2\mathbf{i}, t) G(\mathbf{x} + 2\mathbf{i}, t; \mathbf{x}_0, t_0) \\ & - U_i^\dagger(\mathbf{x} - \mathbf{i}, t) U_i^\dagger(\mathbf{x} - 2\mathbf{i}, t) G(\mathbf{x} - 2\mathbf{i}, t; \mathbf{x}_0, t_0) - 4U_i(\mathbf{x} + \mathbf{i}, t) G(\mathbf{x} + \mathbf{i}, t; \mathbf{x}_0, t_0) \\ & - 4U_i^\dagger(\mathbf{x} - \mathbf{i}, t) G(\mathbf{x} - \mathbf{i}, t; \mathbf{x}_0, t_0) - 6G(\mathbf{x}, t; \mathbf{x}_0, t_0) \end{aligned} \quad (3.30)$$

The terms in the evolution equation involving the chromo-electric fields involves the use of the symmetric difference operator equ (3.8). For the spin-independent term the expression evaluated is

$$\sum_i^3 \Delta_i^{+-} (E_i G(\mathbf{x}, t; \mathbf{x}_0, t_0)) - E_i (\Delta_i^{+-} G(\mathbf{x}, t; \mathbf{x}_0, t_0)) \quad (3.31)$$

For the spin-dependent term involving the electric field the expression is

$$\sum_i^3 \sigma_i \epsilon_{ijk} \Delta_j^{+-} (E_k G(\mathbf{x}, t; \mathbf{x}_0, t_0)) - \sum_i^3 \sigma_i c_{ijk} E_j (\Delta_k^{+-} G(\mathbf{x}, t; \mathbf{x}_0, t_0)) \quad (3.32)$$

The term with the chromo-magnetic field is straight forward and is just simply

$$\left( \sum_i \sigma_i B_i \right) G(\mathbf{x}, t; \mathbf{x}_0, t_0) \quad (3.33)$$

with the appropriate matrix multiplication on spin and colour indices.

The form of the evolution is split up into two for computational reasons. The chromo-electric field at time  $t$  for example will involve the use of  $U$  fields at time  $t-a$ ,  $t$  and  $t+a$  and so the chromo electric field at  $t=0$  can not be calculated. Instead the evolution at  $t=0$  is done as follows. First the  $U$  fields at  $t=0$  are read in and the delta function is evolved according to equ (3.25). Next the  $U$  fields at  $t=1$  and  $t=2$  are read in which will allow the evaluation of the chromo-electric field at  $t=1$ . The quark Greens function at  $t=1$  and at subsequent times is then evolved according to equ (3.26). The fact that  $\delta H$  is not used in the first timestep will not effect the masses of the mesons since effective masses are extracted after several timesteps in the evolution equation where the full Hamiltonian has been used. However the normalization of the quark's wavefunction will be effected at  $\mathcal{O}(\delta H)$ .

### 3.5 Improved Perturbation

When comparing NRQCD to low energy QCD or performing the FWT transformation to compute the coupling constants in NRQCD it is done only at tree level. Quantum corrections will need to be estimated and the coupling constants shifted away from their tree level values appropriately. This will rely on perturbation theory to do the calculation. The coefficients of these perturbative corrections are expected to scale as powers of  $\frac{1}{ma}$  for a lattice spacing cut-off  $a$ . Perturbation theory is then expected to hold so long as  $ma > 1$ . However it has been thought for a long time that perturbation in the bare lattice coupling constant at present values of the lattice spacing has a poor convergence series. The origin of this is the presence of tadpole diagrams caused by the lattice version of the gluonic field. The way to overcome this is to use the method of [26]. It was recognised in [26] that the presence of tadpoles will cause the lattice gluonic field in a fixed gauge to fluctuate about a value different from unity. For example in Landau gauge the quantity

$$\langle 1 - \frac{1}{3} \text{Tr} U_\mu \rangle = 0.139 \quad (3.34)$$

is non zero. This in turn suggests that  $\langle U_\mu \rangle$  is significantly different from one which is naively expected if  $\langle A^\mu \rangle = 0$  as in the continuum. The problem arises from the naive connection between lattice and continuum operators where the connection is made by explicitly taking  $a$  to zero. For example it is assumed that

$$U_\mu \rightarrow 1 + ig a A_\mu \quad (3.35)$$

forgetting quantum corrections. When calculating the expectation value of  $U_\mu$  in a fixed gauge there will be terms like  $\langle A_\mu A_\mu \rangle$  which quadratically diverge as  $\frac{1}{a^2}$  and so

$$g^2 a^2 \langle A_\mu A_\mu \rangle \rightarrow \mathcal{O}(g^2) \quad (3.36)$$

producing a large renormalization between the lattice and the continuum. It would then seem appropriate to redefine the  $U_\mu$  fields as

$$U_\mu \rightarrow u_0 (1 + iag A_\mu) \quad (3.37)$$

where the term in parenthesis has a much improved connection with the continuum. The term  $u_0$  is a gauge-invariant number. A gauge invariant expression which we use in our simulation is

$$u_0 = \langle \frac{1}{3} \text{Tr} U^P \rangle^{\dagger} \quad (3.38)$$

This is important when the chromo-magnetic and electric fields are evaluated. This involves the evaluation of the plaquette which contains four  $U_\mu$  fields and tadpole-improving using the above prescription will change the definition of the cloverleaf term according to

$$\begin{aligned} \mathbf{E} &\rightarrow \frac{\mathbf{E}}{u_0^3} \\ \mathbf{B} &\rightarrow \frac{\mathbf{B}}{u_0^3} \end{aligned} \quad (3.39)$$

This increases the strengths of the fields and neglecting tadpole-improvement will severely underestimate spin-dependent splittings. Tadpole-improvement will also effect other operators, for example, the  $(\Delta)^2$  and  $(\Delta)^4$  terms since these have  $U$  fields in as well. Working out explicitly the effect of the term  $(\Delta)^4$  on the quark Greens function there will be a term

$$-4G(\mathbf{x}, t; \mathbf{x}_0, t_0) - 2U^\dagger(\mathbf{x}, t)U(\mathbf{x}, t)G(\mathbf{x}, t; \mathbf{x}_0, t_0) \quad (3.40)$$

After tadpole-improvement this term will become

$$-(4 + \frac{2}{\beta_3}) G(\mathbf{x}, t; \mathbf{x}_0, t_0) \quad (3.41)$$

which is a slight modification on the corresponding term given in equ (3.30). The importance of tadpole-improvement is that removing tadpole contributions which are responsible for the bulk of the radiative corrections means that now it is possible to keep tree-level values for the arbitrary coupling constants.

### 3.6 Meson Correlation functions

Meson operators  $O(x)$  are defined according to

$$O(x) = \chi_A^\dagger(x) \Gamma \psi_Q(x) \quad (3.42)$$

where  $\Gamma$  determines the specific quantum numbers of the meson. Generically the meson correlation function is evaluated by the expression

$$\langle M \rangle = \sum_U \text{Tr} [G(U) \Gamma G^\dagger(U) \Gamma^\dagger] \quad (3.43)$$

The summation is over gauge configurations generated with weight  $e^{-S(U)}$  where  $S(U)$  is the gluonic action. To define each type of meson correlation function requires  $\Gamma$  to be explicitly defined.

We need first to decide on the spectroscopic notation of Quarkonium. Quarkonium states are normally labelled by their spin  $S$ , angular momentum  $L$  and the total angular momentum  $J$  by  $^{2S+1}L_J$ . In QCD as well as NRQCD the total angular momentum  $J$ , parity  $P$  and charge conjugation  $C$  are individually conserved. In Quarkonium  $P = (-1)^{L+1}$  and  $C = (-1)^{L+S}$  and it is possible to use the quantum numbers  $J^{PC}$  instead. From this we can see that states with the same  $J^{PC}$  will mix, for example, the  $^3S_1$  with the  $^3D_1$ . In our simulation we have looked at S,P and D states with different spin orientation for each L. Below are derived the meson operators corresponding to these states.

### 3.7 Meson operators

The most fundamental operator which can be used is the product of the quark and anti-quark fields. To find out the properties of these fields one needs to look first at the action of the quark and anti-quark. The actions for the quark and anti-quark are defined by

$$S = S_Q + S_A =$$

$$\psi_Q^\dagger(x)K_Q(U)\psi_Q(x) + \psi_A^\dagger(x)K_A(U)\psi_A(x) \quad (3.44)$$

where  $K(U)$  is the inverse of the quark or anti-quark Greens function. The quark fields transform under the representation  $\mathbf{3}$  of  $SU(3)$  colour ie  $\psi(x) \rightarrow G(x)\psi(x)$  with  $G(x) = e^{i\Lambda(x)\cdot A(x)}$ .  $K_Q$  transforms as  $K_Q(U) \rightarrow G(x)K_Q G^\dagger(x)$  for gauge invariance. Alternatively anti-quarks transform as the complex conjugate  $\bar{\mathbf{3}}$  of  $SU(3)$  and so  $K_A(U)$  transforms as  $K_A(U) \rightarrow G^*(x)K_A(U)G^T$ . This in turn suggests that  $K_A(U^*) = K_Q(U)$ . It is then possible to write the lagrangian as

$$S = S_Q + S_A =$$

$$\psi_Q^\dagger(x)K_Q(U)\psi_Q(x) + \psi_A^\dagger(x)(K_Q(U^*))\psi_A(x) \quad (3.45)$$

It is convenient at this point to redefine the anti-quark fields  $\psi_A(x)$  as  $\tilde{\chi}_A^*(x)$  so  $S_A = -\tilde{\chi}_A^\dagger(x)K_Q^\dagger\tilde{\chi}_A(x)$ . The field  $\tilde{\chi}_A(x)$  now creates an anti-particle which is the familiar representation in the dirac theory. The hermitian conjugate is taken in colour space at the moment and if we have dirac matrices in our action then another redefinition of the anti-quark fields will be necessary if one wants to take the hermitian conjugate in spin space as well. For example with a  $\sigma\cdot\mathbf{B}$  term in the action  $K_A(U) = \sigma_2 K_Q^*(U)\sigma_2$  with the complex conjugation now in colour as well as spin space since

$$-g\sigma\cdot\mathbf{B}^* = \sigma_2(g\sigma\cdot\mathbf{B})^*\sigma_2 \quad (3.46)$$

This is the  $U(1)$  case where  $\mathbf{B}^* = \mathbf{B}$  and the difference is then only due to the sign of the charge  $g$ . Rewriting the anti-quark action as

$$S_A = -\tilde{\chi}_A^T(x)i\sigma_2\sigma_2K_A(U)\sigma_2i\sigma_2\tilde{\chi}_A^*(x) \quad (3.47)$$

and defining  $\chi_A^*(x) = i\sigma_2\tilde{\chi}_A^*(x)$  so that  $\chi_A^T(x) = -\tilde{\chi}_A^T(x)i\sigma_2$  the anti-quark action is now

$$S_A = \chi_A^T(x)(K_Q(U))^*\chi_A^*(x) = -\chi_A^\dagger(x)K_Q^\dagger\chi_A(x) \quad (3.48)$$

With the action for both the quark and anti-quark now defined the Greens functions can be written down in terms of these redefined fields as

$$G_A^{\alpha\beta} = (G_Q^{\alpha\beta})^* = \langle 0|\chi_A^{*\alpha}\chi_A^\beta|0\rangle \quad (3.49)$$

$$G_Q^{\alpha\beta} = \langle 0|\psi_Q^\alpha\psi_Q^{*\beta}|0\rangle \quad (3.50)$$

where  $\alpha$  and  $\beta$  are generic indices for the colour and spin components. Under charge conjugation  $\psi_Q(x) \leftrightarrow \psi_A(x)$  and so from this

$$\chi_A^*(x) \rightarrow i\sigma_2\psi_Q(x)$$

$$\psi_Q(x) \rightarrow \psi_A(x) = -i\sigma_2\chi_A^*(x) \quad (3.51)$$

After introducing the quark and anti-quark fields it is now possible to show how these can be formed to produce the meson operators with specific quantum numbers. In particular it is now possible to write down explicitly what  $\Gamma$  should be in equ (3.42). The most basic meson operator is when  $\Gamma$  is equal to one.

$$\mathcal{O}(\mathbf{x}, t) = \chi_A^\dagger(\mathbf{x}, t)\psi_Q(\mathbf{x}, t) \quad (3.52)$$

Under parity the quark and anti-quark will transform as

$$\psi_Q(\mathbf{x}, t) \rightarrow \psi_Q(\mathbf{x}, t)$$

$$\psi_A(\mathbf{x}, t) \rightarrow -\psi_A(\mathbf{x}, t) \quad (3.53)$$

The minus sign is because of the opposite intrinsic parity. Then  $\chi_A^\dagger(\mathbf{x}, t)\psi_Q(\mathbf{x}, t)$  has negative parity. Under charge conjugation the individual fields will transform as equ (3.51) hence

$$\chi_A^\dagger(\mathbf{x}, t)\psi_Q(\mathbf{x}, t) = \sum_{\alpha\beta} i\sigma_2^{\alpha\beta} \psi_A^\beta(\mathbf{x}, t)\psi_Q^\alpha(\mathbf{x}, t) \quad (3.54)$$

under charge conjugation goes to

$$\begin{aligned} \sum_{\alpha\beta} i\sigma_2^{\alpha\beta} \psi_Q^\beta(\mathbf{x}, t)\psi_A^\alpha(\mathbf{x}, t) &= - \sum_{\alpha\beta} \psi_A^\alpha(\mathbf{x}, t)i\sigma_2^{\alpha\beta} \psi_Q^\beta(\mathbf{x}, t) = \\ \sum_{\alpha\beta} i\sigma_2^{\beta\alpha} \psi_A^\alpha(\mathbf{x}, t)\psi_Q^\beta(\mathbf{x}, t) &= \sum_{\beta} \chi_A^{\beta\dagger}(\mathbf{x}, t)\psi_Q^\beta(\mathbf{x}, t) = \chi_A^\dagger(\mathbf{x}, t)\psi_Q(\mathbf{x}, t) \end{aligned} \quad (3.55)$$

This particular operator has then charge conjugation number  $C = +1$ , parity  $P = -1$  and since it is a scalar there is no angular momentum associated with it and hence  $J = 0$ . We can then identify this meson operator with the  $^1S_0$  state. Next consider

$$\mathcal{O}(\mathbf{x}, t) = \chi_A^\dagger(\mathbf{x}, t)\sigma_i\psi_Q(\mathbf{x}, t) \quad (3.56)$$

This still has  $P = -1$  and going through the same process as above it is straight forward to show it has  $C = -1$ . However it now has  $J = 1$  in that it transforms like

Meson ${}^{2S+1}L_J (J^{PC})$	$\chi_A^\dagger(\mathbf{x})\Gamma\psi_Q(\mathbf{x})$
${}^1S_0 (0^{-+})$	$\chi_A^\dagger(\mathbf{x})\psi_Q(\mathbf{x})$
${}^3S_1 (1^{--})$	$\chi_A^\dagger(\mathbf{x})\sigma_i\psi_Q(\mathbf{x})$
${}^1P_1 (1^{+-})$	$\chi_A^\dagger(\mathbf{x})\bar{\Delta}_i\psi_Q(\mathbf{x})$
${}^3P_0 (0^{++})$	$\chi_A^\dagger(\mathbf{x})\left(\sum_i\bar{\Delta}_i\sigma_i\right)\psi_Q(\mathbf{x})$
${}^3P_1 (1^{++})$	$\chi_A^\dagger(\mathbf{x})\left(\bar{\Delta}_i\sigma_j-\bar{\Delta}_j\sigma_i\right)\psi_Q(\mathbf{x})$
${}^3P_2 (2^{++})$	$\chi_A^\dagger(\mathbf{x})\left(\bar{\Delta}_i\sigma_i-\bar{\Delta}_j\sigma_j\right)\psi_Q(\mathbf{x})$ $\chi_A^\dagger(\mathbf{x})\left(\bar{\Delta}_i\sigma_j+\bar{\Delta}_j\sigma_i\right)\psi_Q(\mathbf{x})$ ( $i \neq j$ )
${}^1D_2 (2^{-+})$	$\chi_A^\dagger(\mathbf{x})\left(\bar{\Delta}_{ii}-\bar{\Delta}_{jj}\right)\psi_Q(\mathbf{x})$ $\chi_A^\dagger(\mathbf{x})\bar{\Delta}_{ij}\psi_Q(\mathbf{x})$ ( $i \neq j$ )

Table 3.1: Meson Operators

a vector and has three independent directions. We can associate this operator with the  ${}^3S_1$  state.

For the rest of the states we have considered in the simulation their operators are listed below in table (3.7) [28], where we have defined

$$\chi_A^\dagger(\mathbf{x}, t)\bar{\Delta}_i\psi_Q(\mathbf{x}, t) = \tag{3.57}$$

$$\left(\frac{1}{4}(\Delta_i+\Delta_{-i})\chi_A(\mathbf{x}, t)\right)^\dagger\psi_Q(\mathbf{x}, t)-\chi_A^\dagger(\mathbf{x}, t)\left(\frac{1}{4}(\Delta_i+\Delta_{-i})\psi_Q(\mathbf{x}, t)\right)$$

Considering next the operator  $\chi_A^\dagger(\mathbf{x}, t)\bar{\Delta}_i\psi_Q(\mathbf{x}, t)$  this has no  $\sigma_i$  operators in so  $S=0$  and  $J=L$ . Since the derivative  $\bar{\Delta}_i$  transforms like a spatial vector with three

independent indices,  $J=1$ . To work out the C and P numbers it is necessary to work out explicitly the effect of the derivative  $\vec{\Delta}_i$  on the fields. In the simulation the gauge fields are fixed to coulomb gauge and so the meson operators will not be gauge invariant. For convenience it is possible to fix all the spatial  $U_\mu$  fields in the meson operators to unity. Doing this can not effect the quantum numbers of the meson which must be gauge invariant since they are physical observables. From equ (3.57)

$$\chi_A^\dagger(\mathbf{x}, t) \vec{\Delta}_i \psi_Q(\mathbf{x}, t) = \quad (3.58)$$

$$\left( \frac{1}{4} (\chi_A^\dagger(\mathbf{x} + \mathbf{i}, t) - \chi_A^\dagger(\mathbf{x} - \mathbf{i}, t)) \right) \psi_Q(\mathbf{x}, t) - \chi_A^\dagger(\mathbf{x}, t) \left( \frac{1}{4} (\psi_Q(\mathbf{x} + \mathbf{i}, t) - \psi_Q(\mathbf{x} - \mathbf{i}, t)) \right)$$

Reflecting along the x axis for the parity operation

$$\chi_A^\dagger(\mathbf{x} + \mathbf{i}, t) \rightarrow \chi_A^\dagger(\mathbf{x} - \mathbf{i}, t) \quad (3.59)$$

so that equ (3.58) becomes under a parity operation

$$\begin{aligned} & \left( \frac{1}{4} (\chi_A^\dagger(\mathbf{x} - \mathbf{i}, t) - \chi_A^\dagger(\mathbf{x} + \mathbf{i}, t)) \right) \psi_Q(\mathbf{x}, t) - \chi_A^\dagger(\mathbf{x}, t) \left( \frac{1}{4} (\psi_Q(\mathbf{x} + \mathbf{i}, t) - \psi_Q(\mathbf{x} - \mathbf{i}, t)) \right) \\ & = -\chi_A^\dagger(\mathbf{x}, t) \vec{\Delta}_i \psi_Q(\mathbf{x}, t) \end{aligned} \quad (3.60)$$

Which makes  $P = +1$  (not forgetting the intrinsic parity). For charge conjugation we know from equ (3.51) that

$$\chi_A^\dagger(\mathbf{x} + \mathbf{i}, t) \psi_Q(\mathbf{x}, t) \rightarrow \chi_A^\dagger(\mathbf{x}, t) \psi_Q(\mathbf{x} + \mathbf{i}, t) \quad (3.61)$$

so then

$$\begin{aligned} & \chi_A^\dagger(\mathbf{x}, t) \vec{\Delta}_i \psi_Q(\mathbf{x}, t) \rightarrow \\ & \chi_A^\dagger(\mathbf{x}, t) \left( \frac{1}{4} (\psi_Q(\mathbf{x} + \mathbf{i}, t) - \psi_Q(\mathbf{x} - \mathbf{i}, t)) \right) - \left( \frac{1}{4} (\chi_A^\dagger(\mathbf{x} + \mathbf{i}, t) - \chi_A^\dagger(\mathbf{x} - \mathbf{i}, t)) \right) \psi_Q(\mathbf{x}, t) \\ & = -\chi_A^\dagger(\mathbf{x}, t) \vec{\Delta}_i \psi_Q(\mathbf{x}, t) \end{aligned} \quad (3.62)$$

which shows that  $C = -1$ . We can then identify this operator to belong to the  $^1P_1$  state with quantum numbers  $1^{+-}$ .

Moving on to the next set of operators this involves the combination of spin  $S = 1$  with  $L = 1$ . In terms of group theory the multiplication of  $\underline{1} \otimes \underline{1}$  where  $\underline{1}$  transforms in the fundamental representation of  $SO(3)$  is

$$\underline{1} \otimes \underline{1} \rightarrow \underline{1} \oplus \underline{3} \oplus \underline{5} \quad (3.63)$$

where the representation  $\underline{1}$  and  $\underline{5}$  are symmetric and  $\underline{3}$  is anti-symmetric. Consider the operator  $\sum_i \chi_A^\dagger(\mathbf{x}, t) \vec{\Delta}_i \cdot \sigma_i \psi_Q(\mathbf{x}, t)$ . This is symmetric and is a scalar since it is a dot product of two vectors. From the above discussion we now know that  $\chi_A^\dagger(\mathbf{x}, t) (\vec{\Delta}_i \cdot \sigma_i) \psi_Q(\mathbf{x}, t)$  has  $C=+1$  and  $P=+1$  and we can then associate this operator with the  ${}^3P_0$  state with quantum numbers  $0^{++}$ . As far as the operator  $\chi_A^\dagger(\mathbf{x}, t) (\vec{\Delta}_i \cdot \sigma_j - \vec{\Delta}_j \cdot \sigma_i) \psi_Q(\mathbf{x}, t)$  is concerned this is a vector product of the two operators  $\vec{\Delta}_i$  and  $\sigma_i$  and so is anti-symmetric and transforms like a three vector. This is the operator for the state  ${}^3P_1$  with quantum numbers  $1^{++}$ . For the operators of the  ${}^3P_2$  these split up into two different representations on the lattice.  $\chi_A^\dagger(\mathbf{x}, t) (\vec{\Delta}_i \cdot \sigma_i - \vec{\Delta}_j \cdot \sigma_j) \psi_Q(\mathbf{x}, t)$  has two independent degrees of freedom and belongs to the E rep. The  $\chi_A^\dagger(\mathbf{x}, t) (\vec{\Delta}_i \cdot \sigma_j + \vec{\Delta}_j \cdot \sigma_i) \psi_Q(\mathbf{x}, t)$  operator has three independent degrees of freedom and belongs to the T rep. Both operators are symmetric and so represent the  ${}^3P_2$  state with quantum numbers  $2^{++}$ . For the  ${}^1D_2$  a similar thing happens and the operators split up into two reps the E and T. It is straight forward to show they correspond to states with quantum numbers  $2^{-+}$ .

### 3.8 Coding up Meson Correlators

In the previous sections we have shown how meson operators can be formed using quark and anti-quark fields combined appropriately. Discussed also was the evolution of the quark (or equivalently the anti-quark) Greens function with time from which it is straight forward to compute the evolution of the meson correlation function. It will now be shown how this is done numerically for the states we want to consider.

For a meson operator  $O(x) = \chi_A^\dagger(x) \Gamma \psi_Q(x)$  we can represent the meson correlation function as

$$M(t; t_0) = \sum_{\mathbf{x}} \langle 0 | \chi_A^\dagger(\mathbf{x}, t) \Gamma \psi_Q(\mathbf{x}, t) \psi_Q^\dagger(\mathbf{x}_0, t_0) \Gamma^\dagger \chi_A(\mathbf{x}_0, t_0) | 0 \rangle \quad (3.64)$$

where the sum over  $\mathbf{x}$  ensures that the meson has zero momentum. The sum over spin and colour indices have not been made explicit yet.

Consider first the  ${}^1S_0$  state where  $\Gamma = 1$ .

$$M(t; t_0) = \sum_{\alpha\beta} \langle 0 | \chi_A^{\alpha\dagger}(\mathbf{x}, t) \psi_Q^\alpha(\mathbf{x}, t) \psi_Q^{\beta*}(\mathbf{x}_0, t_0) \chi_A^\beta(\mathbf{x}_0, t_0) | 0 \rangle \quad (3.65)$$

where  $\alpha$  and  $\beta$  are summations on the spins and colour indices. It is possible to factorize out the quark and anti-quark fields (Wicks theorem). Using the definition

of the quarks Greens function as

$$G_Q^{\alpha\beta}(\mathbf{x}, t; \mathbf{x}_0, t_0) = \langle 0 | \psi_Q^\alpha(\mathbf{x}, t) \psi_Q^{*\beta}(\mathbf{x}_0, t_0) | 0 \rangle \quad (3.66)$$

and the anti-quark Greens function as

$$G_A^{\alpha\beta}(\mathbf{x}, t; \mathbf{x}_0, t_0) = G_Q^{*\alpha\beta}(\mathbf{x}, t; \mathbf{x}_0, t_0) = \langle 0 | \chi_A^{*\alpha}(\mathbf{x}, t) \chi_A^\beta(\mathbf{x}_0, t_0) | 0 \rangle \quad (3.67)$$

the meson correlation function for the  $^1S_0$  state becomes

$$\begin{aligned} M(t; t_0) &= \sum_{\alpha\beta} G_Q^{*\alpha\beta}(\mathbf{x}, t; \mathbf{x}_0, t_0) G_Q^{\alpha\beta}(\mathbf{x}, t; \mathbf{x}_0, t_0) = \\ &= \sum_{\mathbf{x}} \text{Tr} (G^\dagger(\mathbf{x}, t; \mathbf{x}_0, t_0) G(\mathbf{x}, t; \mathbf{x}_0, t_0)) \end{aligned} \quad (3.68)$$

The trace is over spin and colour degrees of freedom which are averaged over in the simulation to increase the statistics. The next state of interest is the  $^3S_1$ . Here for  $\Gamma$  we use the matrices  $\sigma_+$ ,  $\sigma_-$  and  $\sigma_3$  where

$$\begin{aligned} \sigma_+ &= \frac{1}{\sqrt{2}} (\sigma_1 + i\sigma_2) \\ \sigma_- &= \frac{1}{\sqrt{2}} (\sigma_1 - i\sigma_2) \end{aligned} \quad (3.69)$$

Hence

$$\sigma_+ = \begin{pmatrix} 0 & 1 \\ 0 & 0 \end{pmatrix} \quad \sigma_- = \begin{pmatrix} 0 & 0 \\ 1 & 0 \end{pmatrix} \quad \sigma_3 = \begin{pmatrix} 1 & 0 \\ 0 & -1 \end{pmatrix} \quad (3.70)$$

The meson correlation function can be expressed as

$$M(t; t_0) = \sum_{\alpha\beta\gamma\delta} \langle 0 | \chi_A^{*\alpha}(\mathbf{x}, t) \sigma_j^{\alpha\beta} \psi_Q^\beta(\mathbf{x}, t) \psi_Q^{*\delta}(\mathbf{x}_0, t_0) \sigma_j^{\delta\gamma} \chi_A^\gamma(\mathbf{x}_0, t_0) | 0 \rangle \quad (3.71)$$

where the summation on the spin indices have been made explicit. For  $j = +$  this is simply

$$M_+(t; t_0) = \sum_{\mathbf{x}} G^{*22}(\mathbf{x}, t; \mathbf{x}_0, t_0) G^{11}(\mathbf{x}, t; \mathbf{x}_0, t_0) \quad (3.72)$$

for  $j = -$

$$M_-(t; t_0) = \sum_{\mathbf{x}} G^{*11}(\mathbf{x}, t; \mathbf{x}_0, t_0) G^{22}(\mathbf{x}, t; \mathbf{x}_0, t_0) \quad (3.73)$$

and for  $j = 3$  this works out to be

$$M_3(t; t_0) = \sum_{\mathbf{x}} G^{*11}(\mathbf{x}, t; \mathbf{x}_0, t_0) G^{11}(\mathbf{x}, t; \mathbf{x}_0, t_0) -$$

$$\begin{aligned} \sum_{\mathbf{x}} G^{*21}(\mathbf{x}, t; \mathbf{x}_0, t_0) G^{21}(\mathbf{x}, t; \mathbf{x}_0, t_0) - G^{*12}(\mathbf{x}, t; \mathbf{x}_0, t_0) G^{12}(\mathbf{x}, t; \mathbf{x}_0, t_0) \\ + G^{*22}(\mathbf{x}, t; \mathbf{x}_0, t_0) G^{22}(\mathbf{x}, t; \mathbf{x}_0, t_0) \end{aligned} \quad (3.74)$$

An average over colour indices as well as spin polarizations is taken for increased statistics.

For the  $^1P_1$  state this involves a covariant derivative but because we fix to the coulomb gauge in the simulation this can be represented by simple difference operators. The meson correlation function then becomes suppressing spin and colour indices

$$\begin{aligned} M(t; t_0) = \sum_{\mathbf{x}} \langle 0 | \chi_A^\dagger(\mathbf{x}, t) \overline{\Delta}_i \psi_Q(\mathbf{x}, t) \psi_A^\dagger(\mathbf{x}_0, t_0) \overline{\Delta}_i \chi_A(\mathbf{x}_0, t_0) | 0 \rangle = \\ \sum_{\mathbf{x}} \langle 0 | ((\chi_A^\dagger(\mathbf{x} + \mathbf{i}, t) - \chi_A^\dagger(\mathbf{x} - \mathbf{i}, t)) \psi_Q(\mathbf{x}, t) - \\ \chi_A^\dagger(\mathbf{x}, t) (\psi_Q(\mathbf{x} + \mathbf{i}, t) - \psi_Q(\mathbf{x} - \mathbf{i}, t))) (\psi_Q^\dagger(\mathbf{x}_0, t_0) ((\chi_A(\mathbf{x}_0 + \mathbf{i}, t_0) - \chi_A(\mathbf{x}_0 - \mathbf{i}, t_0)) \\ - (\psi_Q^\dagger(\mathbf{x}_0 + \mathbf{i}, t_0) - \psi_Q^\dagger(\mathbf{x}_0 - \mathbf{i}, t_0)) \chi_A(\mathbf{x}_0, t_0)) | 0 \rangle \end{aligned} \quad (3.75)$$

Multiplying this out would involve 16 terms and we need to look for some simplification. Since we are summing over the final position  $\mathbf{x}$  of the fields it is possible to replace part of the operator at the sink

$$-\chi_A^\dagger(\mathbf{x}, t) (\psi_Q(\mathbf{x} + \mathbf{i}, t) - \psi_Q(\mathbf{x} - \mathbf{i}, t)) \quad (3.76)$$

with

$$-(\chi_A^\dagger(\mathbf{x} + \mathbf{i}, t) - \chi_A^\dagger(\mathbf{x} - \mathbf{i}, t)) \psi_Q(\mathbf{x}, t) \quad (3.77)$$

Next if the first term at the source is multiplied out there will be a term

$$\begin{aligned} -\chi_A^\dagger(\mathbf{x} - \mathbf{i}, t) \psi_Q(\mathbf{x}, t) \psi_Q^\dagger(\mathbf{x}_0, t_0) \chi_A(\mathbf{x}_0 + \mathbf{i}, t_0) = \\ \sum_{\mathbf{x}\alpha\beta} G^{*\alpha\beta}(\mathbf{x} - \mathbf{i}, t; \mathbf{x}_0 + \mathbf{i}, t_0) G^{\alpha\beta}(\mathbf{x}, t; \mathbf{x}_0, t_0) \end{aligned} \quad (3.78)$$

and similarly multiplying out the third term at the source will give a term

$$\begin{aligned} -\chi_A^\dagger(\mathbf{x} + \mathbf{i}, t) \psi_Q(\mathbf{x}, t) \psi_Q^\dagger(\mathbf{x}_0 + \mathbf{i}, t_0) \chi_A(\mathbf{x}_0, t_0) = \\ \sum_{\mathbf{x}\alpha\beta} G^{*\alpha\beta}(\mathbf{x} + \mathbf{i}, t; \mathbf{x}_0, t_0) G^{\alpha\beta}(\mathbf{x}, t; \mathbf{x}_0 + \mathbf{i}, t_0) \end{aligned}$$

$$= \sum_{\alpha\beta} G^{\alpha\beta}(\mathbf{x}, t; \mathbf{x}_0, t_0) G^{*\alpha\beta}(\mathbf{x} - \mathbf{i}, t; \mathbf{x}_0 + \mathbf{i}, t_0) \quad (3.79)$$

These two terms equ (3.79) and equ (3.78) are complex conjugates of each other so instead of evaluating both terms it is better just to take twice the real part of one of them. Similarly if we do this for all terms we will find that equ (3.75) reduces to

$$\begin{aligned} \text{Real} \sum_{\mathbf{x}} < 0 | (\chi_A^\dagger(\mathbf{x} + \mathbf{i}, t) - \chi_A^\dagger(\mathbf{x} - \mathbf{i}, t)) \psi_Q(\mathbf{x}, t) \psi_Q^\dagger(\mathbf{x}_0, t_0) (\chi_A(\mathbf{x}_0 + \mathbf{i}, t_0) \\ - \chi_A(\mathbf{x}_0 - \mathbf{i}, t_0)) | 0 > = \text{Real} \sum_{\alpha\beta} G^{\alpha\beta}(\mathbf{x}, t; \mathbf{x}_0, t_0) G^{*\alpha\beta}(\mathbf{x} + \mathbf{i}, t; \mathbf{x}_0 + \mathbf{i}, t_0) \\ - G^{\alpha\beta}(\mathbf{x}, t; \mathbf{x}_0, t_0) G^{*\alpha\beta}(\mathbf{x} + \mathbf{i}, t; \mathbf{x}_0 - \mathbf{i}, t_0) - G^{\alpha\beta}(\mathbf{x}, t; \mathbf{x}_0, t_0) G^{*\alpha\beta}(\mathbf{x} - \mathbf{i}, t; \mathbf{x}_0 + \mathbf{i}, t_0) \\ + G^{\alpha\beta}(\mathbf{x}, t; \mathbf{x}_0, t_0) G^{*\alpha\beta}(\mathbf{x} - \mathbf{i}, t; \mathbf{x}_0 - \mathbf{i}, t_0) \end{aligned} \quad (3.80)$$

Again the summation is over spin and colour indices for increased statistics and the average is also taken over the different angular momentum polarization directions.

For the meson correlators belonging to the  $^3P$  states it is convenient to define

$$\begin{aligned} M(t, t_0)_{\{ij\}\{ij\}} = \\ \sum_{\mathbf{x}} < 0 | \chi_A^\dagger(\mathbf{x}, t) \vec{\Delta}_j \sigma_i \psi_Q(\mathbf{x}, t) \psi_Q^\dagger(\mathbf{x}_0, t_0) \vec{\Delta}_i \sigma_j \chi_A(\mathbf{x}_0, t_0) | 0 > \end{aligned} \quad (3.81)$$

from which the  $^3P$  correlators can be expressed as

$$M_{^3P_0} = \sum_{ij} M_{\{ii\}\{jj\}} \quad (3.82)$$

$$M_{^3P_1} = \sum_{i,j,i \neq j} M_{\{ij\}\{ij\}} - M_{\{ji\}\{ij\}} \quad (3.83)$$

$$M_{^3P_{2,0}} = \sum_{ij} M_{\{ii\}\{ii\}} - M_{\{jj\}\{ii\}} \quad (3.84)$$

$$M_{^3P_{2T}} = \sum_{i,j,i \neq j} M_{\{ij\}\{ij\}} + M_{\{ji\}\{ij\}} \quad (3.85)$$

The evaluation of these correlators then essentially just involves evaluating equ (3.81). In equ (3.81) the derivative  $\vec{\Delta}_j$  can be replaced by a symmetric difference operator just as in equ (3.80) reducing the number of terms. Summing over spin indices is no different than in the case of the  $^3S_1$  correlator except that here there are now a few more terms to deal with because of the derivative.

Lastly we need to evaluate the  ${}^1D_2$  meson correlator. In the simulation we have only considered the operators corresponding to the T rep. That is

$$M(t; t_0) = \sum_{\mathbf{x}} \langle 0 | \chi_A^\dagger(\mathbf{x}, t) \bar{\Delta}_i \bar{\Delta}_j \psi_Q(\mathbf{x}, t) \psi_Q^\dagger(\mathbf{x}_0, t_0) \bar{\Delta}_i \bar{\Delta}_j \chi_A(\mathbf{x}_0, t_0) | 0 \rangle \quad (3.86)$$

where to sum over polarization directions a sum over  $i$  and  $j$  is done for  $i \neq j$ . The  ${}^1D_2$  operator is

$$\chi_A^\dagger(\mathbf{x}, t) \bar{\Delta}_j \bar{\Delta}_i \psi_Q(\mathbf{x}, t) = \quad (3.87)$$

$$(\chi_A^\dagger(\mathbf{x} + \mathbf{i} + \mathbf{j}, t) - \chi_A^\dagger(\mathbf{x} + \mathbf{i} - \mathbf{j}, t) - \chi_A^\dagger(\mathbf{x} - \mathbf{i} + \mathbf{j}, t) + \chi_A^\dagger(\mathbf{x} - \mathbf{i} - \mathbf{j}, t)) \psi_Q(\mathbf{x}, t)$$

and so in principle the  ${}^1D_2$  correlator involves 16 terms. In practice we do not do this but instead use smeared operators where for example the terms in parenthesis are replaced by an appropriate smearing wavefunction. More will be said of this in the next section.

To sum up an outline has been given on how meson correlation functions can be evaluated numerically. First by deriving meson operators with specific quantum numbers and then evolving the meson correlation function using the basic evolution equation of the quark Greens function. One last piece of work which needs to be done is to introduce the idea of smeared operators which can considerably help the numerical procedure. This will now be explained in the next section.

### 3.9 Smeared Operators

In Lattice QCD simulations effective masses are extracted from the asymptotic fall off of the meson correlation function equ (1.35). For this to be the case in principle one would like to take the time to infinity. In practice this is not possible because not only is there a restriction on the size of the lattice in the time direction but also noise will tend to dominate the signal before the asymptotic behaviour occurs. In simulations the noise is dominated by the meson which has the lowest possible ground state energy. [19]. For our case this will be the  ${}^1S_0$  state and the ratio of signal to noise for a particular state with a mass above that of the  ${}^1S_0$  is

$$\frac{\text{noise}}{\text{signal}} \approx e^{(M_{state} - M_{{}^1S_0})t} \quad (3.88)$$

which will grow exponentially with time. To increase the numerical accuracy of the simulation the signal needs to be extracted at earlier times where noise has not started to dominate. To do this it is necessary to use smeared operators. Previously

only local operators have been considered where for example in the  $^1S_0$  case the quark and anti-quark started from the same point on the lattice. Similarly in the case of the  $^1P_1$  state the anti-quark was displaced by a minimal amount of one lattice spacing relative to the quark to project out the required angular momentum. In smearing the quark or anti-quark is smeared over the whole of the lattice relative to the anti-quark or quark with an appropriate weighting function. For our smearing function we have used hydrogen type wavefunctions from solving a  $\frac{1}{r}$  potential.

To put it on a more formal basis our meson correlation function is

$$M(t; t_0) = \sum_{\mathbf{x}} \langle 0 | \chi_A^\dagger(\mathbf{x}, t) \Gamma \psi_Q(\mathbf{x}, t) \psi_Q^\dagger(\mathbf{x}_0, t_0) \Gamma^\dagger \chi_A(\mathbf{x}_0, t_0) | 0 \rangle \quad (3.89)$$

and to smear for example the anti-quarks the replacement

$$\chi_A(\mathbf{x}_0, t_0) \rightarrow \tilde{\chi}_A(\mathbf{x}_0, t_0) = \sum_{\mathbf{z}} S(\mathbf{z} - \mathbf{x}_0) \chi_A(\mathbf{z}, t_0) \quad (3.90)$$

is made where  $S(\mathbf{z} - \mathbf{x}_0)$  is the appropriate wavefunction for that meson state. Smearing is possible either at the source or at the sink or both. A general expression for our smeared meson correlator is

$$M(t; t_0) = \sum_{\mathbf{x}, \mathbf{y}, \mathbf{z}} S(\mathbf{y} - \mathbf{x}) \langle 0 | \chi_A^\dagger(\mathbf{y}, t) \Gamma \psi_Q(\mathbf{x}, t) \chi_A^\dagger(\mathbf{z}, t_0) \Gamma^\dagger \psi_Q(\mathbf{x}_0, t_0) S(\mathbf{z} - \mathbf{x}_0) | 0 \rangle \quad (3.91)$$

with smearing at both the source and the sink.

To implement smearing at the source numerically, it is known that at  $t=0$

$$\langle 0 | \chi_A^\dagger(\mathbf{y}) \chi_A(\mathbf{x}_0) | 0 \rangle = \delta_{\mathbf{y}, \mathbf{x}_0} \quad (3.92)$$

and so

$$\langle 0 | \chi_A^\dagger(\mathbf{y}) \tilde{\chi}_A(\mathbf{x}_0) | 0 \rangle = \sum_{\mathbf{z}} \langle 0 | \chi_A^\dagger(\mathbf{y}) \chi_A(\mathbf{z}) | 0 \rangle S(\mathbf{z} - \mathbf{x}_0) = \sum_{\mathbf{z}} \delta_{\mathbf{z}, \mathbf{y}} S(\mathbf{z} - \mathbf{x}_0) = S(\mathbf{y} - \mathbf{x}_0) \quad (3.93)$$

Therefore instead of starting off with a delta function in the evolution this can be simply replaced by the function  $S(\mathbf{y} - \mathbf{x}_0)$  over the whole of the lattice. For smearing at the sink this involves the evaluation of a convolution and to evaluate this it is best to transform the anti-quark Greens function firstly into momentum space. Defining

$$G_A(\mathbf{x}, t; \mathbf{x}_0, t_0) = \frac{1}{\sqrt{N}} \sum_{\mathbf{p}} G_A(\mathbf{p}, t; t_0) e^{-i\mathbf{p} \cdot (\mathbf{x} - \mathbf{x}_0)} \quad (3.94)$$

the final smeared meson correlation function is

$$M(t; t_0) = (N)^{\frac{3}{2}} \sum_{\mathbf{p}} S(\mathbf{p}) \Gamma G_Q(\mathbf{p}, t; t_0) \Gamma^\dagger \tilde{G}_A(\mathbf{p}, t; t_0) \quad (3.95)$$

where  $\tilde{G}_A(\mathbf{p}, t; t_0)$  represents the anti-quark Greens function smeared at the source. The fourier transforms can be performed using a Fast Fourier Transform routine [27].

The solutions to the wavefunctions for a  $\frac{1}{r}$  potential are known exactly and it is relatively straight forward to substitute local for smeared operators. The following substitutions have been made to the various meson operators. For the  $^1S_0$  the replacement

$$\chi_A^\dagger(\mathbf{x}_0, t_0) \psi_Q(\mathbf{x}_0, t_0) \rightarrow \left( \sum_{\mathbf{z}} \chi_A^\dagger(\mathbf{z}, t_0) e^{-\frac{|\mathbf{z}-\mathbf{x}_0|}{r_0}} \right) \psi_Q(\mathbf{x}_0, t_0) \quad (3.96)$$

is made.  $r_0$  is a free parameter which can be adjusted comparing to wavefunctions coming out of NRQCD simulations of heavy-heavy mesons. This smearing function is the ground state wavefunction for the  $^1S_0$  state and should help the ground state signal to decay to its asymptotic value much earlier on. The same substitution has been made to the  $^3S_1$  using the same S state smearing function. Also done for the S states was to use an excited state wavefunction to help project out an excited state. For this the smearing function

$$S(\mathbf{z} - \mathbf{x}_0) = \left( 1 - \frac{|\mathbf{z} - \mathbf{x}_0|}{r_0} \right) e^{-\frac{|\mathbf{z}-\mathbf{x}_0|}{2r_0}} \quad (3.97)$$

was used. Different combinations of smearing at the source and sink can be done for example smearing at the source with a ground state and then using an excited smearing wavefunction at the sink. In all for the S states all different combinations were done using local, ground state and excited state smearing functions.

For the  $^1P_1$  state it is sufficient to use the following meson operator

$$\chi_A^\dagger(\mathbf{x}_0, t_0) \overleftrightarrow{\Delta}_i \psi_Q(\mathbf{x}_0, t_0) = (\chi_A^\dagger(\mathbf{x}_0 + \mathbf{i}, t) - \chi_A^\dagger(\mathbf{x}_0 - \mathbf{i}, t)) \psi_Q(\mathbf{x}_0, t_0) \quad (3.98)$$

which represents polarization in the  $i$  direction. The wavefunction for a  $^1P_1$  state polarized in the  $z$  direction is given by

$$S(r, \theta, \phi) = r \cos \theta e^{-\frac{r}{r_0}} \quad (3.99)$$

were spherical polar co-ordinates have been used. Note that the exponential term in equ(3.98) is not precisely that coming from a  $\frac{1}{r}$  potential since the wavefunction equ(3.98) models well a Richardson wavefunction. For the operator in equ (3.98)

to be polarized in the  $z$  direction  $i = 3$  and so the operator is smeared by making the replacement

$$\chi_A^\dagger(\mathbf{x}_0, t) \vec{\Delta}_3 \psi_Q(\mathbf{x}_0, t) \rightarrow \left( \sum_{z'} \chi_A^\dagger(z', t_0) z e^{-\frac{|z'-z_0|}{r_0}} \right) \psi_Q(\mathbf{x}_0, t) \quad (3.100)$$

A similar substitution for the polarized states  $i = y$  and  $i = x$  has been done. For the  ${}^3P$  states the same smearing function is used too. Only the ground state smearing function has been used for the P states and no attempt to extract an excited state will be attempted.

Lastly for the  ${}^1D_2$  states the wavefunction of  ${}^1D_2$  polarized in the  $z$  direction with magnitude  $M_2 = +1$  can be used. This wavefunction in the  $y$  plane, again with the exponential term modified, is given by

$$S(r, \theta, \phi) = r^2 e^{-\frac{r}{r_0}} \sin\theta \cos\theta \quad (3.101)$$

and so it is straight forward to to make the replacement

$$\chi_A^\dagger(\mathbf{x}_0, t_0) \vec{\Delta}_1 \vec{\Delta}_3 \psi_Q(\mathbf{x}_0, t_0) \rightarrow \left( \sum_z \chi_A^\dagger(z, t_0) x z e^{-\frac{|x-z_0|}{r_0}} \right) \psi_Q(\mathbf{x}_0, t_0) \quad (3.102)$$

Similar replacements can be made for shift operators  $\vec{\Delta}_1 \vec{\Delta}_2$  and  $\vec{\Delta}_2 \vec{\Delta}_3$ .

To illustrate the effectiveness of smearing, S and P states have been used to compare results from using smearing operators to that when using local operators. The results are from a run of 200 UKQCD configurations at  $\beta = 5.7$  on a  $12^3 \times 24$  lattice using a quark mass appropriate for the Bottom quark with a smearing radius of  $r_0 = 1.0$ . The values of the fitted masses from a single exponential fit are given in table (3.2) and table (3.3). The notation  $(n_{s,t}, n_{s,e})$  has been used where for example  $n_{s,t}$  represents the type of smearing at the sink. For a local operator *loc* is used and for smearing with a ground state 1 is used and 2 used for smearing with an excited state wavefunction. Effective mass plots are given in figures (3.1), (3.2) and (3.3) together with the corresponding Q values. The Q value is a measure of the probability that a particular value of  $\chi^2$  can be exceeded by chance. Since at minimization we want  $\chi^2$  to be the smallest possible value it then seems reasonable to have a high probability of having higher values of  $\chi^2$  at this point. In general a good fit is for  $Q > 0.1$  and  $< 0.9$  although a fit  $Q > 0.001$  is acceptable.

The results for the  ${}^1S_0$  show convincingly that the effective mass plateaus much earlier on in the smeared case. For the  $(loc, loc)$  operator even at times of  $t_{min} = 10$  the Q value is poor and the effective mass still has not reached a steady value. Even after times of  $t_{min} = 18$  there is still evidence that the effective mass is decaying.

	$N_{exp}$	$t_{min}/t_{max}$	$aE_1$	$Q$
fits to (loc,loc)	1	10/24	0.5038(6)	$1 \times 10^{-3}$
		12/24	0.5035(6)	0.07
		14/24	0.5034(6)	0.10
		16/24	0.5032(6)	0.16
		18/24	0.5031(7)	0.068
fits to (1,1)	1	2/24	0.5028(6)	0.048
		4/24	0.5027(6)	0.25
		6/24	0.5027(6)	0.17
		8/24	0.5029(6)	0.27
		10/24	0.5028(6)	0.20

Table 3.2: Examples of single exponential fits to the  $^1S_0$ .

	$N_{exp}$	$t_{min}/t_{max}$	$aE_1$	$Q$
fits to (loc,loc)	1	5/24	0.909(6)	0.20
		6/24	0.893(7)	0.72
		7/24	0.89(1)	0.66
		8/24	0.89(1)	0.59
		9/24	0.88(2)	0.69
		10/24	0.87(2)	0.62
		11/24	0.88(3)	0.60
fits to (1,1)	1	2/24	0.846(3)	0.78
		3/24	0.840(4)	0.92
		4/24	0.840(6)	0.90
		5/24	0.841(6)	0.88
		6/24	0.845(9)	0.85
		7/24	0.86(1)	0.95

Table 3.3: Examples of single exponential fits to the  $^1P_1$ .

On the other hand using the  $(1, 1)$  operator it is possible to get acceptable  $Q$  values as early as  $t_{min} = 4$ . Not only that there is a definite plateau in the effective mass from these times onwards as well as steady  $Q$  values. The effective mass in the two cases although agrees within errors does show in the  $(loc, loc)$  case that the effective mass is consistently higher in comparison to the values from the  $(1, 1)$ . This indicates that there are still higher excitations present using a  $(loc, loc)$  source. Other comparisons which can be made are that the errors are the same in both cases as one would naively expect since the noise is dominated by the ground state. Therefore for the  $^1S_0$  case smearing has worked well and if not done so the effective mass extracted from using a  $(loc, loc)$  operator would not have plateaued. As a result the value which would have been extracted would be too high.

Considering next the behaviour for the  $^1P_1$  case in table (3.3) this also shows well that a plateau can be reached much earlier on with smearing. In the  $(loc, loc)$  case a plateau has been reached at times  $t_{min} = 7$  onwards whereas in the  $(1, 1)$  case  $t_{min} = 3$  is where a plateau can be seen. More importantly is that the errors of the effective mass for  $(1, 1)$  at the point at which a plateau can be seen are smaller by a factor of about two in comparison to the  $(loc, loc)$ . This will allow the extraction of an effective mass to be made with a greater accuracy. The effective masses in the two cases do not agree, the  $(loc, loc)$  ones being much higher. This is too probably because of higher excitations being present and if smearing was not done an inaccurate value for the effective mass for the  $^1P_1$  would have been taken.

The effectiveness of smearing is illustrated very well in figures (3.1), (3.2) and (3.3). Clearly earlier plateaus can be seen in the smearing case. For the  $^3S_1$  smearing has worked equally well as in the case of the  $^1S_0$ . This shows that at this level of accuracy in the smearing technique used, smearing is independent of the spin orientation for a particular angular momentum state. This was also found to be the case for the  $^3P$  states. It was also checked that smearing worked for the  $^1D_2$  states.

### 3.10 Dispersion Relation

In the original action of QCD and also of NRQCD there are two arbitrary constants, the bare quark mass and the strong coupling constant. The coupling constant is fixed when the lattice spacing is determined. To fix the bare quark mass this is tuned so that some physical observable, which is dependent on the quark mass, coming out of the simulation agrees with its experimental value. For our physical observable the ground state  $^1S_0$  or the  $^3S_1$  mass is used. As well as deciding this it

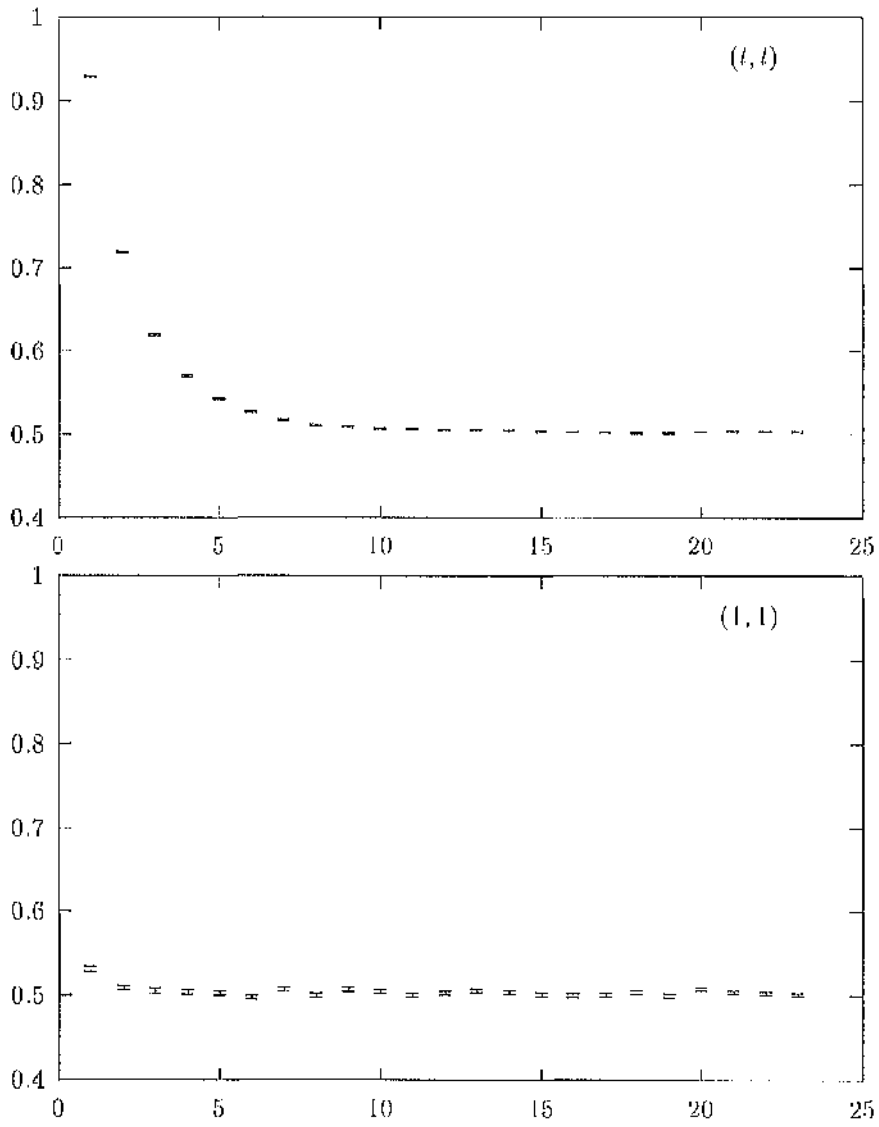


Figure 3.1: Examples of effective mass plots using local and smeared operators for the  $^1S_0$  state.

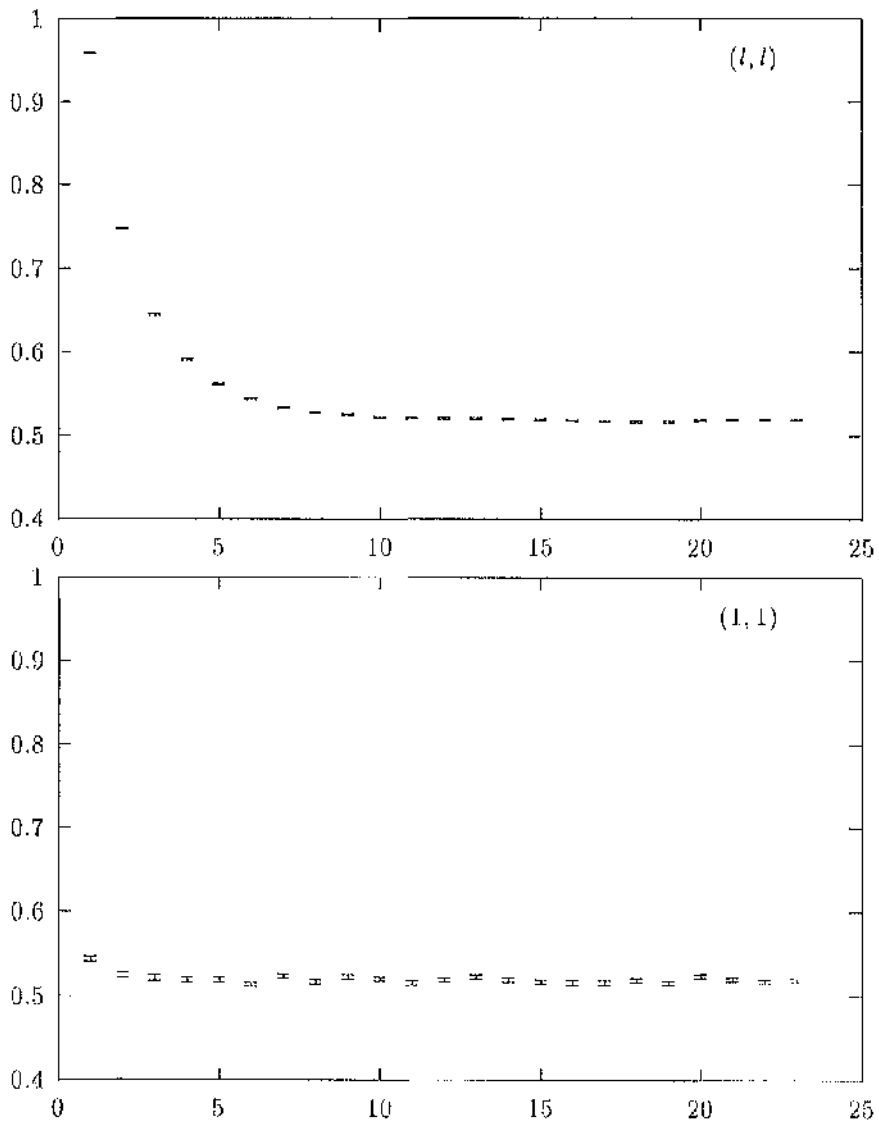


Figure 3.2: Example of effective mass plots for local and smeared operators for the  ${}^3S_1$  state.

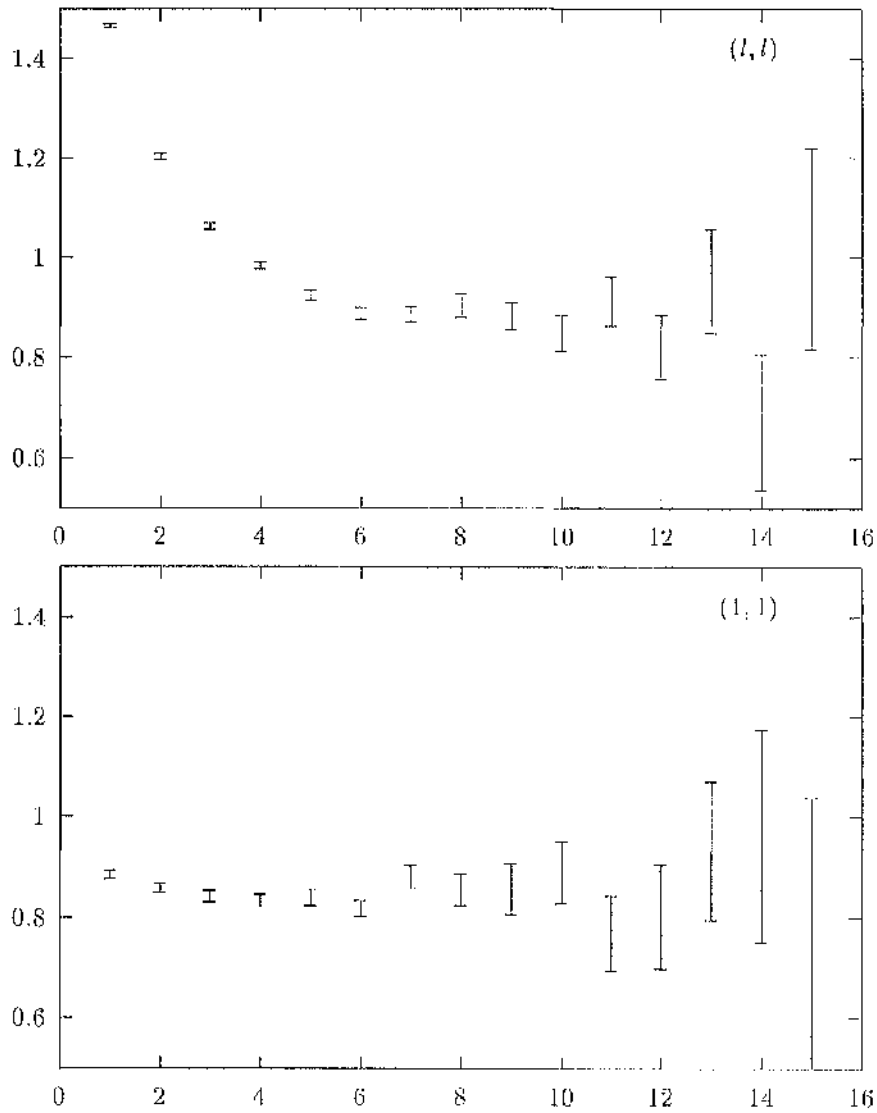


Figure 3.3: Examples of effective mass plots for local and smeared operators for the  ${}^1P_1$  state.

is necessary to decide on the definition of the mass of the  $^1S_0$ .

In NRQCD the non relativistic dispersion relation of a meson with momentum  $\mathbf{p}$  is

$$E_{\mathbf{p}} = M_0 + \frac{\mathbf{p}^2}{2M_1} - \frac{\mathbf{p}^4}{8M_2^3} \dots \quad (3.103)$$

and  $M_0 \neq M_1$  because the rest mass of the heavy quark has been removed from the theory. In turn  $M_1 \neq M_2$  because relativistic corrections away from the  $p^4$  term have not been included. Full Lorentz invariance can only be achieved when all relativistic corrections are added.  $M_1$  in equ (3.103) is used as the definition of the ground state mass for the  $^1S_0$  and will be referred to as the kinetic mass. The value of  $M_1$  should be accurate to  $\mathcal{O}(v^4)$  because of relativistic corrections and in turn  $M_2$  should then agree with  $M_1$  to an accuracy of  $\mathcal{O}(v^2)$ . To extract the value  $M_1$  in the simulation a dispersion relation similar to equ (3.103) will need to be plotted. This will involve knowing the energy of the meson for several different values of momentum. This energy of a meson state with momentum  $\mathbf{p}$  can be found by measuring the exponential fall-off of the correlation function defined by

$$\begin{aligned} M(\mathbf{p}, t; t_0) &= \sum_{\mathbf{x}} \langle 0 | \chi_A^\dagger(\mathbf{x}, t) \Gamma \psi_Q(\mathbf{x}, t) \psi_Q^\dagger(\mathbf{x}_0, t_0) \Gamma^\dagger \chi_A(\mathbf{x}_0, t_0) | 0 \rangle e^{i\mathbf{p} \cdot \mathbf{x}} \\ &= \sum_{\mathbf{x}} C_A(\mathbf{x}, t; \mathbf{x}, t) \Gamma G_Q(\mathbf{x}, t; \mathbf{x}_0, t_0) \Gamma^\dagger e^{i\mathbf{p} \cdot \mathbf{x}} \end{aligned} \quad (3.104)$$

and can be simply evaluated using Fast Fourier Transforms.

### 3.11 Wavefunctions

Of phenomenological interest is the wavefunction of the meson coming out of the simulation. This can not only provide information on the size of the meson but can be used to estimate correction terms in the NRQCD action as well as providing improved smearing functions. The meson wavefunction is defined as

$$\Psi_n(\mathbf{x}, t) = \langle 0 | \chi_A^\dagger(\mathbf{x}, t) \Gamma \psi_Q(0, t) | n, \mathbf{p} = 0 \rangle \quad (3.105)$$

The correlation function then has the asymptotic behaviour

$$\begin{aligned} C(\mathbf{n}, t; t_0) &= \sum_{\mathbf{x}} \langle 0 | \chi_A^\dagger(\mathbf{x} + \mathbf{n}, t) \Gamma \psi_Q(\mathbf{x}, t) \psi_Q^\dagger(\mathbf{x}_0, t_0) \Gamma^\dagger \chi_A(\mathbf{x}_0, t_0) | 0 \rangle = \\ &= \sum_{\mathbf{n}} \psi_n(\mathbf{n}) \psi_n(0) e^{-M_n t} \rightarrow \psi_0(\mathbf{n}) \psi_0(0) e^{-M_0 t} \end{aligned} \quad (3.106)$$

from which the wavefunction can be extracted. To evaluate equ (3.106) the quark Greens function is first transformed into momentum space after which the meson correlation function becomes

$$C(\mathbf{n}, t; t_0) = \sum_{\mathbf{p}} G_A(\mathbf{p}, t; t_0) \Gamma G_Q(\mathbf{p}, t; t_0) \Gamma^\dagger e^{i\mathbf{p} \cdot \mathbf{n}} \quad (3.107)$$

This can then be evaluated for all  $\mathbf{n}$  by fourier transforming back the product  $G_A(\mathbf{p}, t; t_0) \Gamma G_Q(\mathbf{p}, t; t_0) \Gamma^\dagger$ .

## Chapter 4

# Simulation Results

In this chapter the spectrum for Charmonium, Upsilon and the  $B_c$  meson will be given in detail. How the spectrum can be found using a variety of multi-exponential and multi-correlated fits is described. This will allow a precise determination of ground state masses at early times as well as values for excited state masses.

### 4.1 Multi-Exponential and Multi-Correlated Fitting Routines

To extract meaningful results from simulations it is necessary to fit the raw data coming out of the simulation to some functional form. From equ (1.31) we know the form of the behaviour of the asymptotic fall off for a meson correlation function. It would then seem reasonable to fit the data to the function

$$C(t; t_0) = Ae^{-M(t-t_0)} \quad (4.1)$$

This is the most simplest function possible in that the contribution from excited states have been neglected. As well as defining a function to fit to it is necessary to define a measure of the goodness of fit as well as some sort of standard deviation on the fitted parameters. For the goodness of fit the minimization of  $\chi^2$  is chosen which in its simplest form is defined as

$$\chi^2 = \sum_{i=1}^N \frac{(y_i - y(a_1 \dots a_M))^2}{\sigma^2} \quad (4.2)$$

$y(a_1 \dots a_M)$  is the function depending on  $M$  parameters which are determined in the minimization procedure and  $N$  are the number of independent data points. The

standard deviation is taken to be

$$\sigma^2 = \sum_{i=1}^N \frac{(y_i - \langle y \rangle)^2}{N-1} \quad (4.3)$$

There is no real specific value of  $\chi^2$  which needs to be reached in the minimization. In general if  $\chi^2$  per degree of freedom is less than one the fit is taken to be acceptable. The number of degrees of freedom in this case is defined as  $N - M$ . This is however a very naïve model to use to extract effective masses from the data. For example, correlation between successive data points will need to be taken into account when defining the standard deviation and  $\chi^2$ . Also a more general function will have to be used instead of eqn (4.1) to take into account of higher state contamination.

When fitting the spectrum results we have used two functional forms. These not only have more exponential terms in to extract higher excitations but also allow a simultaneous fit between meson correlators which have different types of smearing. Firstly define the meson correlation function as

$$M_{\{sk,sc\}}(t) = \langle 0 | O_{sk}(t) O_{sc}^\dagger(0) | 0 \rangle \quad (4.4)$$

where for example  $O_{sk}$  represents the type of smearing at the sink. This expression can be easily decomposed into energy eigenstates so that

$$M_{\{sk,sc\}}(t) = \sum_n \langle 0 | O_{sk}(0) | n \rangle \langle n | O_{sc}^\dagger(0) | 0 \rangle e^{-M_n t} \quad (4.5)$$

The first functional form that can be fitted to is called the row fit and has the decomposition

$$M_{\{sk,sc\}}(t) = \sum_n b_n(sk; sc) e^{-M_n t} \quad (4.6)$$

The next is called the matrix fit which has the decomposition

$$M_{\{sk,sc\}}(t) = \sum_n a_n^\dagger(sk) a_n(sc) e^{-M_n t} \quad (4.7)$$

with the identification

$$a_n(sk) = \langle n | O_{sk}^\dagger(0) | 0 \rangle \quad a_n(sc) = \langle n | O_{sc}^\dagger(0) | 0 \rangle \quad (4.8)$$

Different combinations of smearing at the sink and at the source can be used simultaneously in the fit restraining the energy to be the same for each different correlation function. This will involve using data which is correlated. There is also correlation between measurement for meson correlation functions taken at different

times which too will need to be taken into account. To do this we define a generalized version of equ (4.2) for the  $\chi^2$  to be minimized. Taking into account of the correlation between the data, the  $\chi^2$  to be minimized is defined as

$$\chi^2 = \sum_{\alpha\beta t t' > t_{min}} (M - M^{theo})_{\alpha t} (\sigma^2)_{\alpha t \beta t'}^{-1} (M - M^{theo})_{\beta t'} \quad (4.9)$$

The  $\alpha, \beta$  indices represent different meson correlation functions ie different types of smearing combinations and  $t$  and  $t'$  are time indices.  $M^{theo}$  is the functional form fitted to which is either equ (4.6) or equ (4.7). The covariance matrix is defined as

$$\begin{aligned} \sigma_{\alpha t \beta t'}^2 &= \frac{1}{N-1} \sum_N (M_\alpha(t) - \langle M_\alpha(t) \rangle) (M_\beta(t') - \langle M_\beta(t') \rangle) = \\ &\langle M_\alpha(t) M_\beta(t') \rangle - \langle M_\alpha(t) \rangle \langle M_\beta(t') \rangle \end{aligned} \quad (4.10)$$

where the average is taken over gauge configurations. The covariance matrix will be a  $N_{corr} \times N_t$  square matrix where  $N_{corr}$  is the number of correlators which are used in the simultaneous fit and  $N_t$  is the range in time in which the fitting is performed. In the minimization of the  $\chi^2$  it will be necessary to invert the covariance matrix which can be singular. In general if the number of gauge configurations  $N$  is much greater than  $N_{corr} \times N_t$  then all the eigenvalues of the covariance matrix will be non zero and the inverse will exist. If this is not the case a singular value decomposition will have to be done on the matrix using routines given in [27]. In practice in our simulations the number of configurations is several times greater than  $N_{corr} \times N_t$ . A singular value decomposition (SVD) routine is still used since it is possible to have a large range of eigenvalues which can be greater than the machine precision and cause false fits to be performed. In general in the majority of cases of fitting we did, it was found that there was not a large spread in eigenvalues of the covariance matrix. The minimization of the  $\chi^2$  is done using conjugate gradient methods with the routines taken out of Numerical Recipes and will not be discussed here. After minimization, and assuming an acceptable  $\chi^2$  has been achieved, it is necessary to quote some sort of error on the fitted parameters. To simplify things for the moment consider that there is only one parameter in the theory  $\lambda$  and that a minimum  $\chi^2$  has been reached. So then

$$\chi_{min}^2 \equiv \chi^2(\lambda_{fit}) \quad (4.11)$$

Expanding  $\chi^2$  around its minimum value

$$\delta\chi^2 = \chi^2(\lambda_{fit} + \delta\lambda) - \chi^2(\lambda_{fit}) =$$

$$\delta\lambda \frac{\partial\chi^2}{\partial\lambda} + \frac{1}{2}\delta\lambda^2 \frac{\partial^2\chi^2}{\partial^2\lambda} = \frac{1}{2}\delta\lambda^2 \frac{\partial^2\chi^2}{\partial^2\lambda} \quad (4.12)$$

since the partial derivative at minimum is zero. If  $\delta\lambda$  is chosen so

$$\delta\lambda^2 = \left( \frac{1}{2} \frac{\partial^2\chi^2}{\partial^2\lambda} \right)^{-1} \quad (4.13)$$

then  $\delta\chi^2 = 1$ . Changing  $\lambda_{\text{fit}}$  by such an amount will cause the fitted function  $\mathcal{F}(\lambda)$  to change in the range  $\mathcal{F}(\lambda_{\text{fit}} + \delta\lambda)$  to  $\mathcal{F}(\lambda_{\text{fit}} - \delta\lambda)$ . The range of the function will then span 68 % of the input data i.e by one  $\sigma$ . If the number of parameters is greater than one, the generalization of equ (4.13) is

$$M_{ab} = \left( \frac{1}{2} \frac{\partial^2\chi^2}{\partial\lambda_a\partial\lambda_b} \right)^{-1} \quad (4.14)$$

and the associated errors are the diagonal matrix elements of  $M_{ab}$ .

## 4.2 Charmonium Spectroscopy

In the next sections the spectrum for Charmonium will be presented in detail together with various techniques used to fit the spectrum. In the simulations we have used the quark evolution equation defined by equ (3.26). Using the notation  $^{2S+1}L_J$  we have looked at meson propagators for the following states:  $^1S_0$ ,  $^3S_1$ ,  $^1P_1$ ,  $^3P_0$ ,  $^3P_1$ ,  $^3P_2$  for both the E and T representation and the  $^1D_2$  in the T representation. For the S states, smearing functions both for the ground and first radially excited state were used as well as a local  $\delta$  function ( $n = loc$ ). From this all possible combinations of smearing at the source and sink were formed making a  $3 \times 3$  matrix of S state correlation functions. For the P and D states only a ground state smearing function and a local  $\delta$  function was used. We calculated the dispersion relation for the  $^1S_0$  by looking at the meson propagator for small momentum components using  $(n_{sc}, n_{sk}) = (loc, loc)$  and  $(1, loc)$ . For the  $^3S_1$ ,  $^1P_1$ ,  $^3P_1$ ,  $^3P_2$  and  $^1D_2$  an average over individual polarization directions is done making a total of 30 S, P and D meson propagators to analyse. Before it is possible to under-take a large simulation it is necessary to determine the remaining arbitrary parameters left. The strong coupling constant is determined for us in advance by the particular gluonic gauge configurations we will use. The heavy bare quark mass will need to be tuned numerically to determine a suitable value appropriate for the Charm quark. To do this we have used the  $^1S_0$  mass as an input from experiment and tuned the heavy quark mass so that our simulation value is in agreement with the experimental value of 2.98 GeV. For this a dispersion relation is used in order to evaluate the  $^1S_0$  energy

for small momentum components. The method outlined in section (3.103) is used here.

In the first simulation performed we used 40 configurations supplied by the FermiLab group with  $\beta = 5.7$  quenched gauge configurations on a 16 lattice. The bare quark mass in lattice units  $aM_Q$  was taken to be 1.2. To fix the lattice spacing the spin averaged 1P-1S splitting is used. More of this will be said in the next section. Only the lowest non-zero momentum component  $p = (1, 0, 0)$  as well as the zero momentum energy was extracted here for the  $^1S_0$ . A ratio fit (again more will be said on this) was performed on the two meson propagators and fitted to a single exponential. Hence

$$\frac{\text{Meson Propagator}_{\{p\}}}{\text{Meson Propagator}_{\{0\}}} = A e^{-\frac{p^2}{2M_{\text{kin}}}t} \quad (4.15)$$

The value  $M_{\text{kin}}$  is taken, for reasons discussed in sections (3.103), as the mass for the lowest  $^1S_0$  state. The momentum on the lattice for the lowest momentum component is  $pa = 4\sin\frac{\pi}{16}$  so using this with the fitted value for the ratio in equ (4.15) a value for  $M_{\text{kin}}$  can easily be found. For a heavy bare quark mass of 1.2 a value for  $M_{\text{kin}}$  in physical units is found to be a value much larger than 2.98 GeV. A better estimation for  $aM_Q$  is chosen to be 0.8. It is this value which we will use in all simulations involving the Charm mass. The results for Charmonium which will be presented in the next sections were obtained using 273 quenched gauge configurations produced from the standard Wilson action and were provided by the UKQCD collaboration. The configurations are at  $\beta = 5.7$  for a  $12^3 \times 24$  lattice and are fixed to Coulomb gauge. The value of the smearing radius used was  $r_0 = 1.0$ . A summary of the Charmonium spectrum using these configurations is given in figures (4.1) and (4.2).

### 4.2.1 Fitting Simulation Data

In the simulation it is necessary to maximize the available statistics, for example by averaging over spin or colour indices in the meson propagator. We can also take advantage of the fact that heavy mesons like Charmonium are relatively small and different starting sites on the lattice can be used to propagate the meson. As well as this, since the evolution equation is an initial value one, it is possible to choose different starting times in the time direction as well. In the spatial direction 8 different starting sites maximally spaced are used and two different starting times. There will inevitably be some correlation between meson propagators starting at different sites. To decide on the amount of correlation a simple test can be used

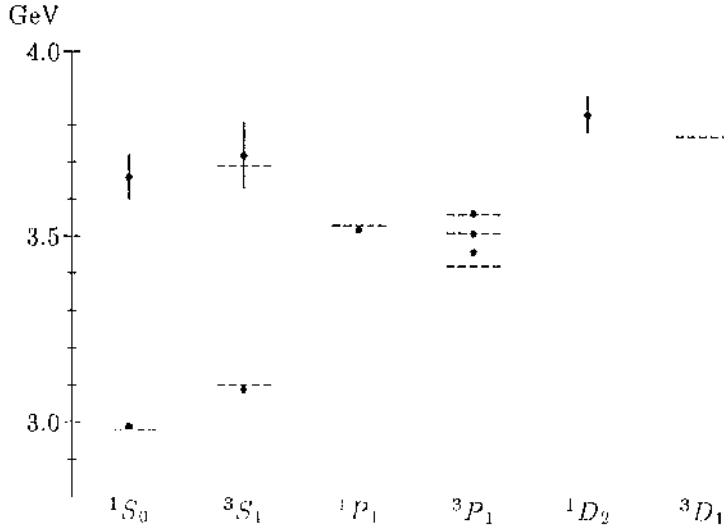


Figure 4.1: NRQCD simulation results for the spectrum of the Charmonium system plotted relative to the  $^1S_0$  using an inverse lattice spacing of 1.23 GeV. Experimental values are indicated by dashed lines. The  $^1S_0$  was used to set the zero of energy for simulation results while the spin-averaged S-P was used to set  $a^{-1}$ . Error bars are shown where visible, and only indicate statistical uncertainties.

where the propagators are binned. Here two sets of propagators starting at different sites are averaged and the error of the mean of the new set of propagators calculated. An increase in the error will be a sign of correlation. To test for correlation the effective mass together with its naive error was calculated. By binning propagators only in the spatial direction there was a small but significant increase in the error suggesting some correlation was present. Bining in the time direction showed there was no correlation at all. In most cases when we fit the data we bin over spatial points as well as time.

The quantity which needs first to be extracted from the simulation is the lattice spacing. This will allow conversion from dimensionless quantities calculated on the lattice to physical units in GeV for example. To do this it is necessary to fix some simulation result with experiment so that

$$M_{lat} \equiv aM_{exp} + \mathcal{O}(a)^2 \quad (4.16)$$

where the  $\mathcal{O}(a)^2$  error is from the gluonic action. If the lattice spacing corrections are ignored and knowing  $M_{exp}$ ,  $a^{-1}$  can be extracted. In Quarkonium systems there is a very natural quantity which can be used to set the scale. Spin-independent

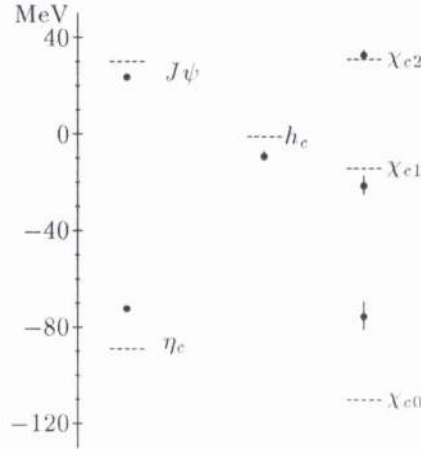


Figure 4.2: Simulation results for the spin structure of the Charmonium family, using an inverse lattice spacing of 1.23 GeV. Energies for S and P hyperfines are measured relative to their center of mass. Error bars for points are statistical.

splittings such as the spin-averaged  $\Delta M_{2S-1S}$  or the  $\Delta M_{1P-1S}$  in Quarkonium are independent of the heavy quark mass and of spin-dependent relativistic corrections. It is then expected that  $a^{-1}$  can be extracted with much higher accuracy than say with light meson systems. There will however be a systematic error from quenching which will cause  $a^{-1}$  to be dependent on the momentum scale appropriate to the physical quantity which has been used in determining  $a^{-1}$ . For example  $a^{-1}$  will be different if  $\Delta M_{2S-1S}$  is used to fix the scale in comparison to using  $\Delta M_{1P-1S}$ . More will be said on this. Here the  $\Delta M_{1P-1S}$  splitting was used to extract the lattice spacing because the noise of the 2S states was poor in comparison to the 1P states. The spin-averaged  $\Delta M_{1P-1S}$  is given by

$$\Delta M_{1P-1S} = M_{1P_1} - \left( \frac{3M_{3S_1} + M_{1S_0}}{4} \right) \quad (4.17)$$

and extracting the lattice value for this will involve a ratio fit of the various meson propagators. In general there will be some correlation between meson propagators calculated on the same configuration and most certainly between propagators with the same orbital angular momentum but different spin orientations. To reduce this correlation a collection of bootstrap ratios are produced which can then be fitted to some functional form. For each bootstrap ratio  $N$  configurations (where  $N$  is the number of independent configurations) are chosen at random and the ratio calculated. For the number of bootstrap ratios a total of 500 are chosen although

the final outcome has very little dependence on the number of bootstrap samples. Using the preliminary experimental value of the  $1P^1-1S_0$  splitting of 457 MeV [17] and fitting the bootstrap ratios to only a single exponential fit a value for  $a^{-1}$  is found to be 1.23(4) GeV. Errors quoted here are only statistical and no attempt has been made at this stage to add in systematic errors. Fixing the scale has then determined the bare coupling constant  $g_0(a^{-1})$  to be  $\frac{6}{5.7}$  at the scale  $a^{-1} = 1.23$  GeV.

With one of the free parameters now determined the next stage in the analysis of the data is to see what mass for the  $^1S_0$  is found using a bare mass  $aM_Q = 0.8$ . In the previous study where a dispersion relation was used in order to fine tune  $aM_Q$  only the first order kinetic term up to  $p^2$  was taken into account. Here a more refined method needs to be used to take into account of relativistic effects and lattice spacing errors. Since we have a  $p^4$  operator in the original kinetic energy Hamiltonian operator it is expected  $p^4$  contributions should be present. Also Charmonium is quite relativistic (ie more so than Upsilon) and only having a  $p^2$  term in the fit to the dispersion relation is inappropriate. From section (3.103) we know that because Lorentz invariance is broken in NRQCD the kinetic mass appropriate to say the  $p^2$  term is not the same as the mass appropriate for the  $p^4$  term in the dispersion relation. Two functional forms for the dispersion relation are used in the fitting. They are

$$E(\mathbf{p}) - E(0) = \frac{\mathbf{p}^2}{2M_1^A} - \frac{(\mathbf{p}^2)^2}{8(M_2^A)^3} \quad (4.18)$$

and

$$E(\mathbf{p}) - E(0) = \frac{\mathbf{p}^2}{2M_1^B} - C_1 \frac{(\mathbf{p}^2)^2}{8(M_1^B)^3} - C_2 \frac{\sum p_i^4}{8(M_1^B)^3} \quad (4.19)$$

The second form of the dispersion relation equ (4.20) has a lattice artifact due to the lattice form of the continuum laplacian in the kinetic energy operator. This is a non-rotational term which is allowed on the lattice since rotational invariance is broken. Since  $\mathcal{O}(a)^2$  errors in the lattice laplacian have been removed we expect this term to be zero. It is also expected that  $(C_1)^{\frac{1}{2}}$  is unity up to corrections of  $\mathcal{O}(v^2)$ . The difference in energies  $E(\mathbf{p}) - E(0)$  is chosen in the fits because this will remove the zero of energy from the fitted form. It is known that this zero of energy will not be equal to  $M_{\text{kin}}$  because the bare quark rest mass was explicitly removed from the theory. To take into account of this difference in mass another parameter would have to be introduced into the functional form for the dispersion relation. Since a value for the difference of energies is needed a ratio of meson

propagators are produced. In the fitting routines ratio of propagators are produced using a jackknife procedure which in turn are then fitted to single exponentials. A jackknife data point  $M_{jack}(i)$  for  $i = 1, N$  is defined to be

$$M_{jack}(i) = \langle M \rangle - M(i) \quad (4.20)$$

where  $M(i)$  is the original data point and  $\langle M \rangle$  is the mean of  $M(i)$ 's over the data sample  $N$ . This is then repeated say 40 times to produce 40 jackknife energies  $E(\mathbf{p}) - E(0)$  which are then fitted to the functional forms equ (4.19) or equ (4.20).

When doing the fit 4 different meson propagators with different momentum components are used and fitted simultaneously. To start with the lowest four components are used,  $\mathbf{p} = (1, 0, 0), (1, 1, 0), (1, 1, 1)$  and  $(2, 0, 0)$  in units of  $\frac{2\pi}{12}$ , not only to reduce extra  $p^6$  contributions but also the noise to signal ratio will become much worse for higher momentum values since the noise will be determined by the lowest momentum component. Using equ (4.19) first it is found in lattice units that  $M_1^A = 2.430(6)$  and  $M_2^A = 2.09(4)$ . For the second fit equ (4.20) the parameters were found to be  $M_1^B = 2.429(7), C_1 = 1.7(1)$  and  $C_2 = -0.12(13)$ . For our definition of kinetic mass which should be compared to the experimental mass of the  $^1S_0$  state the value of  $M_1^A$  or  $M_1^B$  is used. They are both the same within errors and converting to physical units our value for the  $^1S_0$  is found to be  $2.99(10)$  GeV. This is expected to be accurate to  $\mathcal{O}(v^4)$  and so taking into account of the systematic errors as well this mass agrees with experiment. The bare mass  $aM = 0.8$  is appropriate for the Charm case at this lattice spacing. The mass in the  $p^4$  term is found to be  $2.6(1)$  GeV and  $2.5(1)$  GeV from equ (4.19) and equ (4.20) respectively. Again both masses agree within errors and so there is little variation on the type of function used in the fit. The two masses in the  $p^2$  and  $p^4$  terms are expected to agree with  $\mathcal{O}(v^2)$  because of omitted relativistic corrections breaking Lorentz invariance. This is found to be the case for Charmonium where  $v^2 \approx 0.3$ . A similar analysis using instead Upsilon [28] found this to be case as well although the differences in the masses was smaller. For the parameter  $C_2$  this is indeed zero within errors as expected.

It now needs to be decided whether or not the fitting procedure has been optimized. For example have the right momentum components been used and would higher momentum components reveal more of a  $p^4$  structure present and help to account for some of the discrepancy in say the parameters  $M_1^A$  and  $M_2^A$ . Conversely it needs to be tested whether there is a  $p^6$  present in the dispersion relation or whether in fact there is no  $p^4$  present at all and we are constraining the fit to

	$\frac{100}{000}$	$\frac{110}{000}$	$\frac{111}{000}$	$\frac{200}{000}$
Ratio fits	0.0554(2)	0.1089(4)	0.1597(7)	0.210(1)
$\frac{p^2}{2M_1^4}$	0.0564	0.1128	0.1692	0.226
$\frac{p^2}{2M_1^4} - \frac{(p^2)^2}{8(M_1^2)^3}$	0.0554	0.1087	0.1599	0.210

Table 4.1: Comparison of ratio fits of  $E(\mathbf{p}) - E(0)$  to values of  $E(\mathbf{p}) - E(0)$  using fitted parameter values

be so. Simply fitting the dispersion relation to only a  $p^2$  term produces a totally unacceptable Q value and the fit can be ruled out. To see if any  $p^4$  term is present in the dispersion relation a term  $C_2 \frac{(p^2)^3}{16(M_1^2)^3}$  is added to eqn (4.20). The  $p_i^4$  term which is known not to contribute much to the fit is removed to reduce the number of parameters in the fit. Fitting to this form shows there is no  $p^6$  present and the parameters  $M_1^B$  and  $C_1$  remain unchanged within errors. As a last check higher momentum components have been used in eqn (4.19) and eqn (4.20). For example using  $\mathbf{p} = (1, 1, 0), (1, 1, 1), (2, 0, 0)$  and  $(1, 1, 2)$  produced the same values for the parameters but with a lower Q value suggesting higher momentum values will not reveal more  $p^4$  in the dispersion relation. To test whether the parameters from the fit are acceptable or not we can simply work out  $E(\mathbf{p}) - E(0)$  using the fitted parameters and compare that to the energies from fitting a ratio of meson propagators to

$$\frac{\text{meson propagator}_{\{1\}}}{\text{meson propagator}_{\{0\}}} = A e^{-E_1 t} \quad (4.21)$$

This is summarized in table (4.1) where the parameters from eqn (4.19) have been used. The table show that the fitted parameters produce the same  $E(\mathbf{p}) - E(0)$  as from the ratio fit only if a  $p^4$  term is present. There is disagreement if only a single  $p^2$  term is used verifying that a  $p^4$  contribution is definitely present.

In summary we have used two inputs from experiment, the spin-averaged 1P-1S splitting and the lowest lying  $^1S_0$  state to fix the two free parameters in the theory. All results now will be predictions, for example the P and S hyperfines and the 2S-1S splitting. The extraction of these quantities will be described in the next subsections.

### 4.2.2 Fitting results for the S, P and D states

In this sub-section multiple exponential fits will be used to extract not only the ground state to high precision for the  $^1S_0$  and  $^3S_1$  but also their first excited state. Fitting to the ground state of the P and D states will also be done but no attempt will be made to extract any excited states. Using multi-exponential fits will involve fitting several meson correlation functions simultaneously as described in the previous section. Doing multiple exponential fits, for example fitting to  $n$  exponentials will give an accurate value for  $n - 1$  states with higher excited state contamination contained in the last exponential. When using several meson correlation functions it is necessary to use different types of smearing at the source and sink. All possible permutations of smearing at the sink and source have been calculated using delta function smearing, ground state and excited state smearing for the S states.

The results from various types of smearing for the S states are summarized in figure (4.3) where effective masses defined by  $m_{eff}(t) = -\log(G(t+1)/G(t))$  are plotted together with bootstrap errors. From these plots of effective masses smearing works reasonably well and plateaus can be seen early on in the  $(n_{sc}, n_{sk}) = (1, 1)$  than in comparison to the  $(loc, loc)$  case for example. For plots with an excited smearing function no steady plateau can be seen for the first excited state and the signal decays to the ground state. This is in contrast to the Upsilon case where excited state plateaus are just present. This could reflect the fact that their smearing functions have a better overlap to the excited meson state. However another possibility is that the effect is due to the fact that Upsilon was simulated at a higher  $\beta$  value of 6.0. Here the lattice spacing is smaller so effective masses in lattice units are smaller in turn. Therefore higher radial states are less exponentially suppressed relative to the ground state. When lower  $\beta$  values are used as in the case of Charmonium, it is expected that excited states will decay more quickly making it more difficult to extract a value. It is also expected that ground states will plateau earlier on for the same reason and so at lower  $\beta$ 's the method of smearing and multi-exponential fits will become more and more redundant. Plotted in figure (4.4) are effective masses for the  $^1P_1$  and  $^1D_2$  states where as can be seen the noise is much worse, as expected from equ (3.88), although a reasonable plateau can be seen.

Two functional forms have been used in the multi-exponential fits which are described in the previous section. For the row fit equ (4.6) two meson correlation functions  $(n_{sc}, n_{sk}) = (1, loc)$  and  $(2, loc)$  are used. The fit will involve fitting  $n_{par} = n_{exp}(n_{cor} + 1)$  parameters where  $n_{exp}$  is the number of exponentials and  $n_{cor}$

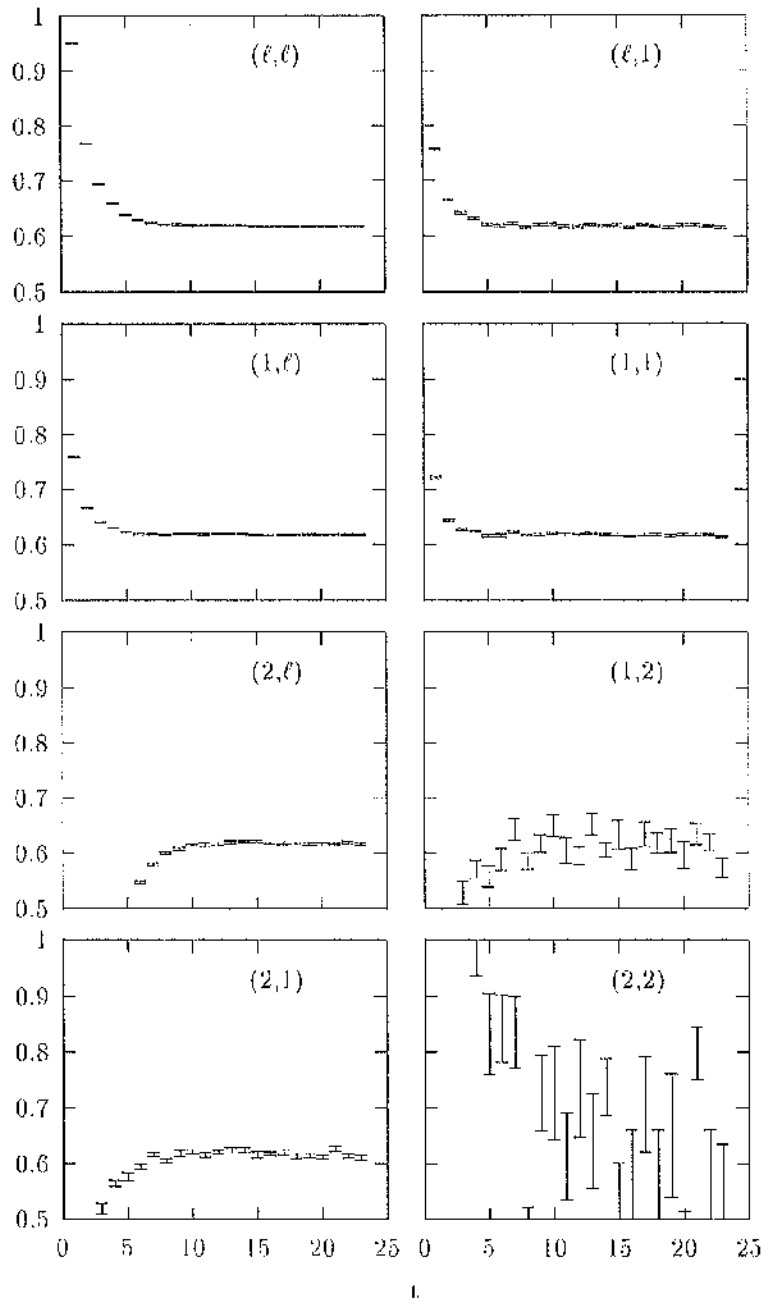


Figure 4.3:  $^1S_0$  Effective masses by (source, sink).

is the number of meson correlation functions. The maximum  $n_{exp}$  is 3 and  $n_{cor} = 2$  making in this case  $n_{par} = 9$ . No *(loc, loc)* correlation functions are used in these fits since it is expected that they will have significant contamination of higher radial states. In general if a certain radial state is to be extracted accurately it must have an appropriate smearing function for that state in the meson correlation function used in the fit. The second functional form used is the matrix fit eqn (4.7) where different correlation functions are made up using the combination  $n_{sc} = 1, 2$  and  $n_{sk} = 1, 2$  forming a  $2 \times 2$  matrix. The number of parameters fitted to in this case is given by  $n_{par} = n_{exp}(n_{row} + 1)$  where  $n_{row}$  is the dimension of the matrix. For the matrix fit we use  $n_{row} = 2$  and the maximum number of exponentials is  $n_{exp} = 3$  giving the maximum number of fitted parameters  $n_{par} = 9$  as in the correlated fits.

In Tables 4.2 and 4.4 are data from the correlated and matrix fits for the  $^1S_0$  and  $^3S_1$ . The errors stated are those causing a change  $\delta\chi^2 = 1$  and we also quote the quality of the fit, Q. To improve our statistics we only bin correlation functions which start from different spatial origins but not ones which have different starting timeslices. This has little effect on the central value but does increase the Q value giving us more confidence in the fit.

From both tables it is clear that an accurate ground state mass can be obtained at very early times. Only a  $t_{min}$  of 2 gives an unacceptable Q for the 2 exponential fit. Adding a 3rd exponential then produces an acceptable fit. Again this contrasts with the Upsilon spectroscopy results at  $\beta = 6.0$ . Here it takes much longer for the ground state effective mass to plateau with worse Q values at early values of  $t_{min}$ . The fitted parameters obtained from the two fits are independent of the type of fitting routine within errors, although the values for Q are lower for the matrix fits. At this point it is constructive to test how effective the multiple exponential fits are for the ground states at  $\beta = 5.7$ . In Table 4.3 are values for a single exponential fit to the  $(n_{sc}, n_{sk}) = (1, loc)$  and  $(1, 1)$  for the  $^1S_0$  state. In both cases an acceptable Q can only be obtained at  $t_{min}$  larger than when using a multiple exponential fit. This demonstrates the need for multiple fits in extracting ground states even at these relatively low  $\beta$ 's.

For the first excited state the choice of fitted value is far more difficult. To have confidence in the value we should use a 3 exponential fit although this gives larger errors in the fitted masses. We look for both a steady value in the fitted mass as  $t_{min}$  is changed and a steady value for Q. It is also useful to look at the amplitude for the second excited state in the 3 exponential fit to see at what  $t_{min}$  values it has decayed away. For the  $^1S_0$  row fit we choose a value 1.17(5) for the excited state mass

	$N_{exp}$	$t_{min}/t_{max}$	$aE_1$	$aE_2$	$Q$	
fits to (1,loc) and (2,loc)	2	2/24	0.6171(6)	1.172(6)	$2 \times 10^{-4}$	
		3/24	0.6178(6)	1.16(1)	0.65	
		4/24	0.6176(6)	1.16(1)	0.64	
		5/24	0.6179(7)	1.14(1)	0.79	
		6/24	0.6182(7)	1.21(5)	0.94	
		7/24	0.6183(7)	1.27(8)	0.93	
		3	2/24	0.6180(7)	1.15(2)	0.38
	3/24		0.6177(20)	1.15(4)	0.53	
	4/24		0.6181(6)	1.16(2)	0.79	
	5/24		0.6183(7)	1.30(16)	0.94	
	6/24		0.6183(7)	1.19(8)	0.87	
	7/24		0.6183(7)	1.25(24)	0.85	
	fits to (1,1), (1,2) (2,1), (2,2)		2	3/24	0.6185(6)	1.18(2)
		4/24		0.6183(6)	1.17(3)	0.15
5/24		0.6178(6)		1.16(4)	0.25	
6/24		0.6177(6)		1.08(6)	0.16	
7/24		0.6181(6)		0.90(6)	0.42	
3		3/24	0.6186(6)	1.19(2)	0.27	
		4/24	0.6178(6)	1.14(4)	0.23	
		5/24	0.6179(6)	1.21(7)	0.16	
		6/24	0.6180(6)	1.26(11)	0.18	
		7/24	0.6181(6)	0.91(6)	0.33	

Table 4.2: Examples of simultaneous multi-exponential fits to the  $^1S_0$  using row and matrix fits respectively.

	$N_{exp}$	$t_{min}/t_{max}$	$aE_c$	$Q$
fits to (1,loc)	1	5/24	0.6188(8)	0.01
		6/24	0.6184(8)	0.66
		7/24	0.6183(8)	0.72
fits to (1,1)	1	4/24	0.6184(8)	0.05
		5/24	0.6181(8)	0.22
		6/24	0.6181(8)	0.18
		7/24	0.6182(8)	0.15

Table 4.3: Examples of single exponential fits to the  $^1S_0$ .

(average of  $t_{min} = 3, 4, 6$ ) and from the matrix fit 1.18(4) (average of  $t_{min} = 3, 4, 5$ ). There is then agreement within errors between the two fits and we choose 1.17(5) as the global average. For the  $^3S_1$  state there is a significant deterioration in the  $Q$  values over those for the  $^1S_0$  and the fitting errors are slightly larger. This is presumably a reflection of the additional noise in the  $^3S_1$  channel coming from the  $^1S_0$ . For the row fit a value of 1.19(7) (average for  $t_{min} = 4, 5, 6$ ) is chosen and a value of 1.22(3) (average for  $t_{min} = 3, 4, 5$ ) from the matrix fit. A global average for the excited  $^3S_1$  is chosen to be 1.20(7). All the fitted values are collected in Table 4.13.

An alternative test which can be used to extract an excited state is that suggested by [29]. Here a matrix of correlation functions which all have the same quantum numbers is formed. Explicitly diagonalizing this matrix will produce orthogonal eigenstates consisting of the ground state and higher excitations. The dimension of the matrix determines the number of eigenvalues and hence the number of excited states which can be extracted. In our case we have used correlators which differ by the type of smearing to form our matrix of correlators and restricted the dimension of the matrix to be a 2 one. Define the matrix of correlators to be

$$C(t) = \begin{pmatrix} M_{\{a,a\}} & M_{\{a,b\}} \\ M_{\{b,a\}} & M_{\{b,b\}} \end{pmatrix} \quad (4.22)$$

where  $M_{\{a,b\}}$  is given in equ (4.5) and  $a$  and  $b$  denote different smearing combinations. Inserting a complete set of energy eigenstates one has

$$C(t) = \sum_n e^{-M_n t} \begin{pmatrix} |a_n(a)|^2 & a_n(a)a_n^*(b) \\ a_n(b)a_n^*(a) & |a_n(b)|^2 \end{pmatrix} \quad (4.23)$$

Diagonalizing the matrix by solving for the eigenvalues it is relatively simple to

	$N_{exp}$	$t_{min}/t_{max}$	$aE_1$	$aE_2$	$Q$	
fits to (1,loc) and (2,loc)	2	2/24	0.6951(8)	1.247(7)	$4 \times 10^{-5}$	
		3/24	0.6961(8)	1.23(1)	0.23	
		4/24	0.6958(9)	1.22(2)	0.23	
		5/24	0.6961(9)	1.18(2)	0.46	
		6/24	0.6966(9)	1.21(5)	0.56	
		7/24	0.6968(10)	1.25(8)	0.56	
		3	2/24	0.6964(9)	1.21(4)	0.10
	3/24		0.6957(9)	1.20(4)	0.17	
	4/24		0.6964(10)	1.16(5)	0.47	
	5/24		0.6967(10)	1.22(8)	0.55	
	6/24		0.6966(7)	1.19(6)	0.41	
	7/24		0.6969(10)	1.25(16)	0.40	
	fits to (1,1), (1,2) (2,1), (2,2)		2	3/24	0.6970(8)	1.22(1)
		4/24		0.6967(8)	1.21(3))	0.05
5/24		0.6965(8)		1.24(5)	0.07	
6/24		0.6966(8)		1.31(9)	0.09	
7/24		0.6967(9)		0.95(8)	0.08	
3		3/24	0.6966(8)	1.23(2)	0.08	
		4/24	0.6965(8)	1.20(3)	0.06	
		5/24	0.6964(8)	1.23(4)	0.04	
		6/24	0.6969(8)	1.46(13)	0.06	
		7/24	0.6967(9)	1.00(9)	0.07	

Table 4.4: Examples of simultaneous multi-exponential fits to the  ${}^3S_1$  using row and matrix fits respectively.

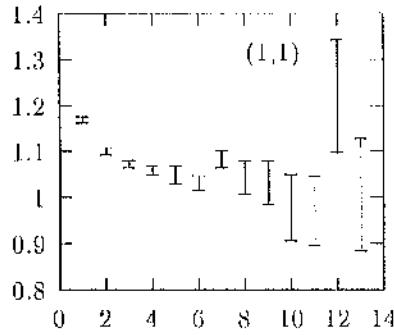


Figure 4.4:  $^1P_1$  Effective masses by (source, sink).

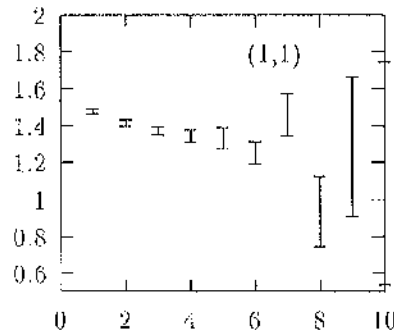


Figure 4.5:  $^1D_2$  Effective masses by (source, sink).

show that the behaviour of the two eigenvalues with time is

$$\begin{aligned}\lambda_+ &\sim e^{-M_0 t} (1 + g_+(a_i(a), a_i(b))e^{-\Delta E_1 t}) \\ \lambda_- &\sim e^{-M_1 t} (1 + g_-(a_i(a), a_i(b))e^{-\Delta \mathcal{E} t})\end{aligned}\quad (4.24)$$

where

$$\begin{aligned}\Delta E_n &= E_n - E_0 \\ \Delta \mathcal{E} &= \min(E_1 - E_0, E_2 - E_1)\end{aligned}\quad (4.25)$$

Therefore we expect  $\lambda_+$  to be dominated by the ground state very early on in time and  $\lambda_-$  to plateau to the first excited state. To start a local smearing function is used for  $a$  and the ground state for  $b$ . When diagonalizing the matrix there will be correlation between different elements of the matrix which needs to be removed. To do this a bootstrap ensemble of matrices are produced from the original data set and for each bootstrap matrix this can be diagonalized by solving a simple quadratic equation. The two bootstrap eigenvalues are then fitted to a single exponential. The ground state and first excited state plateaus are shown in figure (4.6). The

$N_{exp}$	$t_{min}/t_{max}$	$aE_1$	$Q$
1	3/15	1.284(7)	$3 \times 10^{-4}$
	4/15	1.24(1)	$9 \times 10^{-2}$
	5/15	1.20(2)	0.32
	6/15	1.20(3)	0.24
	7/15	1.19(6)	0.17

Table 4.5: Fits from a single exponential for the first excited state eigenvalue

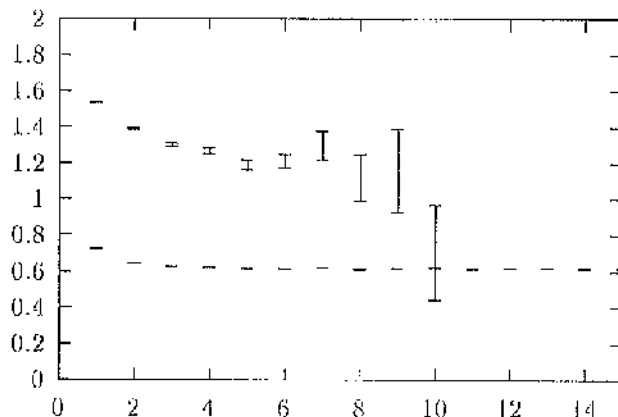


Figure 4.6: First excited and ground state obtained by diagonalization for the  $^1S_0$  state.

fitted results obtained for the first excited state are tabulated in table (4.5). There it can be seen that it takes a relatively large time for the first excited state to plateau to a steady value in comparison to the values from the multi-exponential fits. These higher state contributions are probably caused by having a (*loc, loc*) correlation present. However the values in table (4.5) agree within errors with the multi-exponential fits which acts as a test for the validity of both methods.

In Tables (4.6) and (4.7) are the amplitudes from the various fits for particular values of  $t_{min}/t_{max}$ . The value of  $t_{min}/t_{max}$  from which the amplitudes were taken are from the fit for which the first excited state was closest to the average result quoted above. In both the correlated and matrix fits it was found that the amplitude for a second excited state is essentially zero. This indicates that contamination from higher states in our fits are negligible. Consider first the amplitudes from the matrix fit given in table (4.6). The amplitude coefficients are defined by

$$a_n(sc) = \langle n | \mathcal{O}^\dagger_{sc} | 0 \rangle \quad (4.26)$$

so that for example  $a_1(1) = \langle 1 | \mathcal{O}^\dagger_1 | 0 \rangle$  is the projection of the ground state

onto the ground state smearing operator. It can be seen from the table that the smearing functions are doing a reasonable job in projecting out the desired state (on diagonal amplitudes) and suppressing unwanted states (off-diagonal amplitudes). For example  $a_1(1) > a_2(1)$  and in turn  $a_2(2) > a_1(2)$ . For the amplitude coefficients in table (4.7) these are from the row fit and are defined by

$$b_n(sk; sc) = \langle 0 | \mathcal{O}_{sk} | n \rangle \langle n | \mathcal{O}_{sc} | 0 \rangle \quad (4.27)$$

Again the smearing functions are projecting out the required state, for example the off-diagonal amplitudes again are more suppressed compared to the on-diagonal ones. Thus it is of advantage to have smearing functions although they are clearly not optimal. It may be better to use the output wavefunctions to produce input smearing functions in an improved calculation.

To illustrate the quality of the multi-exponential fits into early times effective amplitude plots given by the average of  $e^{M_1 t} \mathcal{M}(t)$  for some meson correlation function are plotted. Also plotted is the function

$$e^{M_1 t} \mathcal{M}(t) = a + b e^{-(M_2 - M_1)t} \quad (4.28)$$

where the parameters are taken from the fit. It can be seen from all the fits that the functional form for the effective amplitude lies well within the error bars giving confidence in the quality of the fitted parameters.

For the singlet P and D states because we have only included the ground state smearing function in the simulation, multiple exponential fits are not possible. Instead a single exponential fit was performed to the  $(n_{sc}, n_{sk}) = (1, 1)$  meson propagators of the  $^1P_1$  and  $^1D_2$ . The results are shown in Tables (4.8) and (4.9). In both cases a reasonable  $Q$  can be obtain with relatively small statistical errors although these are larger for the D states as expected. To isolate the ground state early on and achieve better errors higher radial smearing functions need to be added. Work has begun on this for the P states.

### 4.2.3 Fits to Spin Splittings

The operators in the NRQCD action responsible for the S and P hyperfine splittings involve the chromo-magnetic and electric fields. Hence spin splittings are very dependent on the tadpole-improved coupling constants  $c_i$ 's. This makes the spin-splittings a good test of the tadpole-improvement scheme. It is also true that potential models find it hard to produce spin-splittings in agreement with experiment so we would hope that they are also a good test of the differences between a full

Fit	$t_{min}/t_{max}$	k	$a_k(n_{sc,sk} = 1)$	$a_k(n_{sc,sk} = 2)$
$N_{exp} = 2$ for ${}^1S_0$	4/24	1	0.681(1)	0.1188(8)
		2	0.18(9)	0.52(2)
$N_{exp} = 2$ for ${}^3S_1$	5/24	1	0.700(3)	-0.164(1)
		2	0.29(2)	0.53(5)

Table 4.6: Examples of fit results for amplitudes  $a_k(n_{sc,sk})$

Fit	$t_{min}/t_{max}$	k	$b(n_{sc} = 1, k)$	$b(n_{sc} = 2, k)$
$N_{exp} = 2$ for ${}^1S_0$	4/24	1	0.1037(7)	-0.0184(4)
		2	0.032(3)	0.064(2)
$N_{exp} = 2$ for ${}^3S_0$	5/24	1	0.103(1)	-0.0253(4)
		2	0.036(7)	0.069(3)

Table 4.7: Examples of fit results for amplitudes  $b(n_{sc}, k)$

	$N_{exp}$	$t_{min}/t_{max}$	$aE_1$	$Q$
fits to (1,1)	1	3/24	1.959(4)	0.45
		4/24	1.952(5)	0.68
		5/24	1.049(7)	0.66
		6/24	1.046(9)	0.62
		7/24	1.048(14)	0.55

Table 4.8: Example of a  ${}^1P_1$  fit.

	$N_{exp}$	$t_{min}/t_{max}$	$aE_1$	$Q$
fits to (1,1)	1	3/24	1.35(1)	0.62
		4/24	1.32(2)	0.77
		5/24	1.30(3)	0.78
		6/24	1.26(5)	0.78
		7/24	1.26(9)	0.72

Table 4.9: Example of a  ${}^3D_2$  fit.

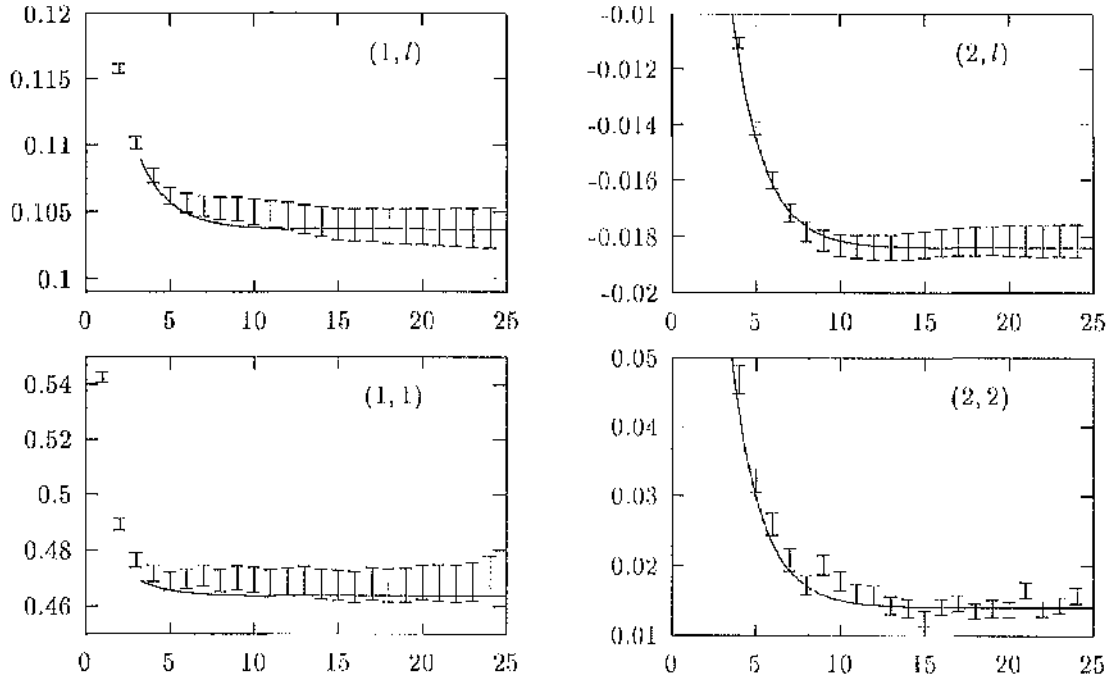


Figure 4.7:  ${}^1S_0$  Effective amplitudes  $G(t) \cdot e^{E_1 t}$  from two-exponential row fits (1, $\ell$ ) (2, $\ell$ ) and two-exponential matrix fits (1, $i$ ) (2,2) with  $t_{min} = 4$ ,  $t_{max} = 24$ .

calculation in QCD, such as ours, and a potential model. The calculation of these hyperfine splittings are direct predictions of QCD, the remaining free parameters have been fixed previously using spin-independent quantities.

It is expected that meson operators with the same orbital angular momentum but different spin orientations will be highly correlated. To take this into account a bootstrap ensemble of ratios of correlation functions are produced. Doing a ratio fit has the advantage of reducing statistical errors because the high correlation between the numerator and denominator is divided out. In most cases a single exponential fit is used in ratio fits which has the form

$$\text{Ratio}(t) = A e^{-\delta E t} \quad (4.29)$$

where  $\delta E$  is the energy difference between the two mesons in the ratio. Meson correlation functions with smearing  $(n_{sk}, m_{sk}) = (1,1)$  are used. Binning on time and spatial origin have been used in all cases and it is found that very high Q values in general can be achieved. Shown in Table (4.11) are values obtained for various combinations of spin-splittings using equ (4.30). The  $\delta E$  obtained for the  ${}^3S_1$  to  ${}^1S_0$  fit is in agreement with that obtained from the separate row and matrix fits of Tables (4.2) and (4.4). There a value of 0.0780(14) was obtained which has a higher

error than in the ratio fit case showing that a ratio fit can indeed reduce statistical noise.

If instead a ratio fit was done between two meson correlators with different angular momentum it is not necessarily true that the noise will be reduced. The Monte Carlo noise experienced by the quark in the D state is different than the noise experienced by the quark in the S state because of the greater separation between quark and anti-quark in the D state. The two different types of noise will not then cancel out when a ratio is taken. As an example a ratio fit to  ${}^1D_2 - {}^1S_0$  gave a value 0.69(3) where as fitting the two states directly gave a splitting 0.68(4). Hence the noise and central value remains the same. For the P states all different types of splitting between different spin orientations were done. Using these values P splittings relative to the centre of mass can be calculated. For example with the centre of mass for the P states defined by

$$P_{CM} = \frac{(5^3 P_2 + 3^3 P_1 + 3 P_0)}{9} \quad (4.30)$$

then

$${}^3P_2 - P_{CM} = \frac{3}{9} ({}^3P_2 - {}^3P_1) + \frac{1}{9} ({}^3P_2 - 3 P_0) \quad (4.31)$$

The quality of the data also allows direct fits to the P states to extract P hyperfine splittings. Again the central value is unchanged but the errors are increased. From table (4.11) it can be seen that the splittings involving the P states in the E rep give the same values within errors as P states in the T rep. This is a good indication that rotational symmetry is restored on the particular lattice which we have used.

To estimate the effect of higher radial excitations in the ratio fit for the  ${}^3S_1$  and  ${}^1S_0$  we have used a correlated  $\delta E$  fit and fitted to the form

$$G_{meson A}(n_{sc}, loc; t) = \sum_{k=1}^{N_{exp}} c_A(n_{sc}, k) e^{-E_k^A t} \quad (4.32)$$

$$G_{meson B}(n_{sc}, loc; t) = c_B(n_{sc}, 1) e^{-(E_1^B + \delta E)t} + \sum_{k=2}^{N_{exp}} c_B(n_{sc}, k) e^{-E_k^B t}$$

for  $n_{sc} = 1, 2$  for each meson. The results shown in Table (4.12) show that the  ${}^3S_1 - {}^1S_0$  splitting can be obtained at early times with smaller errors than in the ratio fit. The extra excited states have been absorbed in the extra terms in the correlated fit. The results from the row and matrix fits are not able to give a clear signal for the 2S hyperfine splitting and we are also unable to obtain this with the ratio fit either, for example by adding additional exponentials.

Splitting	$N_{exp}$	$t_{min}/t_{max}$	$a\delta E$	$Q$
${}^3S_1 - {}^1S_0$	1	4/24	0.0794(3)	$4.0 \times 10^{-5}$
	1	6/24	0.0784(4)	0.35
		8/24	0.0784(4)	0.32
		10/24	0.0783(5)	0.21
		12/24	0.0778(6)	0.25

Table 4.10: S hyperline splitting from a ratio fit.

Splitting	$N_{exp}$	$t_{min}/t_{max}$	$a\delta E$	$Q$
${}^3P_{3E} - {}^3P_0$	1	3/13	0.090(2)	0.94
		4/13	0.089(4)	0.91
		5/13	0.090(6)	0.85
		6/13	0.086(9)	0.81
${}^3P_{3E} - {}^3P_1$	1	3/13	0.045(1)	0.99
		4/13	0.046(3)	0.99
		5/13	0.045(4)	0.99
		6/13	0.044(6)	0.97
${}^3P_{2T} - {}^3P_0$	1	3/13	0.086(2)	0.87
		4/13	0.086(4)	0.57
		5/13	0.087(5)	0.64
		6/13	0.083(9)	0.65
${}^3P_{2T} - {}^3P_1$	1	3/13	0.041(1)	0.97
		4/13	0.043(3)	0.97
		5/13	0.043(4)	0.95
		6/13	0.042(7)	0.90
${}^3P_1 - {}^3P_0$	1	3/13	0.045(1)	0.13
		4/13	0.043(2)	0.13
		5/13	0.045(3)	0.12
		6/13	0.041(5)	0.09

Table 4.11: P hyperfine splitting from a ratio fit.

$t_{min}/t_{max}$	$1^1S_0$	$2^1S_0$	$1^3S_1 - 1^1S_0$	$2^3S_1$	$Q$
3/24	0.6179(6)	1.17(1)	0.0779(3)	1.23(1)	0.29
4/24	0.6178(6)	1.17(1)	0.0778(3)	1.24(2)	0.33
5/24	0.6180(6)	1.16(2)	0.0777(3)	1.19(2)	0.72
6/24	0.6183(6)	1.20(4)	0.0780(4)	1.20(4)	0.88
7/24	0.6183(7)	1.20(6)	0.0781(4)	1.20(6)	0.82
8/24	0.6184(7)	1.16(11)	0.0781(4)	1.25(13)	0.76

Table 4.12: Example of correlated  $\delta E$  fit for the  $^3S_1$  and  $^1S_0$  states

	Simulation Results
$1^1S_0$	0.618(1)
$1^3S_1$	0.697(1)
$2^1S_0$	1.17(5)
$2^3S_1$	1.20(7)
$1^1P_1$	1.050(7)
$1^1D_2$	1.30(4)
$^3S_1 - ^1S_0$	0.0782(4)
$^3P_2 - ^3P_0$	0.088(8)
$^3P_2 - ^3P_1$	0.044(5)
$^3P_1 - ^3P_0$	0.044(3)

Table 4.13: Fitted dimensionless energies.

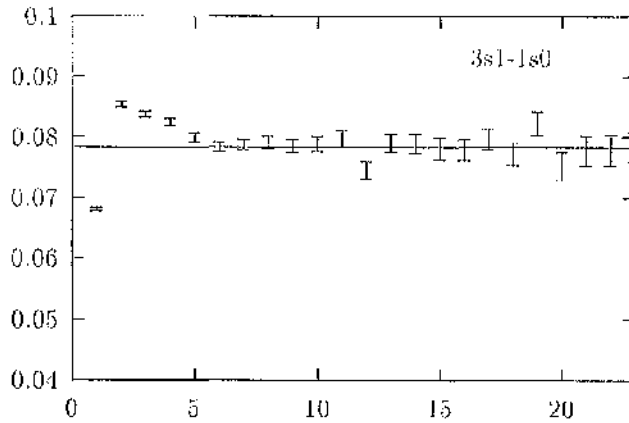


Figure 4.8: Example of a S hyperfine fit using  $(n_{s\sigma}, n_{sk}) = (1, 1)$  meson propagators.

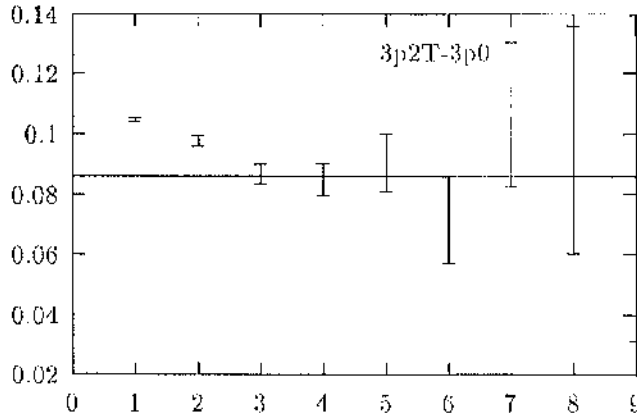


Figure 4.9: Example of a P hyperfine fit using  $(n_{sc}, n_{sk}) = (1, 1)$  meson propagators.

#### 4.2.4 Wavefunctions

As well as determining the spectrum of Charmonium, wavefunctions for the  $^1S_0, ^3S_1$  and the  $^1P_1$  ground states have been calculated. Wavefunctions are interesting from a phenomenological point of view but can also help to determine the size of the heavy meson and estimate for finite volume effects. Wavefunctions coming out of the simulation can be used to estimate the expectation values of operators in the correction program of NRQCD instead of relying on potential- inspired wavefunctions. More importantly is that the wavefunctions can be used to extract a heavy quark potential using a simple inverse Schrödinger equation. A program now exists to do this [30]. The potential extracted here will have the advantage over more conventional techniques because relativistic corrections should be present and comparison to the conventional static heavy quark potentials can be made. If, for example, the heavy quark potential is found using a  $^1S_0$  wavefunction and another potential from the  $^3S_1$  wavefunction the two potentials can be subtracted and the potential responsible for the S hyperfine splitting found. This can then be compared to what is expected from potential models eqn (4.34). Another use for simulation wavefunctions is that they can offer a much improved smearing function for future simulations.

Shown in figure (4.10), (4.11) and (4.12) is the radial wavefunction component for the  $^1S_0, ^3S_1$  and the  $^1P_1$  respectively. For the S states their wavefunctions are normalized so that the modulus of the wavefunction squared summed over the whole lattice is equal to one. As for the  $^1P_1$  state the wavefunction is normalized so that it is equal to one at a distance of one from the origin. The distinctive feature of all three radial wavefunctions is that they all are coulombic in behaviour. The radial wavefunctions of the S states goes as  $e^{-\frac{r}{r_0}}$  whereas for the P states they behave as  $re^{-\frac{r}{r_0}}$ . A fit to the wavefunctions gives  $r_0$  to be about 1.6. Clearly the wavefunctions are dominated by a  $\frac{1}{r}$  potential in the Charmonium case and suggests

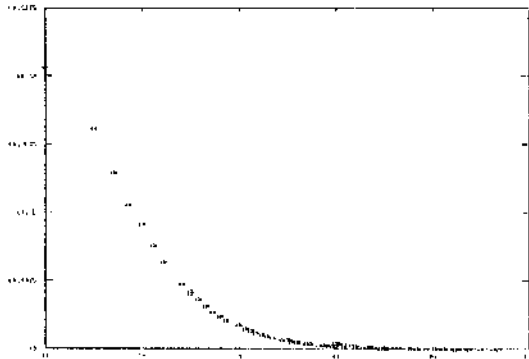


Figure 4.10: Wavefunction for the  ${}^1S_0$  state.

that the original choice of smearing functions is a satisfactory one. Looking at the difference between the different spin states  ${}^1S_0$  and  ${}^3S_1$  it can be seen that for the  ${}^3S_1$  the wavefunction at the origin is slightly less than in the  ${}^1S_0$  case. This is to be expected since the  ${}^3S_1$  has a higher excitation energy relative to the  ${}^1S_0$  case and hence a slightly greater separation between the quark and anti-quark is expected. In all cases it is possible to see the effect of periodic boundary conditions at a separation of six lattice spacings.

#### 4.2.5 Comparison with Experiment

To compare simulation results to experiment it is necessary to fix the scale  $a^{-1}$ . If the spin-averaged 1P-1S splitting is used eqn (4.18) it is found that  $a^{-1} = 1.23(4)$  GeV where the error is only statistical. It is also possible in principle to use the 2S-1S splitting to set the scale because this splitting also has the property of being insensitive to the quark mass and relativistic corrections. Using this splitting would give a slightly different  $a^{-1}$  as a result of quenching and taking an average of the two  $a^{-1}$  would help to limit the quenching effect. However in practice the statistical error on the 2S state is too high for this to be done. In Table (4.14) we compare the splittings obtained from the simulation with experimental results. The results are plotted in figures (4.1) and (4.2). It is important to remember that there is a potential  $\mathcal{O}(Mv^6) \approx 30 - 45$  MeV systematic error in all splittings coming from relativistic corrections not included in the heavy quark action.

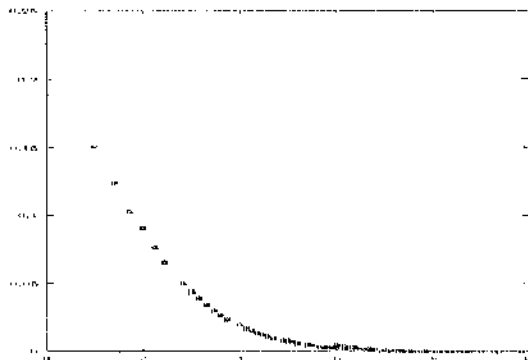


Figure 4.11: Wavefunction for the  ${}^3S_1$  state.

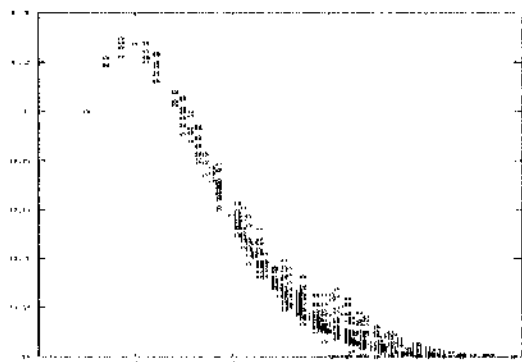


Figure 4.12: Wavefunction for the  ${}^1P_1$  state.

	Simulation Results [GeV]	Experiment [GeV]
$2^1S_0 - 1^1S_0$	0.679(62)	
$2^3S_1 - 1^3S_1$	0.619(87)	0.586
$1^1D_2 - 1^1S_0$	0.84(5)	
$3^3D_1 - 1^1S_0$		0.789
$3^3S_1 - 1^1S_0$	0.096(2)	0.116
$3^3P_2 - 3^3P_0$	0.108(10)	0.141
$3^3P_2 - 3^3P_1$	0.054(6)	0.045
$3^3P_1 - 3^3P_0$	0.054(4)	0.095
$3^3P_{CM} - 1^1P_1$	0.012(2)	

Table 4.14: NRQCD spectrum results and comparison with experiment for  $a^{-1} = 1.23(4)$  GeV and  $aM = 0.8$ .

As discussed the statistical error on the 2S state is too large to see any significance in the disagreement with experiment. The fact that it comes out larger than experiment, when the scale is fixed from the  $1^3P-1^3S$  splitting in a quenched calculation, is in agreement with results from the Upsilon where the difference there is thought to be mostly from quenching [28]. To test for this in Charmonium it is necessary to reduce the statistical errors and systematic errors from the heavy quark action in the 2S state.

The mass of the  $1^1D_2$  state is rather higher than that found for the  $\psi(3770)$ , thought to be a  $3^3D_1$  state. From the spin splittings alone you would expect this difference. The  $\psi(3770)$  is also above threshold for decay to  $\bar{D}D$  so quenching might have a significant effect on masses in this region. The  $3^3D_1$  has the same quantum numbers as the  $3^3S_1$  and will appear as a third excited state in that channel. In order to observe such a state the cross-correlation between the meson correlators  $3^3S_1$  and the  $3^3D_1$  would have to be calculated and we have not attempted to do this here.

Spin splittings have been calculated for the ground S and P states. From Table (4.14) we can see that the hyperfine splitting  $M(3^3S_1) - M(1^1S_0)$  has a very small statistical error. The difference from experiment then shows up clearly and is presumably a result of our systematic errors. For spin-splittings there is an approximate 45 MeV systematic error from higher order relativistic, discretisation and radiative corrections to the heavy quark action. The discretisation errors are  $\mathcal{O}(a^2)$

errors in the chromo-magnetic and electric fields and the radiative corrections are  $\mathcal{O}(g^2)$  corrections to the coefficient  $c_i$ 's away from tadpole-improvement. This could easily account for the difference in the S hyperfine splitting with experiment that is observed. Quenching though is also expected to have a significant effect certainly in the case where S states are concerned. From potential models the S hyperfine splitting is given by

$$\Delta M_{\text{hf}} = \frac{32\pi \alpha_s(M_Q)}{9 M^2} |\psi(0)|^2, \quad (4.33)$$

where the effect of quenching on the running of  $\alpha_s$  up to the Charm mass scale will cause it to be reduced by approximately  $\frac{(\beta_0^{n_f=0} - \beta_0^{n_f=3})}{\beta_0^{n_f=3}} \approx 20\%$  which again can explain the discrepancy with experiment. It is also possible for the wavefunction at the origin to change on going from quenching to unquenching. This change is found to be small which will be explained in chapter (5). Recent results for Upsilon using unquenched configurations show a significant increase in the S hyperfine, reinforcing the above argument of the effect of quenching on the S hyperfine splitting. One advantage of the Charmonium system is that an experimental value for the hyperfine splitting does exist and this should enable us to monitor how we are improving the result as we remove systematic errors including, eventually, that of the quenched approximation. A comparison to other methods of calculating the Charmonium S hyperfine can be made. For example the Fermilab group [31] give for the S hyperfine a rather smaller value than ours. Here they use a tadpole-improved Wilson fermion action eqn (2.40) for the heavy quarks and this approach has different systematic errors than ours. In terms of an expansion in powers of  $v^2/c^2$  their current calculation is not as accurate since the relativistic corrections of type  $p^4/M^3$  are not included correctly, as ours are. This will produce errors in their calculation in fixing the bare heavy quark mass from the meson dispersion relation. The hyperfine splitting is rather sensitive to this, as can be seen from eqn (4.34). The Fermilab group have, however, pieces of yet higher order terms which are entirely missing from our calculation. A similar calculation from the UKQCD collaboration [32] using an unimproved Wilson as well as an improved Wilson fermion action found also that the S hyperfine was much smaller in comparison to a NRQCD calculation. Here it was clear that using an improved Wilson action increased the hyperfine splitting significantly. However the improvement was only done at tree-level and the hyperfine splitting from the tree-level improved Wilson action gave a value smaller than the Fermilab group.

In the case of the P state splittings it is expected that the correction as a result

of quenching will be less. This is because the momentum scale causing the splittings in the P states lies more closely to the average momentum scale in the Charmonium. In contrast the momentum scale causing the S hyperfine splitting is larger and this splitting will be effected more by quenching. Nevertheless there is a discrepancy in P state splittings between our results and experiment which is due to higher order relativistic and/or discretisation errors in the heavy quark action. In the Upsilon spectrum calculation there was no significant disagreement with experiment but the results had the same qualitative tendency as here i.e. the overall splitting between  $\chi_2$  and  $\chi_0$  is too small and the  $\chi_1$  state tends to be equidistant between  $\chi_2$  and  $\chi_0$  instead of much closer to  $\chi_2$ . The experimental values for the ratio

$$\frac{M(\chi_2) - M(\chi_1)}{M(\chi_1) - M(\chi_0)} \quad (4.34)$$

are 0.48(1) for  $c\bar{c}$ , 0.66(2) for  $b\bar{b}$  (1P) and 0.58(3) for  $b\bar{b}$  (2P). The values from our simulation at  $\beta = 5.7$  are 1.0(2) for  $c\bar{c}$  and 0.7(3) for  $b\bar{b}$  at  $\beta = 6.0$ . Future calculations which include higher orders terms should be able to resolve this discrepancy.

The main conclusion from the calculation of the S and P hyperfine splitting is that the simulation results have very small statistical errors allowing for the observation of systematic errors. The disagreement with experiment can be put down to these errors which are the omission of relativistic corrections in the heavy quark action and quenching. The fact that this is the case is a success of tadpole improved perturbation theory. When tadpole-improving the chromo-magnetic and electric fields are divided by  $u_0^4$ . For  $\beta = 5.7$  it is found from Monte-Carlo simulations that  $u_0 = 0.861$  and so tadpole-improvement will increase the strength of the chromo-magnetic and electric fields by a factor of 1.8. Not doing this will severely reduce the value of spin-dependent splittings. The reduction being such that it could not be accounted for by the remaining systematic errors. Tadpole-improvement is then fundamental to the success and predictive power of NRQCD.

### 4.3 Upsilon and $B_c$ Spectroscopy

In this section the spectroscopy of Upsilon and  $B_c$  at  $\beta = 5.7$  will be given. An extensive calculation of the Upsilon spectrum at  $\beta = 6.0$  already exists [28] and doing the same calculation at lower  $\beta$ 's will enable to help quantify errors arising from lattice spacings. As for the  $B_c$  spectrum none of these mesons have been experimentally observed. Unlike Quarkonium systems the  $B_c$  is charged. This means it can not be produced in electron positron annihilation into a quark and

anti-quark as in the case of Charmonium or Upsilon. It is likely that  $B_c$  bound states will be produced from b and c quarks coming from the separate decays of  $Z^0$  particles or hadronization of b quarks. When the bound states are formed below  $B\bar{D}$  threshold they will be even more stable than Quarkonium. Being charged they are unable to decay into gluons and must do so via electromagnetic transitions to the ground state which will then decay by the weak interaction.

The results from the simulation can then act as predictions. In the simulation both the Upsilon and  $B_c$  spectrum are calculated at the same time to save on computation time. The code will essentially be the same as for Charmonium but some slight adjustments are necessary. No attempt to calculate any of the D states has been made because for these to be of use the  $^3D_1$  states really need to be done for a comparison to experiment. When calculating the quark Greens functions it is best to keep the Charm quark local and smear the Bottom quark propagator instead. This is because it is computationally quicker to calculate the Bottom quark Greens function. For the Bottom quark the stabilizing factor  $\alpha$  in the evolution equation is smaller in comparison to using a Charm quark. This will reduce the number of loops in the kinetic energy operator has to perform. The only change needed in the evolution part of the code is to add an extra Greens function which is local and must be evolved with a mass appropriate to that of the Charm. An important change will come about when calculating the P states in the  $B_c$  system. For Quarkonium the states were represented by the quantum numbers  $J^{PC}$  which were all individually conserved. It was then impossible for states differing in these numbers to mix. However since the  $B_c$  system is charged, the charge conjugation quantum number C is not defined. Therefore this means that states which have the same J and P quantum number will mix. In conclusion  $B_c$  states can be labelled by the quantum numbers  $J^P$  and states like the  $^1P_1$  and  $^3P_1$  with  $J^P = 1^-$  will mix. The problem with mixing will cause the meson propagator to be a linear combination of mass energy eigenstates with quantum numbers  $J^P$ . For example the meson propagator has the following decomposition

$$\langle 0 | \mathcal{O}_{^3P_1} \mathcal{O}_{^1P_1}^\dagger | 0 \rangle = A r^{-M_{^3P_1}} + B r^{-M_{^1P_1}} \dots \quad (4.35)$$

To extract both masses is equivalent to the problem of extracting both the ground and excited states containing the same quantum numbers when there is no mixture of states with different quantum numbers. It was shown in section (4.2.2) how this is possible. A cross-correlation matrix is formed using operators which have the same  $J^P = 1^-$  quantum numbers. Upon diagonalization this will produce

eigenvalues of the form  $\sim e^{-M_3 v_1 t}$  and  $\sim e^{-M_1 v_1 t}$  from which the masses can then be extracted. Here since the masses  $M_3 P_1 \sim M_1 P_1$  one will not have to worry about the higher mass state being exponentially suppressed relative to the lower mass state. Defining the operator

$$\langle 0 | \mathcal{O}_a \mathcal{O}_b^\dagger | 0 \rangle = \langle a | b \rangle \quad (4.36)$$

the cross-correlation matrix which needs to be evaluated is

$$\begin{pmatrix} \langle {}^3 P_1 | {}^3 P_1 \rangle & \langle {}^3 P_1 | {}^1 P_1 \rangle \\ \langle {}^1 P_1 | {}^3 P_1 \rangle & \langle {}^1 P_1 | {}^1 P_1 \rangle \end{pmatrix} \quad (4.37)$$

For this it is necessary to add in the correlation functions  $\langle {}^3 P_1 | {}^1 P_1 \rangle$  and  $\langle {}^1 P_1 | {}^3 P_1 \rangle$  into the code. Another modification from the Quarkonium case is that as well as the real parts of the correlation function being kept the imaginary parts for the  $B_c$  also will be required. This is a reflection on the fact that  $B_c$  has no C number. In Quarkonium the correlation function will be purely real because of charge conjugation. If C does not exist then the correlation function is in general complex.

For the operators appropriate to  $B_c$  states these do not have to be the same as those for Quarkonium. For Quarkonium the various operators are chosen with specific  $J^{PC}$  where as here only the quantum numbers  $J^P$  needs to be considered and so some simplifications might arise. As an example consider the angular momentum operator

$$\chi_A^\dagger(\mathbf{x}, t) \overleftrightarrow{\Delta}_i \psi_Q(\mathbf{x}, t) - \quad (4.38)$$

$$\chi_A^\dagger(\mathbf{x}, t) \left( \frac{1}{4} (\psi_Q(\mathbf{x} + \mathbf{i}, t) - \psi_Q(\mathbf{x} - \mathbf{i}, t)) \right) - \left( \frac{1}{4} (\chi_A^\dagger(\mathbf{x} + \mathbf{i}, t) - \chi_A^\dagger(\mathbf{x} - \mathbf{i}, t)) \right) \psi_Q(\mathbf{x}, t)$$

Both terms in parenthesis have the required angular momentum and parity for a  $J^P = 1^-$  state. But because of charge conjugation it was necessary to have both of the terms present in the final operator for Quarkonium. For the  $B_c$  case then only one of the terms will be needed. However from section (3.8) it was shown that this spatial derivative could be simplified so that only one term in the parenthesis needs to be used. This however used the property that some terms were complex conjugates of one another. This will not be the case in  $B_c$  and to use that argument for the simplification of the operator is incorrect. So it turns out that even though the  $B_c$  has one less quantum number compared to Quarkonium the same operators can be used.

The cross-correlation function which needs to be evaluated is

$$M(t; t_0)_{\{1P_3\}\{3P_1\}} = \sum_{\mathbf{x}, k, i, j} \langle 0 | \chi_A^\dagger(\mathbf{x}, t) \bar{\Delta}_k \psi_Q(\mathbf{x}, t) \psi_Q^\dagger(\mathbf{x}_0, t_0) (\bar{\Delta}_i \sigma_j - \bar{\Delta}_j \sigma_i) \chi_A(\mathbf{x}_0, t_0) | 0 \rangle \quad (4.39)$$

and similarly for the correlation function  $M(t, t_0)_{\{3P_1\}\{1P_3\}}$ . The summation over spatial indices is such that  $k \neq i \neq j$ . The determination of these cross-correlation functions is very much like that of the on diagonal terms ie  $M(t; t_0)_{\{1P_1\}\{1P_1\}}$  and involves the procedure outlined in section (3.8).

As previously with the Charmonium spectrum it is necessary to fix the bare quark masses. It is known what the Charm bare mass is from the simulation of Charmonium and to get the Bottom bare quark mass it is possible to scale down the value used at  $\beta = 6.0$  to  $\beta = 5.7$ . By doing this the bare quark mass in physical units is being kept fixed and independent of the lattice size. A more physical definition which should be kept fixed is the pole quark mass which can be written as the bare quark mass multiplied by a renormalization constant. This renormalization constant will depend on the cut-off [33], ie the lattice spacing, and hence the bare quark mass will scale in a non trivial way. If the renormalization constant is known at  $\beta$ 's of 5.7 and 6.0 then it is possible to find the value of the bare quark mass for the Bottom case at  $\beta = 5.7$ . However it will be necessary to convert from physical units to lattice units once the bare quark mass is fixed and for this the inverse lattice spacing  $a^{-1}$  needs to be used which has been extracted at the moment using the Charmonium spectrum. This is not the appropriate  $a^{-1}$  for the Upsilon case because of quenching, see section (5.3). It then seems reasonable to fine tune the Bottom bare quark mass in a simulation extracting the correct value for  $a^{-1}$  in the process. For this it is necessary to calculate the dispersion relation for the  $^3S_1$  state in the Upsilon case until the simulation value agrees with the experimental value of 9.46 GeV. The  $^1S_0$  state could not be used since this has not been observed experimentally and to calculate the dispersion relation for the  $^3S_1$  state requires only a slight change in the code. After several trial runs a value for the Bottom bare quark mass at  $\beta = 5.7$  was found to be 3.15 in lattice units. Comparing known coulombic wavefunctions to simulation wavefunctions the parameter  $r_0$  best suited was found to be 1.0 for Upsilon and 1.45 for  $B_c$ . It is too costly in computer time to change the present code to include two sets of smearing functions for the two  $r_0$ 's. It was decided to choose  $r_0$  appropriate to the Upsilon system since here one wants to maximize the statistics to see any deviation from

the already high statistics calculation at  $\beta = 6.0$ . The fact that  $r_0$  is greater for Upsilon than  $B_c$  which in turn is greater for Charmonium is as expected since the size of the meson should decrease with increasing quark mass.

The main reason for doing simulations of Upsilon at lower  $\beta$ 's is to try and quantify lattice spacing errors. It is expected from potential models and perturbation theory that the dominant source of error will be coming from  $\mathcal{O}(a^2)$  errors in the gluonic action. This will have the effect, of for example, reducing the 1P-1S splitting and increasing the determination of  $a^{-1}$ . In the next chapter it is shown that the correction could be anything up to the order of 10 %. However if we forget this for the while and just go ahead and fit the data to extract physical mass splittings and then try to see if any disagreement to the values found at  $\beta = 6.0$  occurs. Any disagreement can then be corrected for in the next chapter.

### 4.3.1 Upsilon Spectroscopy

To find the kinetic mass we fit to two forms of the dispersion relation equ (4.19) and (4.20) just as in the case of Charmonium. However because Upsilon is more non-relativistic a problem arises in extracting a value for the kinetic mass in the  $p^4$  term. Even though it was possible to do this at  $\beta = 6.0$  our kinetic bare mass in lattice units at lower  $\beta$ 's is higher which can offer more suppression of the  $p^4$  term relative to the  $p^2$  one. In the fit we used the four highest sets of momentum available in the dispersion fit. From the fitted parameters there was very little  $p^4$  present to make the fit worthwhile. Instead a simultaneous fit using the two lowest sets of momentum was fitted to just a  $p^2$  term. To set the scale the spin-averaged 1P-1S splitting defined by equ (4.18) was used. From this it is found that  $a^{-1} = 1.37(4)$  GeV where the error is only statistical. Using this a value for the kinetic mass for the  $^3S_1$  state is found to be 9.65(30) GeV to be compared to the experimental value of 9.46 GeV.

In table (4.15) are fits for the  $^3S_1$  states. In contrast to the fits of Charmonium a clear signal for the first excited state can be seen. A more stable plateau can be seen for the Upsilon case and could be a reflection on the fact that the effective mass in lattice units for the splitting 2S-1S is smaller in comparison and so less exponentially suppressed. In physical units the splittings are very similar and the fact that they differ in lattice units is a direct consequence of quenching producing different values of  $a^{-1}$  for Charmonium and Upsilon. The Upsilon's excited state can be observed out to a timeslice of  $t_{min} = 9$  which was not possible for Charmonium. Again adding a third exponential in the correlated fit produces a much better  $Q$

	$N_{exp}$	$t_{min}/t_{max}$	$aE_1$	$aE_2$	$Q$		
fits to (1,loc) and (2,loc)	2	3/24	0.5186(6)	0.888(5)	$1.3 \times 10^{-2}$		
		4/24	0.5186(6)	0.901(7)	0.37		
		5/24	0.5186(6)	0.91(1)	0.64		
		6/24	0.5188(6)	0.93(1)	0.73		
		7/24	0.5188(6)	0.95(3)	0.70		
		8/24	0.5187(6)	0.93(4)	0.65		
		9/24	0.5186(6)	0.93(6)	0.70		
	3	3/24	0.5187(6)	0.93(3)	0.77		
		4/24	0.5188(6)	0.94(4)	0.73		
		5/24	0.5189(6)	0.98(3)	0.68		
		6/24	0.5188(6)	0.94(6)	0.60		
		7/24	0.5188(3)	0.93(3)	0.57		
		fits to (1,1), (1,2) (2,1), (2,2)	2	3/24	0.5185(5)	0.95(1)	$2.0 \times 10^{-4}$
				4/24	0.5185(5)	0.97(2)	$3.5 \times 10^{-4}$
5/24	0.5183(5)			0.92(5)	$8.6 \times 10^{-4}$		
6/24	0.5184(5)			0.95(5)	$2.9 \times 10^{-4}$		
7/24	0.5191(6)			0.95(9)	$2.4 \times 10^{-4}$		
3	3/24		0.5184(5)	0.95(2)	$1.0 \times 10^{-4}$		
	4/24		0.5185(5)	0.97(2)	$1.3 \times 10^{-4}$		
	5/24		0.5183(5)	0.91(3)	$3.8 \times 10^{-4}$		
	6/24		0.5184(5)	0.95(5)	$1.1 \times 10^{-4}$		
	7/24		0.5191(6)	0.95(9)	$1.1 \times 10^{-3}$		

Table 4.15: Examples of simultaneous multi-exponential fits to the  $^3S_1$  using row and matrix fits respectively.

Fit	$t_{min}/t_{max}$	k	$a_k(n_{sc,sk} = 1)$	$a_k(n_{sc,sk} = 2)$
$N_{exp} = 2$	5/24	1	0.901(1)	0.1380(6)
		2	0.04(1)	0.49(3)

Table 4.16: Examples of fit results for amplitudes  $a_k(n_{sc,sk})$  to the  $^3S_1$  state.

Fit	$t_{min}/t_{max}$	k	$b_k(n_{sc} = 1)$	$b_k(n_{sc} = 2)$
$N_{exp} = 2$	6/24	1	0.344(2)	0.0524(6)
		2	0.02(1)	0.151(8)

Table 4.17: Examples of fit results for amplitudes  $b_k(n_{sc})$  to the  $^3S_1$ .

	$N_{exp}$	$t_{min}/t_{max}$	$aE_1$	$Q$
fits to (1,1)	1	2/24	0.846(3)	0.78
		3/24	0.840(4)	0.92
		4/24	0.840(6)	0.90
		5/24	0.841(6)	0.88
		6/24	0.845(9)	0.85
		7/24	0.86(1)	0.95

Table 4.18: Example of a  $^1P_1$  fit.

value at earlier times. As for the matrix fit the  $Q$  values are certainly not as good as in the correlated fits although the fitted parameters are consistent. Adding a third exponential does not help for the matrix fit suggesting the poor  $Q$  values are not from higher excited state contamination.

Comparing the values of the amplitudes in table (4.16) and (4.17) again the off-diagonal values are more heavily suppressed than the on-diagonal ones as expected. Here it is useful to compare these values to the ones from Charmonium. Looking at the amplitudes from both types of fitting for  $n_{exp} = 2$  the smearing function for the ground state of Upsilon is far more effective in projecting out the ground state and suppressing the excited case. In both the Charmonium and Upsilon runs the same smearing radius  $r_0 = 1.0$  was used which is appropriate for Upsilon but not so for Charmonium. From the fits to the simulation wavefunctions a radius of  $r_0 = 1.6$  should be used in the future for Charmonium. If one compares the effective mass plots figure (3.3) and (4.4) of the  $^1P_1$  states for Upsilon and Charmonium respectively it is clear that a plateau is reached earlier on in Upsilon case even though the value of the effective mass is smaller. Again this indicates the smearing function is more well suited to Upsilon.

To extract S and P spin-splittings a jackknife ensemble was fitted to the ratio equ (4.30). The results are summarized in table (4.19). As with the Charmonium

Splitting	$N_{conf}$	$t_{min}/t_{max}$	$a\delta E$	$Q$
${}^3S_1 - {}^1S_0$	1	4/24	0.01576(7)	0.50
	1	6/24	0.01574(7)	0.41
		8/24	0.01578(9)	0.44
		10/24	0.01573(9)	0.43
		12/24	0.01573(10)	0.33
${}^3P_{2E} - {}^3P_0$	1	3/24	0.0182(6)	0.72
		4/24	0.019(1)	0.76
		5/24	0.019(2)	0.70
		6/24	0.020(3)	0.65
		7/24	0.022(4)	0.60
${}^3P_{2E} - {}^3P_1$	1	3/24	0.0104(4)	0.79
		4/24	0.0109(7)	0.78
		5/24	0.011(1)	0.74
		6/24	0.012(2)	0.70
		7/24	0.013(3)	0.67

Table 4.19: S and P hyperfine splitting from a ratio fit.

data there is near degeneracy between the splittings from the E and T rep for the  ${}^3P_2$  state and only results from the E reps are quoted here. The final fitted values in dimensionless units are given in table (4.20) which are then converted to dimensionful energies in table (4.21).

Even though gluonic corrections have not been taken into account yet it is still instructive to compare the simulation results at  $\beta = 5.7$  to experiment and the simulation values given at  $\beta = 6.0$ . The splitting between the first excited state and the ground state for the  ${}^3S_1$  agrees with experiment although the errors are quite high. This result is expected to increase using a corrected gluonic  $a^{-1}$ . This splitting should then turn out to be higher than experiment which is in accord with the fact that the scale has been set by the 1P-1S splitting in the quenched approximation. More interesting is to look at the S and P spin-splittings. Comparing to experiment for the P fine structure it can be seen that the splittings from the simulation are too small. If the S hyperfine is compared to the value found at  $\beta = 6.0$  of 29 MeV, since no experimental value exists, again there is a reduction in the value obtained at  $\beta = 5.7$ . An increase in these values are expected from gluonic corrections but if ratios of P spin-splittings are calculated these should not depend on which type of

	Simulation Results
$1^1S_0$	0.5030(5)
$1^3S_1$	0.5187(6)
$2^1S_0$	0.93(4)
$2^3S_1$	0.94(4)
$1^1P_1$	0.843(6)
$^3S_1 - ^1S_0$	0.01575(8)
$^3P_2 - ^3P_0$	0.020(2)
$^3P_2 - ^3P_1$	0.011(2)
$^3P_1 - ^3P_0$	0.0079(5)

Table 4.20: Fitted dimensionless energies.

	Simulation Results [GeV]	Experiment [GeV]
$2^1S_0 - 1^1S_0$	0.585(58)	
$2^3S_1 - 1^3S_1$	0.577(58)	0.563
$^3S_1 - ^1S_0$	0.0216(6)	
$^3P_2 - ^3P_0$	0.027(3)	0.053
$^3P_2 - ^3P_1$	0.015(3)	0.021
$^3P_1 - ^3P_0$	0.0108(7)	0.032

Table 4.21: NRQCD spectrum results and comparison with experiment for  $\alpha^{-1} = 1.37(4)$  GeV and  $\alpha M = 3.15$ .

lattice spacing is used. From these ratios there is still disagreement with experiment which can not be understood for example in terms of possible relativistic corrections still to be included. For example the ratios calculated here are

$$\frac{M(\chi_2) - M(\chi_1)}{M(\chi_1) - M(\chi_0)} = 1.4(3) \quad (4.40)$$

which are very different from the experimental value of 0.66(2) and the lattice value of 0.7(3) at  $\beta = 6.0$  even taking into account of systematic errors of 10%. Also the splitting  $M(\chi_2) - M(\chi_0) = 27(3)$  MeV is much smaller than experiment and the result at  $\beta = 6.0$  but gluonic corrections are expected to alter the result somewhat. From the 2S-1S splitting it seems reasonable to assume that spin-averaged splittings are well reproduced at these relatively low  $\beta$  values. The problem could then arise from the operators which effect spin splittings, notably the chromo-magnetic and electric fields. Here there are  $\mathcal{O}(a)^2$  corrections in these fields which have not been taken into account.

### 4.3.2 $B_c$ Spectroscopy

In this section the spectrum of  $B_c$  is presented. In contrast to Quarkonium systems the correlation functions will in general be complex. The fitting routines have not been modified to take into account of this. However this is not a severe problem because it is still possible to use the row fit method to do multiple fits. With the matrix fits this is not possible since the decomposition of the correlated functions involves a product of amplitudes and imaginary terms will need to be kept at all times in the fitting. Taking the real part of the correlation function and fitting to eqn (4.30) will produce the correct energies. The amplitudes will just be the real parts of the amplitudes found from fitting both the real part and imaginary part of the correlation function. In the ratio fits the imaginary terms will need to be taken into account. Here a jackknife of correlation functions with both the real and imaginary terms in is produced and the real value of the ratio taken. This is then fitted to a single exponential as before.

To start with the kinetic mass needs to be found. As with the Upsilon case there was no real evidence of a  $p^4$  contribution and just fitting to a  $p^2$  term gave a value for the  $^1S_0$  state in lattice units to be 4.79. To set the scale requires an input from experiment which we do not have. A sensible choice would again be to use the 1P-1S splitting which is known not to vary by much through the Bottom to Charm quark mass scale. Taking a naive average of the 1P-1S splitting from Charmonium, 457 MeV, and Upsilon, 452 MeV, gives for  $B_c$  a possible experimental value of



	Simulation Results
$1^1S_0$	0.6052(8)
$1^3S_1$	0.6353(9)
$2^1S_0$	1.12(6)
$2^3S_1$	1.14(6)
$1^1P_1$	0.971(8)
$^3S_1 - ^1S_0$	0.0305(3)
$^3P_2 - ^3P_0$	0.045(4)
$^3P_2 - ^3P_1$	0.023(2)
$^3P_1 - ^3P_0$	0.022(2)

Table 4.22: Fitted dimensionless energies for  $B_c$  states.

	Simulation Results [GeV]	Potential Model Results [GeV]
$2^1S_0 - 1^1S_0$	0.673(75)	0.592
$2^3S_1 - 1^3S_1$	0.660(75)	0.562
$^3S_1 - ^1S_0$	0.040(1)	0.073
$^3P_2 - ^3P_0$	0.059(5)	0.047
$^3P_2 - ^3P_1$	0.030(3)	0.017
$^3P_1 - ^3P_0$	0.029(3)	0.030

Table 4.23: NRQCD spectrum results for  $B_c$  states and comparison with experiment for  $\alpha^{-1} = 1.32(4)$  GeV

value lies above the potential model predictions as expected since the scale was set by the 1P-1S splitting. As for the spin-dependent splitting one naively expects to get agreement due to relativistic corrections to about 20% or equivalently 20 MeV. Comparing to potential model predictions gives good agreement. However the potential model predictions vary considerably with the type of potential used and in the table the potential model results are just from one type of potential, the Buchmüller-Tye potential. The spread for example in the  $^3P_2 - ^3P_0$  splitting is from 45 MeV to 115 MeV where as for the S hyperfine the spread is from 45 MeV to 96 MeV which limits the predictive power of potential model calculations. It is not so easy to make a firm prediction for the S hyperfine coming from the NRQCD simulation here because of quenching, but our result is consistently lower than all the potential model values. As with the Upsilon results problems could arise with the effect of  $\mathcal{O}(a)^2$  corrections in the E and B fields as well as the gluonic action. Since the  $B_c$  is a larger meson these are not expected to be as severe. If the ratio in equ (4.41) is calculated for the  $B_c$  case it is found to be very close to unity as in Charmonium but not in Upsilon where the ratio was far from correct if compared to experiment. This could suggest that the problems in the P spin-splittings for the Upsilon will not occur here for the  $B_c$ . The large variation in potential model predictions for  $B_c$  make it a good system which NRQCD can improve upon. If higher order relativistic corrections are added in the systematic errors for the P line splittings can be brought down to about 4 MeV. Other known systematic errors will contribute at this level. For example  $\mathcal{O}(g)^2$  corrections away from tadpole improving. But if the next simulation will involve the addition of the relativistic corrections for the Charmonium then it is relatively cheap to use the present code which was used to calculate the Upsilon and  $B_c$  simultaneously. Here one can just substitute the Bottom mass for the Charm mass and vice a versa to calculate the Charmonium and  $\overline{B}_c$  spectrum simultaneously.

## Chapter 5

# Estimates of Quenching and $\mathcal{O}(a)^2$ Gluonic corrections

### 5.1 Introduction

In this chapter a simple Schrödinger equation is used as a method to estimate the effects of quenching in Quarkonium and the effects of  $\mathcal{O}(a)^2$  errors coming from the gluonic action. It is shown that there is agreement between the perturbative estimates for these gluonic lattice spacing errors and the non-perturbative ones from using the Schrödinger equation. Using these results, mass splittings in the Upsilon can be adjusted and it is shown that scaling from  $\beta = 6.0$  down to  $\beta = 5.7$  is successful when using these adjusted results.

### 5.2 Schrödinger equation on the lattice

The Schrödinger equation acting on a wavefunction  $\psi(\mathbf{x}, t)$  in Euclidean time is given by

$$\left( \frac{\partial}{\partial t} + \mathcal{K}_0 + V(\mathbf{x}) \right) \psi(\mathbf{x}, t) = 0 \quad (5.1)$$

where  $\mathcal{K}_0$  is the kinetic energy operator,  $V(\mathbf{x})$  is taken to be the static potential between two heavy quarks. This equation can be readily converted to the lattice by introducing shift operators

$$\Delta_\mu \psi(x) = \frac{1}{2} (\psi(x + \mu) - \psi(x - \mu)) \quad (5.2)$$

which have been expressed in terms of lattice units ( $a = 1$ ). To lowest order the kinetic energy operator  $\mathcal{K}_0$  is given by

$$\begin{aligned} \mathcal{K}_0\psi(\mathbf{x}, t) &= -\frac{\Delta^2}{2M}\psi(\mathbf{x}, t) \\ &= -\frac{1}{2M}\left(\sum_i \psi(\mathbf{x} + \mathbf{i}, t) + \psi(\mathbf{x} - \mathbf{i}, t) - 2\psi(\mathbf{x}, t)\right) \end{aligned} \quad (5.3)$$

which will contain  $\mathcal{O}(a)^2$  corrections. The general solution to eqn (5.1) is

$$\psi(\mathbf{x}, t) = e^{-(\mathcal{K}_0 + V(\mathbf{x}))(t-t_0)}\psi(\mathbf{x}, t_0) \quad (5.4)$$

Decomposing  $\psi(\mathbf{x}, t)$  into energy eigenstates so that  $\psi(\mathbf{x}, t) = \sum_n \psi_n(\mathbf{x}, t)$  one has

$$\psi(\mathbf{x}, t) = \sum_n e^{-E_n(t-t_0)}\psi_n(\mathbf{x}, t_0) \rightarrow e^{-E_0(t-t_0)}\psi_0(\mathbf{x}, t_0) \quad (5.5)$$

with  $E_0$  the lowest ground state possible. To find the lowest energy eigenvalue for a particular angular momentum state an appropriate smearing function is used for the wavefunction at  $t = 0$ . This is then evolved according to eqn (5.4) until a plateau in the effective mass is seen. The advantage over the NRQCD simulations is that it is possible to evolve out in time to as many time steps as is required. There is no problem with noise increasing with time since there are no errors associated with the heavy quark potential  $V(\mathbf{x})$  that we use. This means the ground state can be removed of any excited state contamination. Of course this is only a model and certainly has its limitations, for example, the exclusion of relativistic corrections. Since one is restricted to using smearing functions which will not be true eigenstates of the system there will only need to be a small contribution of ground state in order for it to dominate at large times. This can cause a problem in the extraction of excited states with the signal decaying to the ground state before a plateau can be found in the excited state. To try and avoid this happening a reorthogonalization procedure is introduced. First the ground state S and P wavefunctions are found after evolving many time steps in the evolution equation. The S and P wavefunctions are then used as improved smearing functions for the next set of evolutions. To remove unwanted ground state contamination from excited states the excited state wavefunction at each timestep is found and then made orthogonal to the ground state. Explicitly let  $\psi_{11}(\mathbf{x}, t)$  be the true ground state wavefunction obtained after the first set of evolutions and  $\psi_{12}(\mathbf{x}, t)$  the wavefunction of the first excited state at time  $t$  found by evolving a coulombic type wavefunction at time  $t = 0$  and reorthogonalizing at each time step. Then we want a wavefunction defined by

$$\psi'_{12}(\mathbf{x}, t) = \psi_{12}(\mathbf{x}, t) + \alpha\psi_{11}(\mathbf{x}, t) \quad (5.6)$$

such that  $\sum_{\mathbf{x}} \psi'_{\{2\}}(\mathbf{x}, t) \psi_{\{1\}}(\mathbf{x}, t) = 0$ . Hence the wavefunction which should be evolved at time  $t = t + 1$  is then

$$\psi'_{\{2\}}(\mathbf{x}, t) = \psi_{\{2\}}(\mathbf{x}, t) - \left( \frac{\sum_{\mathbf{x}} \psi_{\{2\}}(\mathbf{x}, t) \psi_{\{1\}}(\mathbf{x}, t)}{\sum_{\mathbf{x}} |\psi_{\{1\}}(\mathbf{x}, t)|^2} \right) \psi_{\{1\}}(\mathbf{x}, t) \quad (5.7)$$

This can easily be extended to include higher excitations, each being orthogonalized with respect to one another in a systematic way.

The heavy quark potential used,  $V(\mathbf{x})$ , is measured on the lattice by finding the average of Wilson loops in a Monte-Carlo simulation [36]. The  $\beta$  at which these simulations are performed defines the lattice spacing for our Schrödinger equation. The volume of the lattice used here is also the same as the one used to extract the heavy quark potential. The potential has not been calculated on all points of the lattice and with the data available the potential will have to be interpolated across the whole of our lattice. For example if the potential at distance  $\mathbf{r}_1$  and  $\mathbf{r}_2$  is known the potential at distance  $\mathbf{r}$  between these two points is calculated from

$$V(\mathbf{r}) = V(\mathbf{r}_1) + \left| \frac{\mathbf{r} - \mathbf{r}_1}{\mathbf{r}_2 - \mathbf{r}_1} \right| (V(\mathbf{r}_1) - V(\mathbf{r}_2)) \quad (5.8)$$

This is assuming a linear relation between the two known potentials. This is a reasonable assumption since at large distances it is expected that the potential is linear with distance and at smaller distances eqn (5.8) should hold irrespective of the form of  $V(\mathbf{x})$ .

The evolution of the wavefunction is performed in two parts. First the wavefunction is transformed into momentum space and evolved according to

$$\psi(\mathbf{p}, t+1) = e^{-\frac{p_L^2}{2M}} \psi(\mathbf{p}, t) \quad (5.9)$$

where the lattice momentum  $p_L^2$  is given by

$$p_L^2 = 4\sin^2 \frac{\mathbf{P}}{2} + \frac{4}{3}\sin^4 \frac{\mathbf{P}}{2} \quad (5.10)$$

defined such that  $\mathcal{O}(a)^2$  corrections are removed from the Laplacian operator, eqn (5.3). Since the exponential has been kept in the evolution no stabilizing factor needs to be introduced as in the case of NRQCD. After this part of the evolution the wavefunction is transformed back into position space and evolved using the term  $e^{-V(\mathbf{x})}$ .

The effective mass can be extracted by taking the dot product of two wavefunctions, which if they are normalized to unity will be

$$\sum_{\mathbf{x}} \psi(\mathbf{x}, t+1) \psi(\mathbf{x}, t) = e^{-E_{eff}} \quad (5.11)$$

	Simulation Results [GeV]	Experiment [GeV]
$2S - 1S$	0.56	0.56
$3S - 1S$	1.00	0.89
$2P - 1S$	0.92	0.81
$1D - 1S$	0.79	

$ R(0) ^2$	Simulation Results [GeV] <sup>3</sup>	Experiment [GeV] <sup>3</sup>
$1S$	5.6	5.1(2)

Table 5.1: Schrödinger spectrum results and comparison with experiment for  $a^{-1} = 2.70$  GeV and  $M_Q \approx 5.0$  GeV.

from which  $E_{eff}$  can be easily extracted. The zero of energy has not been included and only splittings relative to the ground S state are calculable. The quark mass used is that appropriate to the value of its pole mass. The code to solve this Schrödinger equation has been set up to extract effective masses for the 1S, 2S, 3S, 1P, 2P and the 1D state. As a test run the spectrum using a quark mass appropriate for the Bottom quark is tabulated in table (5.1) and compared to experiment. Since there is only the lowest order kinetic energy operator in the evolution equation an accuracy of 10% is possible. The scale is set using the 1P-1S splitting. For this example the heavy quark potential used is obtained at  $\beta = 6.0$  on a volume of  $16^4$ . The splittings obtained show agreement to experiment within the expected 10% accuracy. The experimental value for the 1D-1S is not known but the value obtain using the Schrödinger equation can be compared to the NRQCD result of 0.74(1) GeV [28]. The value for the wavefunction at the origin is consistent with other values obtained by using another discretized form of the Schrödinger equation [19]. The experimental value quoted for the wavefunction at the origin was obtained by looking at branching ratios of the Upsilon into lepton pairs without taking into account of radiative corrections.

### 5.3 Quenching

One of the main errors in Lattice simulation results is that of quenching where internal quark loops are neglected. As a consequence the inverse spacing  $a^{-1}$  which is extracted by comparing to some experimentally known quantity will depend on the typical momentum scale associated with that quantity. The bare strong coupling

constant  $g_0$  is defined through  $\beta = \frac{6}{g_0}$  and hence has a fixed value for a fixed  $\beta$ . However  $g_0$  runs with the momentum scale and the scale at which  $g_0$  is given must also be defined. This scale will be the cut-off and will be of  $\mathcal{O}(a^{-1})$ . Removing virtual quark loops will cause the coupling constant to run too fast with increasing momentum since it is the virtual quark loops which are responsible for the screening effect.

Consider for example extracting two  $a^{-1}$ 's from two different energy scales. With a fixed  $g_0$ , let  $a_{\{1\}}^{-1}$  be the inverse lattice spacing found using an experimental input with typical momentum  $q_1$  and  $a_{\{2\}}^{-1}$  found using an experimental input with typical momentum  $q_2$ . For  $q_2 > q_1$ ,  $a_{\{2\}}^{-1} > a_{\{1\}}^{-1}$ , because of the difference in the running of the coupling constant in the quenched and unquenched theories. To put it another way, when  $a^{-1}$  is fixed from experiment, the unquenched and quenched coupling constants are the same at the typical momentum scale associated with the experiment result. Hence

$$\alpha_{n_f=0}(q^*) = \alpha_{n_f}(q^*) \quad (5.12)$$

where  $q^*$  is the typical momentum and  $n_f$  the number of fermion flavours appropriate for the momentum scale  $q^*$ . With momentum  $q > q^*$  the quenched coupling constant will run too much in comparison to the unquenched and so

$$\alpha_{n_f=0}(q) < \alpha_{n_f}(q) \quad (5.13)$$

The two ways at looking at the effect of quenching are equivalent. In the former case we were keeping the coupling constant the same and showing that a difference in the scale at which  $g_0$  is defined will be different. In the latter the coupling constants at the same momentum  $q$  were being compared.

We can see this variation in  $a^{-1}$  with the NRQCD simulation results from Quarkonium and  $B_c$ . The typical momentum is expected to increase for smaller (or equivalently heavier) mesons ( $\Delta p \Delta x \approx 1$ ) and so  $q_{\{\bar{b}b\}} > q_{\{B_c\}} > q_{\{\bar{c}c\}}$ . The inverse lattice spacings (in GeV) obtained are

$$a_{\{\bar{b}b\}}^{-1} = 1.37(4) \quad a_{\{B_c\}}^{-1} = 1.32(4) \quad a_{\{\bar{c}c\}}^{-1} = 1.23(4)$$

which is in agreement with the argument given above. This effect can also be tested using the Schrödinger equation. The inverse lattice spacing using the string tension from a heavy quark potential gives a value of 1.8 GeV at  $\beta = 6.0$ . If this same potential is used in the Schrödinger equation and the scale set by the 1P-1S splitting in Quarkonium a value for  $a^{-1}$  is 2.70 GeV. This result was also seen in a

NRQCD [42] simulation at  $\beta = 6.2$  where the scale set by the 1P-1S splitting gave 3.4(3) GeV. This compares to the value of 2.6(1) GeV found by setting the scale from the string tension of a heavy quark potential produced using the same set of configurations. The difference can be explained simply by the fact that the string tension part of the heavy quark potential is dominated by momentum exchange of  $\mathcal{O}(\Lambda_{QCD})$  whereas the typical energy scale in Quarkonium like Upsilon is about 0.75-1 GeV and hence larger than  $\Lambda_{QCD}$ .

The effect of quenching on  $a^{-1}$  will affect conversion of lattice results to dimensional quantities. Quenching will also affect dimensionless quantities. This has been mentioned already when the S hyperfine for Charmonium was being compared to experiment. From perturbation theory this splitting is given by

$$\Delta M_{\text{hs}} = \frac{32\pi\alpha(M_Q)}{9M^2} |\psi(0)|^2. \quad (5.14)$$

Since  $\alpha_0(q^*) = \alpha_3(q^*)$  with  $q^* \approx 0.5\text{GeV}$  for Charmonium  $\alpha_0(M_Q) < \alpha_3(M_Q)$  and the S hyperfine splitting will be reduced by quenching. If  $q^*$  is large enough the difference in the running can be estimated perturbatively. In the 1-loop approximation the strong coupling constant evolves with some mass scale  $M$  by the expression

$$\alpha_{n_f}(M) = \frac{2\pi}{\beta_0^{n_f} \log(M/\Lambda_{QCD})} \quad (5.15)$$

where  $\beta_0^{n_f} = 11 - \frac{2}{3}n_f$ . In the limit of large  $M$  the difference in coupling constants should approach the value [38]

$$\frac{\alpha_3 - \alpha_0}{\alpha_3} = \frac{(\beta_0^{n_f=0} - \beta_0^{n_f=3})}{\beta_0^{n_f=3}} \approx 20\% \quad (5.16)$$

The effect of quenching on the wavefunction at the origin will need to be calculated in a non-perturbative way. The Schrödinger equation is used to calculate the spectrum and wavefunctions for Upsilon in both a quenched and unquenched heavy quark potential. The heavy quark mass was fixed by using the same physical pole mass [39] for both potentials. For the unquenched potential we use the potential which has been calculated using the unquenched HEMCCG configurations [40]. For the wavefunction at the origin we find in physical units

$$\frac{\psi(\mathbf{x}, t)_{\{unquenched\}}}{\psi(\mathbf{x}, t)_{\{quenched\}}} = 1.05 \text{ to } 1.07 \quad (5.17)$$

where the variation is due to the kind of sea quarks used ie if they are Wilson or Staggered. The fact that the wavefunction is reduced in the quenched approximation is as expected from arguments above. Since the coupling constant runs too

much in the quenched case the quark and anti-quark are less deeply bound at shorter distances and hence are expected to have a smaller wavefunction at these shorter distances. This finding also agrees with the studies of [41] where the wavefunction at the origin also showed a decrease in going to the quenched theory. Here a continuum Richardson potential was used for the quenched and unquenched potentials. A larger decrease was found for the wavefunction at the origin of  $\approx 15\%$ .

## 5.4 $\mathcal{O}(a)^2$ Gluonic Corrections

The remaining systematic errors are expected to come from the  $\mathcal{O}(a)^2$  lattice spacing errors in the gluonic action. Previous studies have suggested, for example with Upsilon at  $\beta = 5.7$ , that these could be the dominant correction over relativistic corrections at  $\mathcal{O}(v)^2$  and other lattice spacing errors [43]. In the study of [43] Richardson wavefunctions were used to perturbatively calculate the expectation values of the operators causing the  $\mathcal{O}(a)^2$  errors in the gluonic action. There are problems in using Richardson wavefunctions, for example they are only defined in the continuum limit and known with limited accuracy. Here a non-perturbative method on the lattice is used to estimate  $\mathcal{O}(a^2)$  gluonic corrections which are then compared to perturbation theory using NRQCD wavefunctions. In general we find good agreement between the two methods.

For the non-perturbative method the Schrödinger equation is used together with a Cornell type potential. In [36, 37] the results for their heavy quark potential are fitted to the form

$$V(\mathbf{R}) = KR - \frac{c\pi}{(3L)^3} \sum_{\mathbf{q} \neq 0} \frac{\cos(\mathbf{q} \cdot \mathbf{R})}{\sum_i 4\sin^2(q_i/2)} + V_0 \quad (5.18)$$

and this has now been done for  $\beta$ 's of 5.7, 6.0 and 6.2 [44]. The second term in eq (5.18) is the lattice version of the one gluon exchange, which would produce a  $\frac{1}{R}$  Coulombic potential in the continuum. To evaluate this sum on a  $16^3$  lattice for all points will require alot of computer time and hence some sort of simplification is needed. The gluonic lattice momentum is evaluated using the expression

$$4\sin^2((q_i - 1)\pi/3L) \quad (5.19)$$

where the sum for  $q_i$  is from 1 to  $3L$  for a lattice of volume  $L^3$ . This substitution  $L \rightarrow 3L$  helps remove finite volume effects. The fourier transform is done explicitly and is evaluated only once for a particular value of  $\mathbf{R}$ . This enables the potential to be found for different lattice points which have the same  $\mathbf{R}$  saving considerable in

Splittings	5.7	6.0	6.2
$\delta(1P - 1S)$	-0.0394	-0.0041	-0.0018
$\delta(2S - 1S)$	-0.0181	-0.0017	-0.0008

Table 5.2: Differences in splittings for Upsilon between an improved and unimproved heavy quark potential.

Splittings	$B_c$	$\bar{c}c$
$\delta(1P - 1S)$	-0.0105	-0.0060
$\delta(2S - 1S)$	-0.0027	-0.0015

Table 5.3: Differences in splittings for  $B_c$  and  $\bar{c}c$  at  $\beta = 5.7$  between an improved and unimproved heavy quark potential.

computer time. To estimate the size of gluonic corrections the lattice expression for the gluon momentum in equ (5.18) is corrected for  $\mathcal{O}(a)^2$  errors by the substitution given in equ (5.10).

The differences in splittings extracted using an unimproved and improved heavy quark potential in lattice units are given in table (5.7) and (5.3). In table (5.7) are results for Upsilon at  $\beta$ 's of 5.7, 6.0 and 6.2 using an unimproved and improved potential. Also given in table (5.3) are the results for Charmonium and  $B_c$  at  $\beta = 5.7$ . Comparing the change in values in the 1P-1S and 2S-1S splitting in all cases it is the 1P-1S splitting which suffers the most change. This is to be expected qualitatively since the 2S and 1S are meson states which are both relatively small compared to the average size of the meson. Both will experience a greater change in comparison to the P state when  $\mathcal{O}(a)^2$  corrections are removed. On a more quantitative basis as we will see in perturbation theory the expected shift in the mass of a meson state going from an uncorrected to corrected gluonic action depends on the wavefunction at the origin for that state and hence should be zero for P states. Comparing the Upsilon results to  $B_c$  and Charmonium at  $\beta = 5.7$  the changes experienced in the Upsilon case are much larger as one would naively expect. Upsilon is smaller than both  $B_c$  and Charmonium and hence will be more effected by  $\mathcal{O}(a)^2$  corrections. Even though one is comparing results at a constant  $\beta$  the  $a^{-1}$  extracted will be slightly different depending on the type of meson but this should generally not effect the results too much. For Upsilon going from  $\beta = 5.7$  through to  $\beta = 6.2$  it can clearly be seen that the changes in splittings decreases

Splittings	5.7	6.0	6.2
$\delta(1P - 1S)$	-10.2%	-2.3%	-1.5%
$\delta(2S - 1S)$	-4.15%	-0.75%	-0.46%

Table 5.4: Percentage differences in splittings for Upsilon between an improved and unimproved heavy quark potential.

Splittings	5.7	6.0	6.2
$\delta(1P - 1S)$	-10.9%	-2.3%	-1.1%
$\delta(2S - 1S)$	-3.6%	-0.75%	-0.36%

Table 5.5: Scaling results from  $\beta = 6.0$  for Upsilon assuming  $\mathcal{O}(a^2)$  corrections.

appreciably. It is instructive to find the percentage change in the splittings from going from uncorrected to corrected potentials. For example in the Upsilon case it is possible to see if the percentage changes scale as  $\mathcal{O}(a^2)$ . In table (5.4) are given these percentage changes and in table (5.5) are the expected percentage changes scaled from the value at  $\beta = 6.0$ . The lattice spacings were the ones obtained in the uncorrected potential. As can be seen from the table the changes scale in agreement assuming there are only  $\mathcal{O}(a^2)$  corrections. There is obvious a limit to the accuracy in the estimation of these gluonic  $\mathcal{O}(a^2)$  errors using the Schrödinger equation with the heavy quark potential. There might be radiative corrections to the constants associated with the  $\mathcal{O}(a^2)$  errors which would be expected to depend on the lattice spacing and scale in a non-trivial way.

The perturbative formulae for the mass shift in lattice units from  $\mathcal{O}(a^2)$  gluonic corrections is given by [45]

$$\Delta M_q = \frac{4\pi\alpha_s(q_\delta)}{15} |\psi(0)|^2, \quad (5.20)$$

where  $q_\delta$  is approximately twice the reduced mass [46]. The wavefunction at the origin can be found directly from a NRQCD simulation. Define the wavefunction at the origin to be

$$\psi_n(0) = \langle 0 | \mathcal{O}_{loc} | n \rangle \quad (5.21)$$

where  $\mathcal{O}_{loc}$  are the local S state operators defined in table (3.1). In the decomposition of the meson correlation function  $M_{\{loc,loc\}}$  the square of eqn (5.21),  $|\langle 0 | \mathcal{O}_{loc} | n \rangle|^2$ , is just the amplitude for the  $n^{\text{th}}$  state and so  $\psi_n(0)$  can be easily

Meson ( $nS$ )	Direct Fit to $b_n(toc, sc)$	Using $b_n(toc, sc)/a_n(sc)$	
		$sc = 1$	$sc = 2$
$\bar{b}b(1S)$	.389(1)	.382(1)	-----
$\bar{b}b(2S)$	-----	-----	.30(2)
$B_c(1S)$	.2118(4)	-----	-----
$\bar{c}c(1S)$	.1535(6)	.1523(3)	-----
$\bar{c}c(2S)$	-----	-----	.125(4)

Table 5.6: Mesonic wave function at the origin,  $\psi(0)$ , from NRQCD simulations. A dashed line means that no signal could be extracted.

extracted. Since local-local meson correlation functions contain appreciable contamination from higher states a multiple fit is performed using  $M_{\{2,toc\}}$ ,  $M_{\{1,toc\}}$  and  $M_{\{loc,toc\}}$  correlation functions to three exponentials. Using this method a stable ground state wavefunction can be found but not that for the first excited state. An alternative procedure is to calculate the ratio

$$\frac{b_n(toc, sc)}{a_n(sc)} \equiv \langle 0 | \mathcal{O}_{toc} | n \rangle \quad (5.22)$$

The results for the wavefunctions from the two types of fittings are summarized in table (5.6). Using these results for the wavefunction at the origin the perturbative mass shift from gluonic corrections can be calculated. These are compared to the non-perturbative estimates from the Schrödinger equation in the cases of the 1S and 2S states in tables (5.7), (5.8). In general there is good agreement. The results have been scaled so that the lattice spacing at the same  $\beta$  from using the heavy quark potential and the NRQCD simulation agree. The one anomaly is the result for Upsilon at  $\beta = 5.7$  where there are quite large differences, the non-perturbative result being higher. This could mean for example that the wavefunction at the origin in the NRQCD simulation is too small. But scaling the wavefunction at  $\beta = 6.0$  down to 5.7 does show reasonable agreement. This suggests that the potential at short distances, to which the Upsilon is more susceptible, is too singular and changes in going from uncorrected to corrected gluonic potentials is overestimated. In extracting the potential down to  $R = 0$  a coulombic behaviour is assumed and no attempt has been made in taking into account asymptotic freedom in the running of the coupling constant. Evidence of this is found in the wavefunction at the origin, the Schrödinger wavefunctions being too high in comparison to the NRQCD wavefunction results. This is a problem which has been experienced in using a

Non-Pert. Masses	5.7	6.0	6.2
$M_{\{1S\}}$	0.034	0.0041	0.0020
$M_{\{2S\}}$	0.019	0.0024	0.0012
Pert. Masses	5.7	6.0	6.2
$M_{\{1S\}}$	0.023	0.0036	0.0028
$M_{\{2S\}}$	0.014	0.0023	---

Table 5.7: Comparison for Upsilon of perturbative and non-perturbative shifts of effective masses in lattice units between an improved and unimproved heavy quark potential.

Non-Pert. Masses	$B_c$	$\bar{c}c$
$M_{\{1S\}}$	0.011	0.0063
$M_{\{2S\}}$	0.008	0.0049
Pert. Masses	$B_c$	$c\bar{c}$
$M_{\{1S\}}$	0.009	0.0062
$M_{\{2S\}}$	---	0.0041

Table 5.8: Comparison for  $B_c$  and  $\bar{c}c$  at  $\beta = 5.7$  of perturbative and non-perturbative shifts of effective masses in lattice units between an improved and unimproved heavy quark potential.

continuum Cornell potential where it is likely that the potential near  $\mathbf{R} = 0$  is even more singular than on the lattice.

When correcting for gluonic corrections in the 1P-1S splitting we shall use the perturbative estimations. The corrected  $a^{-1}$ 's in GeV are for  $\beta = 5.7$

$$a_{\{\text{bb}\}}^{-1} = 1.46(4) \quad a_{\{B_c\}}^{-1} = 1.36(4) \quad a_{\{\text{cc}\}}^{-1} = 1.25(4) \quad (5.23)$$

and for  $\beta = 6.0$

$$a_{\{\text{bb}\}}^{-1} = 2.61(10) \quad (5.24)$$

With the gluonic improved  $a^{-1}$ 's calculated it is constructive to see how they scale from one  $\beta$  to another. For this the scale  $\Lambda_V$  is used, the dimensionless quantity  $a\Lambda_V$  calculated on the lattice using the expectation values of  $1 \times 1$  plaquettes [47]. Hence using the identity

$$\frac{(a^{-1})_{5.7}}{(a^{-1})_{6.0}} = \frac{(a\Lambda_V)_{6.0}}{(a\Lambda_V)_{5.7}} \quad (5.25)$$

$a_{\{\text{bb}\}}^{-1}$  for example can be scaled from its value at  $\beta = 5.7$  to  $\beta = 6.0$ . A value of 2.53(7) GeV is found which compares well to the value 2.61(10) GeV found by direct simulation. Using the corrected values for  $a^{-1}$  gluonic improved dimensionful energies should be recalculated. For Upsilon at  $\beta = 5.7$  the corrected value for the kinetic mass is 10.28(32) GeV and the corrected  $^1S_0$  mass for the  $B_c$  is 6.47 (20) GeV. Correcting for the  $2^3S_1 - 1^3S_1$  splitting in Upsilon at  $\beta = 5.7$  gives a value of 602(62) MeV. This corrected value is more in line with the value quoted at  $\beta = 6.0$  of 627(26) GeV than the uncorrected value but the error bars are higher for the  $\beta = 5.7$  case. Correcting the S hyperfine for Upsilon at  $\beta = 5.7$  gives a splitting of 23 MeV still significantly smaller than the  $\beta = 6.0$  results of 29 MeV. However the Bottom quark mass we have used in the simulation is too heavy and the S hyperfine is certainly sensitive to this. If one rescales the kinetic mass to the value 9.46 GeV the S hyperfine becomes 25 MeV. The dependence of the heavy quark mass on the S hyperfine is taken to be  $\mathcal{O}(\frac{1}{M})$ . In dimensionless units the S hyperfine will also be affected by gluonic corrections since for S states the wavefunction at the origin is non-zero. However it seems unlikely that the differences in the shift between the  $^3S_1$  and  $^1S_0$  states is large since they have very similar wavefunctions, as can be seen from the plots for Charmonium for example. However as far as the P states are concerned no shift in dimensionless units will occur. The only shift due to gluonic corrections is in the change in the value of  $a^{-1}$ . This should however not affect the ratio of P hyperfine splittings and it is hard to understand the disparity in the ratios eqn (4.41) to the values at  $\beta = 6.0$  in terms of only gluonic corrections.

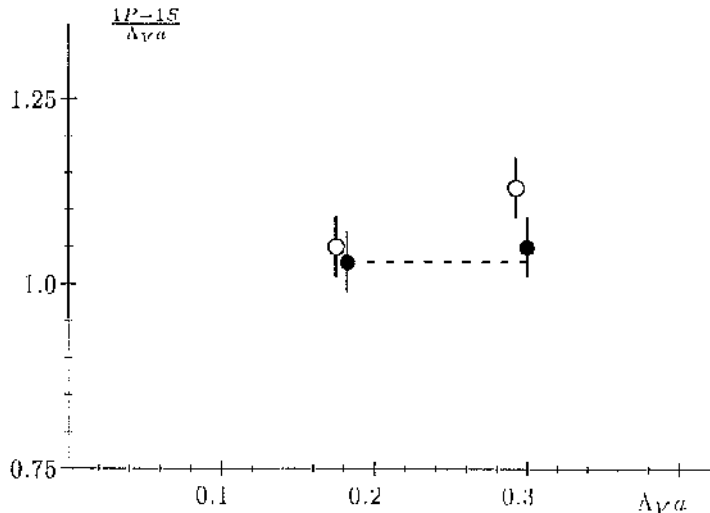


Figure 5.1: Asymptotic scaling of the  $1P - 1S$  splitting for  $b\bar{b}$  for quenched results in the  $V$  scheme. Open circles represent raw results at  $\beta = 5.7$  and  $6.0$  and filled circles represent results corrected for gluonic  $\mathcal{O}(a^2)$  errors.

A good example of the need for gluonic corrections is in the scaling of the ratio  $1P-1S$  to  $\Lambda_V$ , defined by the plaquette, with  $\beta$ . Plotted in figure (5.1) is the ratio which should be constant for asymptotic scaling. Clearly this is not so in the uncorrected case but is within errors when gluonic corrections have been done. So not only is it possible to observe scaling violations but also it is possible to systematically remove them.

## 5.5 Decay Constants

The pseudoscalar decay constant,  $f_{B_c}$ , which will determine the annihilation decay rate for  $B_c$  is defined in the rest frame of the  $B_c$  as

$$\langle 0 | \bar{b} \gamma^0 \gamma_5 c | B_c \rangle = i f_{B_c} M_{B_c} \quad (5.26)$$

The pseudoscalar decay constant can be related to a nonrelativistic wavefunction through the Van Royen-Weisskopf formula [48] by

$$f_{B_c}^2 = \frac{12 |\psi(0)|^2}{M_{B_c}} \quad (5.27)$$

where  $M_{B_c}$  is taken to be the mass of the pseudoscalar particle. When relating wavefunctions from lattice simulations to continuum quantities, renormalization

constants between the continuum and the lattice should really be taken into account. However it is not done here because they have not been calculated yet. It is also expected that large errors coming from the small components of the heavy Dirac spinors will effect the result at the  $\mathcal{O}(v^2) \approx 20\%$  level. Using the value of the wavefunction given in tabel (5.6) a value of  $f_{B_c} = 460(13) \text{ Mev}$  is obtained where the error quoted is only from the error in  $a^{-1}$ . This value for  $f_{B_c}$  is in line with estimates using various potential models [34]. A more accurate method would be to evaluate equ (5.26) directly by expressing this matrix element in terms of matrix elements in NRQCD. To  $\mathcal{O}(\frac{1}{M^2})$  equ (5.26) will be

$$\langle 0 | \bar{b} \gamma^0 \gamma_5 c | B_c \rangle = C_1 \langle 0 | \chi_b^\dagger \psi_c | B_c \rangle + C_2 \langle 0 | (\mathbf{D} \chi_b)^\dagger \cdot \mathbf{D} \psi_c | B_c \rangle + \dots \quad (5.28)$$

For an accuracy of  $\mathcal{O}(v^4)$ , radiative corrections to  $C_1$  need to be evaluated and  $C_2$  evaluated at least to tree-level. This has been done in [49] for the continuum. When  $B_c$  has been observed experimentally and the annihilation decay measured it will be possible to extract an accurate value for  $V_{cb}$  given a value for  $f_{B_c}$  calculated on the lattice.

## Chapter 6

# Conclusion

The first part of the work presented was the calculation of the spectrum of Charmonium to next to leading order using NRQCD. This allowed relativistic effects to be investigated, for example, the calculation of spin-dependent splittings. Agreement with experiment was found within the expected remaining systematic errors which are quenching and the omission of relativistic corrections in the heavy quark action. For agreement with experiment it is essential to use tadpole improved perturbation theory. Not doing so would have severely underestimated spin-splittings to such an extent that the discrepancy to experiment could not have been understood by the remaining systematic errors. Spin-independent splittings, for example the 2S-1S, were also calculated although the noise in the 2S state is found to be quite high for direct comparison to experiment. The extraction of excited states relied on using multi-exponential multi-correlated fits. For this it is necessary to have smeared operators in the meson correlation function to project out at early times the required state. This was successful in obtaining plateaus in the ground state at early times where the noise to signal ratio is smaller.

Presented also was the spectrum for  $\bar{b}b$  at a lower  $\beta$  of 5.7 than has previously been done. Disagreement in spin-splittings to the values at  $\beta = 6.0$  and to experiment was found indicating  $\mathcal{O}(a^2)$  corrections in the chromo-magnetic and electric field are significant at these low  $\beta$  values. The spectrum of  $B_c$  states, none of which have yet been observed experimentally, has also been given. A prediction for the lowest ground state  $^1S_0$  for  $B_c$  is  $6.47(20)$  GeV. These could in the future be observed in the decay modes  $B_c \rightarrow \psi\pi, \psi l\nu$  where the  $\psi$  decays ultimately into a lepton pair [50]. In all cases the scale was set using the 1P-1S splitting as experimental input. The  $a^{-1}$  extracted is quite different depending on the type of meson

used. The values obtained obey the relation  $a_{\{\bar{b}b\}}^{-1} > a_{\{B_c\}}^{-1} > a_{\{\bar{c}c\}}^{-1}$ . This is a direct consequence of quenching and is a good demonstration of it.

A non-perturbative method to determine  $\mathcal{O}(a^2)$  gluonic corrections has been presented, the values obtained are consistent with perturbative estimates. These gluonic corrections are significant for Upsilon at  $\beta = 5.7$ . Asymptotic scaling from  $\beta = 6.0$  to  $\beta = 5.7$  for the 1P-1S splitting, is successful provided these gluonic corrections are taken into account. This increases  $a_{\{\bar{b}b\}}^{-1}$  at  $\beta = 5.7$  to about 7 % which is significant when converting to physical units.

For future work relativistic corrections must be included to reduce the remaining systematic errors. This should be possible for Charmonium. Charmonium is a good system to use in order to gauge the improvement program of NRQCD since for example the S hyperfine is known experimentally. Any changes seen in the Charmonium spectrum can be used to monitor the possible changes expected in Upsilon. Performing unquenched simulations for Charmonium is also necessary which will help to decide the effect of quenching on for example the S hyperfine splitting. Doing such simulations will also enable another value for the strong coupling constant,  $\alpha_s$ , to be extracted. Agreement with the result from Upsilon will be a great success for NRQCD showing that systematic errors are under control. If simulations for Upsilon are done again at  $\beta = 5.7$  then it must be necessary to correct for  $\mathcal{O}(a^2)$  corrections in the chromo-magnetic and electric fields. More importantly configurations from a  $\mathcal{O}(a^2)$  corrected gluonic action should be used. It will be interesting to observe the changes to see if they agree with the perturbative and non-perturbative estimates. This underlines an important principle of NRQCD. One should identify lattice spacing errors and correct for them systematically instead of naively taking the lattice spacing to zero by using higher  $\beta$  values.

# Bibliography

- [1] K. G. Wilson, *Phys. Rev. D* **10**, 2445 (1974).
- [2] A. S. Kronfield, Lectures presented at the TASI summer school 1991, *Perspectives in the Standard Model*, Boulder, USA, (1991).
- [3] R. D. Kenway, *Rep. Prog. Phys.* **52**, 1475 (1989).
- [4] H. J. Rothe, *Lattice Gauge Theories*, World Scientific, Singapore, (1992).
- [5] S. R. Sharpe, Lectures at TASI 1994, to appear in *CP Violation and the Limits of the Standard Model*, Ed. J. Donoghue, to be published by World Scientific.
- [6] K. G. Wilson, *Adv. Math.* **16** 176 (1975).
- [7] J. J. Aubert et al, *Phys. Rev. Lett.* **33**, 1404 (1974).
- [8] J. E. Augustin et al, *Phys. Rev. Lett.* **33**, 1406 (1974).
- [9] S. W. Herb et al, *Phys. Rev. Lett.* **39**, 252 (1977).
- [10] W. R. Innes et al, *Phys. Rev. Lett.* **39**, 1240 (1977).
- [11] W. Lucha, F. F. Schoberl and D. Gromes, *Quarkonia and Quantum Dynamics*, *Phys. Rep.* **200** 127 (1991).
- [12] E. Eichten and F. Feinberg, *Spin dependent forces in Quantum Chromodynamics*, *Phys. Rev. D* **23** 2724 (1981).
- [13] G. S. Bali et al., *Confining forces and String Formation From The Lattice*, Wuppertal preprint WUB 94-32.
- [14] L. D. Landau and E. M. Lifshitz *Quantum Mechanics*, course of Theoretical Physics, Volume 3 Third Edition.
- [15] M. Peskin in *Dynamics and Spectroscopy at High Energy*, Proceedings of the 11th SLAC Summer Institute on Particle Physics, SLAC Report 267.

- [16] W. Kwang, J. Rosner and C. Quigg, *Annu. Rev. Nucl. Part. Sci.* **37**, 325 (1987).
- [17] *Review of Particle Properties*, *Phys. Rev. D* **50** (1994).
- [18] L. L. Foldy and S. A. Wouthuysen, *Phys. Rev.* **78**, 29 (1950).
- [19] B. A. Thacker and G. P. Lepage, *Phys. Rev. D* **43**, 196 (1991).
- [20] G. P. Lepage, L. Magnea, C. Nakhleh, U. Magnea and K. Hornbostel, *Phys. Rev. D* **46**, 4052 (1992).
- [21] K. Symanzik, *Nucl. Phys.* B226:187 (1983), B226:205 (1983).
- [22] B. Sheikholeslami and R. Wohlert, *Nucl. Phys.* B259:572 (1985).
- [23] A. S. Kronfeld, *Nucl. Phys. B (Proc. Suppl.)* **30**, 445 (1993).
- [24] A. S. Kronfeld, *Beauty and the Beast: What Lattice QCD can do for B physics*, Fermilab-Conf-93/277-T.
- [25] B. Sheikholeslami and R. Wohlert, *Nucl. Phys. B* **259**, 572 (1985).
- [26] G. P. Lepage and P. B. Mackenzie, *Phys. Rev. D* **48**, 2250 (1993).
- [27] W. H. Press, B. P. Flannery, S. A. Teukolsky and W. T. Vetterling, *Numerical Recipes*, Cambridge University Press (1986).
- [28] C. T. H. Davies, K. Hornbostel, A. Langnau, G. P. Lepage, A. Lidsey, J. Shigemitsu and J. Sloan, *Precision  $\Upsilon$  Spectroscopy from Nonrelativistic Lattice QCD*, *Phys. Rev. D* **50**, 6963 (1994).
- [29] M. Luscher and U. Wolff, *Nuc. Phys. B* **339**, 222 (1990).
- [30] Tim Klassen, Private Communication.
- [31] A. X. El-Khadra, *Lattice QCD*, Ohio-preprint: OIISTPY-HEP-T-94-020 (1994).
- [32] C. R. Allton et al., UKQCD collaboration, Southampton-preprint: SHEP 91/92-27 (1992).
- [33] C. J. Morningstar, *Phys. Rev. D* **48**, 2265 (1993); *Nucl. Phys. B (Proc. Suppl.)* **34**, 425 (1994); Edinburgh Preprint 94/L.
- [34] E. Eichten and C. Quigg, *Mesons with Beauty and Charm: Spectroscopy*, FERMILAB-PUB-94/032-T, and references therein.

- [35] V. V. Kiselev, A. K. Likhoded and A. V. Tkabladze, Serpukhov preprint IFVE-94-51, hep-ph 9406339.
- [36] G. S. Bali and K. Schilling, Phys. Rev. D **46**, 2636 (1992).
- [37] G. S. Bali and K. Schilling, Phys. Rev. D **47**, 661 (1993).
- [38] A. X. El-Khadra, G. Hockney, A. S. Kronfeld and P. B. Mackenzie, Phys. Rev. Lett. **69**, 729 (1992).
- [39] C.T.H. Davies et al., Phys. Rev. Lett. **73** 2654 (1994).
- [40] U. M. Heller, K. M. Bitar, R. G. Edwards and A. D. Kennedy, *The Heavy Quark Potential in QCD with 2 Flavours of Dynamical Fermions*, Tallahassee preprint, FSU-SCRL-94-09, hep-lat/9401025 (1994).
- [41] A. X. El-Khadra et al., Nucl. Phys. B (Proc. Suppl.) **30**, 449 (1993).
- [42] S. M. Catterall, F. R. Devlin, I. T. Drummond, R. R. Horgan Phys. Lett. B **321**, 246 (1994).
- [43] G. P. Lepage, Nucl. Phys. B (Proc. Suppl.) **26**, 45 (1992).
- [44] Gunnar Bali, Private Communication
- [45] C. T. H. Davies et al., *A Precise Determination of  $\alpha_s$  From Lattice QCD*, hep-ph/9408328, Phys. Lett. B **345**, 42 (1995).
- [46] Kent Hornbostel, Private Communication.
- [47] G. P. Lepage, *Lattice QCD for Small Computers*, lectures presented at TASI 93 and at the UK Summer Institute.
- [48] R. Van Royen and V. F. Weisskopf, Nuovo Cim. **50**, 617 (1967); **51**, 583 (1967).
- [49] E. Braaten and S. Fleming, *QCD Radiative Corrections to the Leptonic Decay Rate of the  $B_c$  Meson*, Northwestern University preprint:NUHEP-TH-95-1, hep-ph 9501296.
- [50] C. Quigg, Fermilab preprint:Fermilab-Conf 93/265-T, contributed to the Workshop on B Physics at Hadron Accelerators, Snowmass.

